International PhD Program in Biomolecular Sciences – XXXIII cycle

Department of Cellular, Computational

and Integrative Biology - CIBIO

Mechanisms of centrosome-dependent PIDDosome activation

PhD Thesis of:

Matteo BURIGOTTO
Mat. 197959

Tutor:

Prof. Massimo PIZZATO

Advisor:

Prof. Luca FAVA

Academic Year 2019/2020

DECLARATION

I, Matteo Burigotto, confirm that this is my own work and the use of all materials from other sources has been properly and fully acknowledged.

ABSTRACT

Centrosome number control is crucial for the faithful segregation of chromosomes during mitosis. Centrosome amplification results into genetic instability and predisposes cells to neoplastic transformation. To preserve tissue homeostasis, the increase in centrosome number in healthy cells is invariably followed by a p53-dependent reduction in the propensity to commit to additional cell cycles. It has been previously shown that supernumerary centrosomes trigger p53 stabilization dependent on the PIDDosome (a multiprotein complex composed by PIDD1, RAIDD and Caspase-2), whose activation results in cleavage of p53's key inhibitor, MDM2.

Herein, I present evidence based on super resolution microscopy, yeast-two-hybrid and reverse genetics demonstrating that PIDD1 is recruited to mature centrosomes by the centriolar distal appendage protein ANKRD26, uncoupling surveillance of centrosome number from ciliogenesis. Furthermore, I show that the centrosome constitutively recruits the PIDD1 full-length precursor, dynamically exchanging it with the cytoplasmic pool. Remarkably, albeit independent from each other, both PIDD1 centrosomal localization and autoproteolysis are required for PIDDosome-dependent Caspase-2 activation, since selective perturbation of either of these aspects resulted into compromised PIDDosome activation, blunting thereby the ability of cells to undergo p53-dependent cell cycle arrest. Moreover, I present evidence supporting the notion that physical clustering of supernumerary centrosomes upon cytokinesis failure is needed to overcome a PIDD1 concentration threshold that is limiting PIDDosome-dependent p53 activation in healthy cells.

In addition, in the context of DNA damage, activation of the complex results from a p53-dependent elevation of PIDD1 levels independently of centrosome amplification. I propose that PIDDosome assembly can in both cases be promoted by an ANKRD26-dependent local increase in PIDD1 concentration close to the centrosome. Collectively, these findings provide a paradigm for how centrosomes can contribute to cell fate determination by igniting a signalling cascade.

TABLE OF CONTENTS

INTRODUCTION

Centrosome architecture

Centrosomes are non-membrane bound organelles found in most eukaryotic cells and constituted by two rod-shaped structures called centrioles. Centrioles display a cylindrical architecture and are characterized by an evolutionary conserved radial symmetry. In fact, their clearest feature is the presence of nine microtubule triplets which are circumferentially arranged to form a hollow scaffold (Gönczy, 2012). Analogously to cytoplasmic microtubules, the centriolar microtubules are made of α- and β-tubulin heterodimers, which, however, carry specific post-translational modifications (such as acetylation, glutamylation or detyrosination), necessary to increase their stability (Bobinnec *et al*, 1998; Gundersen & Bulinski, 1986; Piperno & Fuller, 1985). Centrioles present a distinct polarity in which a distal end can be distinguished from a proximal end thanks to the presence of nine microtubule doublets instead of the triplets which nucleate the entire structure. In a centrosome, the centrioles are connected by a flexible proteinaceous linker and surrounded by a dynamic multi-layered protein network, the pericentriolar material (PCM) (Fig. 1).

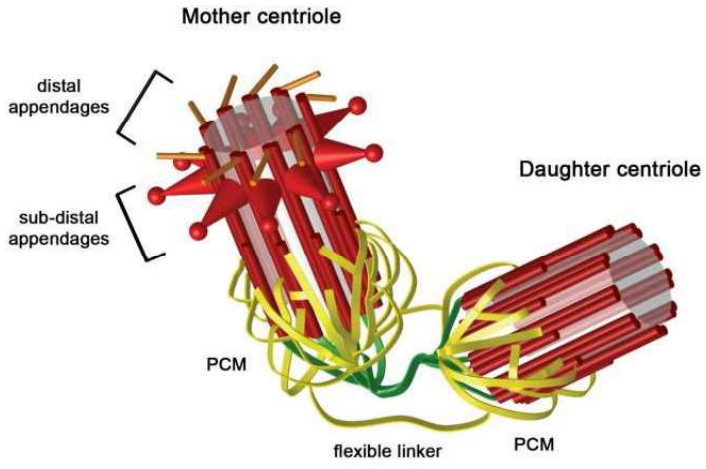

Figure 1. Schematic structure and organization of the centrosome. Parent and daughter centriole are tethered by a flexible linker (green) and embedded in a proteinaceous matrix (PCM, yellow). Only the fully mature centriole carries the distinctive DAs (orange) and SDAs (red cones). Image from (Sillibourne & Bornens, 2010).

The PCM is a highly structured array of proteins which embeds the centrioles and sustains their function, acting as a docking platform for protein complexes involved in regulation of intracellular trafficking and protein degradation (Pimenta-Marques & Bettencourt-Dias, 2020). Its main function resides in the ability to recruit the γ-tubulin ring complex, making the centrosome the dominant microtubule nucleating centre of vertebrate cells. The PCM is a highly dynamic protein condensate but characteristic components have been identified and can be divided in scaffolding proteins (e.g., pericentrin or PCNT, CEP192, CEP152, CPAP, and CDK5RAP2) and effectors (e.g., γ-tubulin).

The fibrous linker is composed of several proteins (among which Rootletin, CEP250/C-Nap1 and CEP68) and, together with microtubule-driven forces, it has the main role of forming a loose tether between the two centrioles, generating the so-called centrosome cohesion (Remo *et al*, 2020). This allows cells to maintain a single microtubule organizing centre until mitosis onset, when the two newly formed centrosomes will migrate apart to serve for mitotic spindle organization thanks to the dissolution of the linker via phosphorylation by the mitotic kinase Nek2A (Fry, 2002).

Another feature of vertebrate centrosomes is the presence of centriolar satellites, electron-dense membrane-less granules that cluster in the vicinity of centrioles. These granules are acentriolar assemblies of centrosomal proteins in which PCM1 seems to be the essential scaffold protein (Quarantotti *et al*, 2019). Even if their precise contributions remain elusive, centriolar satellites are thought to be important regulators of all centrosome activities, from duplication and maturation to microtubule cytoskeleton organization and ciliogenesis.

Inside a centrosome the two centrioles are not equivalent, and they can be distinguished one from another based on their age and structure (Nigg & Stearns, 2011). In fact, the older one (or parent centriole) is the only fully mature centriole and carries two sets of proteins close to its distal end, namely Distal Appendages (DAs) and Subdistal Appendages (SDAs), the latter of which present only in vertebrates (Fig. 1).

Centriole appendages

DAs and SDAs differ quantitatively, morphologically, biochemically, and functionally (Uzbekov & Alieva, 2018). The first difference between the two sets resides in the fact that whereas DAs are present as ninefold symmetrical structures which decorate the very distal part of the centriole wall, SDA number, distribution and shape vary significantly across species and among cell types. In fact, SDA variability could reflect differences in cell age and functional state. Even if both appendage sets were firstly imaged in the '50 thanks to electron microscopy, only recently a more detailed characterization has emerged, shedding light on both their structural composition and their functional role.

Combining centrosome proteomics, immunofluorescence microscopy and RNAi, Tanos and colleagues identified a set of five DA proteins and the presence of a discrete hierarchy in their recruitment to the centriole (Tanos *et al*, 2013). Few years later, two landmark works confirmed these data and refined the definition of DA architecture, employing superresolution techniques such as direct stochastic optical reconstruction microscopy (dSTORM) (Yang *et al*, 2018) and correlative 3D STORM/electron microscopy (Bowler *et al*, 2019). DA assembly begins with the recruitment of C2CD3. This distal end centriole protein resides inside the centriole lumen and is essential for DA priming, despite not being considered a DA protein per se. Downstream to C2CD3, CEP83 occupies the innermost region of a DA and it is responsible for the recruitment of SCLT1 and CEP89. SCLT1, in turn, is the docking site for three other proteins, namely FBF1, CEP164 and ANKRD26 (Fig. 2).

SDA assembly is driven by ODF2 recruitment to the centriole wall, followed by CEP128, CCDC68 and CCDC120. Downstream of these proteins, centriolin, Ninein and CEP170 are recruited (Fig. 2) (Chong *et al*, 2020). In contrast to the well-defined DA epistasis, SDA formation is more elusive, since CCDC68, CCDC120 and Ninein all independently concur in CEP170 localization. Moreover, the fact that both Ninein and CEP170 are present in two distinct pools (one distal, involved in SDA formation, and one at the proximal end of the centriole) makes the fine dissection of epistatic relationships more difficult.

Even if the two appendage sets comprise biochemically and spatially distinct pools of protein, it has been recently demonstrated that a certain degree of coupling between DAs and SDAs exists (Chong *et al*, 2020). In fact, DA depletion induces SDAs

to occupy a broader distal region, implying that DAs act as a physical barrier for SDA positioning. Furthermore, it has been shown that appendage composition exhibits some crosstalk, since both ODF2 and CEP89 display dual localization with one pool dependent on DAs and the other on SDAs (Fig. 2). Another layer of complexity is represented by the fact that, once assembled, appendages are not immutable structures, but they undergo a remodelling process dependent on cell cycle (Bowler *et al*, 2019).

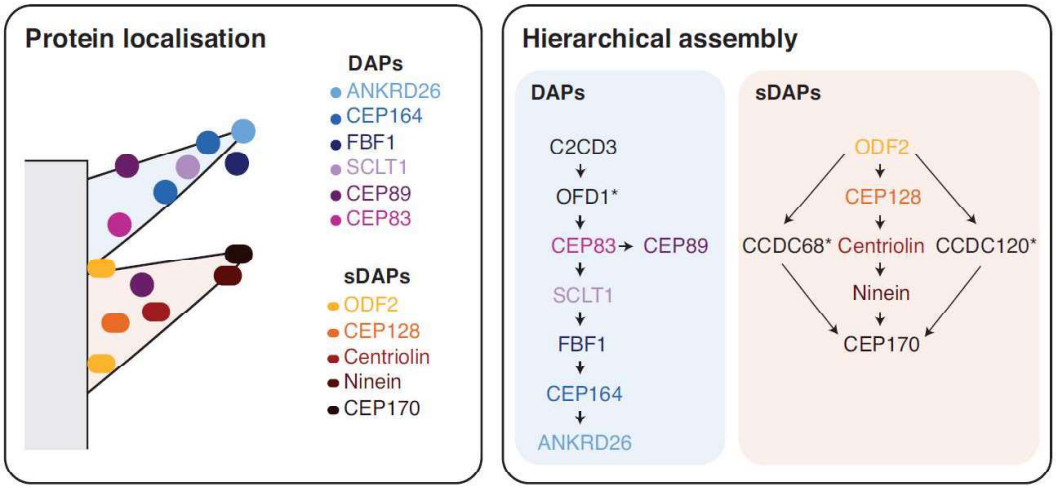

Figure 2. Schematic of DA and SDA architecture. DAs and SDAs are two sets of proteins which decorate the distal end of parent centrioles. Their composition has been described, both in terms of protein localization (left panel) and epistatic relationships (right panel). Of note, C2CD3 is indispensable for DA formation despite not being considered as a DA protein (Ye *et al*, 2014). Asterisks indicate proteins involved in appendage assembly but whose precise localization has not been mapped yet. Image from (Tischer *et al*, 2020).

The centrosome cycle

In proliferating cells, the centriole number is tightly controlled. This is achieved by a multistep centrosome cycle which is tightly synchronized with the cell cycle and allows cells to duplicate their centriole number, building up two centrosomes right before mitosis (Nigg, 2007). This leads to the presence of two structures with microtubule nucleation capability which assist chromosome segregation during mitosis and equip each

daughter cell with its own fully competent centrosome at the end of cell division (Fig. 3) (Nigg & Holland, 2018).

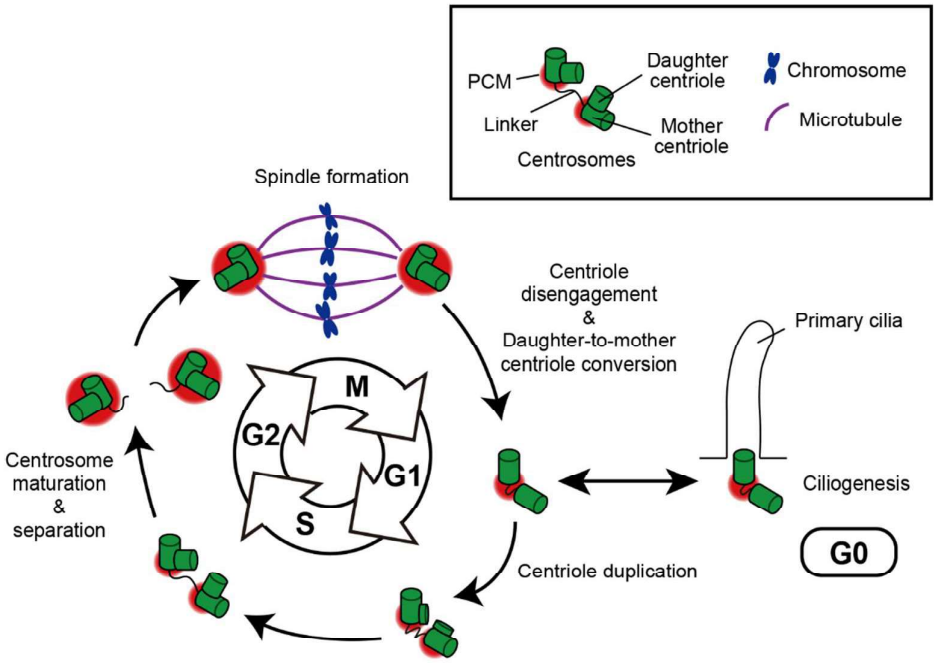

Figure 3. The centrosome cycle in relation to the cell cycle. In S phase, concomitantly to DNA replication, centriole duplication starts by the formation of procentrioles, which elongate to reach full length during G_2 phase. At the same time, both centrioles undergo extreme PCM expansion. At G_2/M transition, the two centrosomes are separated and concur to form the poles of a bipolar mitotic spindle. Following cytokinesis, every daughter cell inherits a centrosome, whose centrioles disengage during the following G_1 phase, licensing them for a new duplication cycle. When cells enter quiescence (G_0), the centrosome can act as basal body for primary cilium nucleation. Image adapted from (Takeda *et al*, 2020).

At the beginning of cell cycle (G_1), each cell has a single centrosome. At the G_1/S transition, both parent and daughter centriole nucleate a new single procentriole, at a proximal site, perpendicular to each existing structure. The first steps of procentriole formation require a well-defined core of five evolutionary conserved proteins: PLK4, CEP192, CPAP, STIL and SAS6 (Gönczy & Hatzopoulos, 2019). Of these, PLK4 is recognized as the master regulator of the process (Habedanck *et al*, 2005; Bettencourt-Dias *et al*, 2005) since it catalyses the formation of the central cartwheel, a ring-like structure with nine-fold symmetry that serves as template for procentriole biogenesis

(Kim *et al*, 2016; Moyer & Holland, 2019). Importantly, when PLK4 is depleted, procentriole formation cannot occur; on the other hand, its overexpression exerts the opposite effect, leading to centrosome amplification (Kleylein-Sohn *et al*, 2007). Once primed, procentrioles elongate and they reach full length before mitosis. Their distinguishing feature is the inability to recruit PCM. As a result, procentrioles do not contribute to microtubule nucleation, remaining functionally quiescent at this stage. Procentrioles enter mitosis still associated with their parent centriole and this association persists until late mitosis/early G_1.

In G_2 phase, substantial changes in centrosome structure occur. In particular, PCM massively expands (a phenomenon called centrosome maturation), increasing the abundance of γ-tubulin ring complexes which will catalyse the formation of the mitotic spindle. This event is mainly guided by phosphorylation events performed by Plk1 and Aurora A kinases. Concomitantly, the daughter centriole begins to be sequentially decorated by both DA and SDA components. This process starts in G_2 phase, continues throughout mitosis, and ends only during the G_1 phase of the subsequent cell cycle. Appendage acquisition marks the conversion of the daughter centriole to a parent centriole. Eventually, once inherited by a daughter cell, this centriole will be the oldest available centriole in that cell. Coupled with the DA epistatic relationships discussed above, a temporal hierarchy in the assembly can be seen: C2CD3 is recruited to the daughter centriole wall during G_2, followed by CEP83, CEP89 and SCLT1 in early mitosis, and FBF1, CEP164 and ANKRD26 in late mitosis (Wang *et al*, 2018; Bowler *et al*, 2019). At the same time, transient remodelling events occur also on the old parent centriole, leading to the loss of more peripheral appendage proteins, which will reappear in late mitosis/early G_1 (whereas the inner components, such as CEP83 and SCLT1 for DAs and ODF2 for SDAs are retained as a permanent scaffold). The functional relevance of this remodelling phenomenon is not entirely clear but it has been hypothesized that it would facilitate appendage-related functions in mitosis, reducing the otherwise imbalanced protein composition of the old and young parent centrioles (Bowler *et al*, 2019; Sullenberger *et al*, 2020).

At mitosis onset (G_2/M transition), the tether between the two original centrioles is resolved (an event called centrosome disjunction) thanks to the Nek2A kinase-dependent phosphorylation of CEP250/C-Nap1 and Rootletin (Bahe *et al*, 2005; Hardy *et al*, 2014). Once the proteinaceous linker is disassembled, the microtubule plus end-directed kinesin Eg5 guides an active centrosome separation (Blangy *et al*, 1995). This

migration culminates in the establishment of two poles in the dividing cell, an event sustained by microtubule motor proteins which exert dynein-dependent forces (Merdes *et al*, 2000). The presence of a bipolar mitotic spindle assists chromosome segregation. Once mitosis is completed, upon physical division of mitotic cells, each daughter cell inherits a single centrosome.

Eventually, in parallel to full appendage re appearance at both parent centrioles, the procentrioles become daughter centrioles by undergoing centriole disengagement, i.e. they lose their tight association with their respective parent centriole (even though a proteinaceous linker persists). At centriole disengagement, the parent centriole reduces its PCM and at the same time the newly formed daughter centriole acquires its PCM, an event termed centriole-to-centrosome conversion, essential for the acquisition of full competence for duplication (Wang *et al*, 2011). Thanks to this highly controlled cycle, each cell can build up a second centrosome which, upon mitotic division, can be passed on to each daughter cell.

Canonical centrosome functions

The centrosome is the main microtubule-organizing centre of mammalian cells, as it is primarily involved in the regulation of the microtubule cytoskeleton during interphase and in the assembly of a bipolar mitotic spindle during cell division. For this reason, it influences a wide range of microtubule-associated processes, such as cell shape determination, cell division, cell fate determination, motility, polarity, intracellular trafficking, and positioning of other organelles inside the cell (Gönczy, 2012).

Remarkably, centrosomes are not strictly necessary for mitotic spindle formation (Debec *et al*, 2010). For example, even if higher plants have evolutionary lost these organelles, they are still able to segregate their chromosomes relying on a microtubule-based mitotic spindle (Schmit, 2002). Laser ablation and microsurgery experiments in animal cells yielded conflicting results about the requirement of centrosomes for cell cycle completion. For example, it has been shown that they are not strictly indispensable for somatic cells to progress into and out of mitosis (Uetake *et al*, 2007). Moreover, it has been reported that the destruction of centrosomes in the preceding interphase does not prevent the formation of a bipolar spindle and a timely mitotic exit (Khodjakov *et al*, 2000; Basto *et al*, 2006) but it rather leads to defects in cytokinesis and to an inability to

enter a subsequent S-phase (Piel *et al*, 2001; Hinchcliffe *et al*, 2001; Khodjakov & Rieder, 2001). However, a major caveat in interpreting these studies lies in the use of techniques as laser ablation and RNA interference to remove centrosomes. In fact, such methods create cellular stresses which can account for the reported phenotypes.

The development of chemical inhibitors which specifically target key regulators of centriole biogenesis (e.g., the PLK4 inhibitor centrinone)(Wong *et al*, 2015) allowed to establish that non-transformed cell lines lacking centrosomes undergo a G_1 arrest after a few cell cycles (Fong *et al*, 2016; Lambrus *et al*, 2016; Meitinger *et al*, 2016). Nowadays it is well established that centrosomes per se are non-essential for mitosis (Meraldi, 2016). Nevertheless, they play a critical role in the completion of a rapid faithful segregation of large chromosome sets (Sir *et al*, 2013; Wong *et al*, 2015) and they are at least important for the control of the positioning and the orientation of the bipolar spindle and for its timely assembly during the early stages of cell division (Meraldi, 2016).

Another centrosome function connected with microtubule-organizing capability resides in their involvement in cilia formation. Cilia are instrumental organelles for cell motility and fluid movement (motile cilia), and for extracellular environment sensing, such as mechano-transduction and signalling transduction (non-motile or primary cilia). Most mammalian cells (including stem, epithelial, endothelial, and muscle cells, as well as connective tissue and neurons) possess a single primary cilium which protrudes from their surface. Primary cilia are specialized compartments enriched with receptors which assist signalling cascades that are fundamental during development and tissue homeostasis, such as Hedgehog, Wnt, and TGF-β pathways (Singla, 2006).

Primary cilia are formed in interphase when the centrosome (specifically the parent centriole) docks at the plasma membrane, at the future site of cilium emanation (Ishikawa & Marshall, 2011). The membrane-docked centriole (basal body) elongates and templates the growth of the cilium microtubule backbone (axoneme), that consists in nine radially disposed microtubule doublets directly emanating from the basal body (Fig. 4).

Centriolar appendages are necessary for ciliogenesis. In fact, the first steps of this process involve the recruitment of Golgi-derived vesicles to the DAs. These give rise to the formation of a ciliary vesicle which covers the parent centriole distal end, enabling the subsequent docking and fusion with the plasma membrane. In the absence of DAs, primary cilia completely fail to form (Tanos *et al*, 2013). Conversely, the role of SDAs in ciliogenesis is less clear since they seem dispensable for this process (Mazo *et al*,

2016). Several functions have been shown for these appendages: they aid basal body positioning through cytoplasmic microtubule anchoring (Mogensen *et al*, 2000), they concur to link the basal body to the Golgi (Mazo *et al*, 2016), and they promote basal body alignment in multiciliated cells (Kunimoto *et al*, 2012; Clare *et al*, 2014).

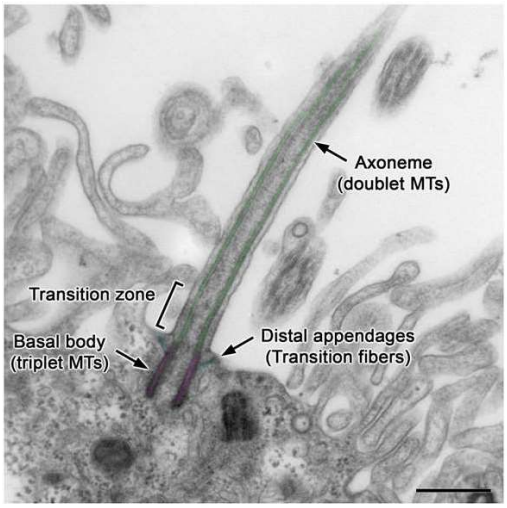

Figure 4. The primary cilium. Transmission electron micrograph depicting a longitudinal section of a primary cilium, emerging from the apical surface of a cell. The parent centriole (magenta), thanks to its distal appendages (cyan), docks at the plasma membrane and nucleates the axoneme (green). MTs: microtubules. Scale bar: 500 nm. Image from (Narita & Takeda, 2015).

Contrary to mitotic spindle assembly, cilia biogenesis categorically depends on the presence of a mature centriole, a notion that is strongly supported by human molecular genetics. In fact, defects in both structural and regulatory centriolar components often result into cilia-related syndromes (referred to as ciliopathies), characterized by distinctive traits such as microcephaly, cerebral malformations, cystic kidneys, retinal degeneration, and infertility (Fliegauf *et al*, 2007). Considering the different requirement of the centrosome in mitotic division and in ciliogenesis, it has been hypothesized that this organelle has evolved to provide the cell the ability to assemble cilia rather than assist it during mitosis (Marshall, 2009).

The centrosome proteome and non-canonical centrosome functions

The centrosome is a dynamic structure whose protein composition varies according to cell cycle and cell state. The definition of a centrosome proteome has been hampered not only by this dynamism but also by experimental challenges due to the fact that this organelle is present in a single copy per cell, it is not delimitated by a membrane and it is usually tightly associated with the nuclear membrane. Large scale proteomic studies of human centrosomes have so far identified more than three hundred proteins as centrosomal components and many of these have been validated (Andersen *et al*, 2003; Jakobsen *et al*, 2011; Danielsson *et al*, 2020). Schematically, centrosomal proteins can be classified in 3 different classes:

1) Centriolar proteins, persistently present during all phases of the cell cycle since structural centriolar components, e.g., α- and β-tubulin or centrin. This category comprises also appendage proteins, which are remodelled in mitosis but fix components of interphasic centrioles.

2) Proteins of the PCM and centriolar satellites, such as γ-tubulin, pericentrin, CDK5RAP2, AKAP450, CEP55, CEP63, CYLD, FOPNL, OFD1, PCM1, BBS4. Co-localization studies coupled with PCM1 co-immunoprecipitation have recently revealed several additional satellite components (Tollenaere *et al*, 2015; Hori & Toda, 2017). Of these, some have been shown to be exclusive satellite proteins (SSX2IP), some are common to satellites and centrosome (e.g., CEP131 and FOP), some common between satellites and primary cilium (e.g., BBS4) and some are shared between all centrosome related compartments (e.g., CEP290) (Staples *et al*, 2012; Lee & Stearns, 2013; Villumsen *et al*, 2013).

3) Proteins transiently associated with centrosomes such as Polo-like kinases, Aurora A kinase, cyclins and cyclin-dependent kinases (e.g., cyclin B and CDK1), DNA damage response proteins (e.g., p53, ATM, ATR, DNA-PK, BRCA1, BRCA2).

The first two categories encompass centrosomal components *stricto sensu.* The latter group instead reveals that the centrosome has a functional complexity which reaches well beyond its primary involvement in microtubule organization. In fact, growing evidence continues to suggest how this organelle could participate in numerous, seemingly unrelated, processes, likely serving as docking platform for the accumulation of regulatory complexes, concentrating and integrating signalling cascades in time and

space. Some of these processes involve: actin cytoskeleton organization (Farina *et al*, 2016), cell cycle regulation (Doxsey *et al*, 2005), support to DNA replication (Tayeh *et al*, 2020), DNA damage response (Mullee & Morrison, 2016), neurogenesis (independently of primary cilia signalling) (Zhang *et al*, 2016; Wang *et al*, 2020), autophagy (Joachim *et al*, 2017; Morleo *et al*, 2020) and protein homeostasis (Freed *et al*, 1999; Wigley *et al*, 1999; Vora & Phillips, 2016), immune response (either by concentrating molecules involved in innate immunity and supporting the activity of the immunological synapse in T cells) (Stinchcombe *et al*, 2006), stress responses (Moser *et al*, 2013; Lee *et al*, 2019), localized storage and translation of specific mRNAs (Filippova *et al*, 2012; Iaconis *et al*, 2017; Ryder *et al*, 2020). Taking into account this, it is not surprising that defects in centrosomal components or in the countless activities of this organelle are implicated in a plethora of diseases, ranging from neurodevelopmental disorders, to ciliopathies, to cancer.

Centrosome number aberrations and cancer

In 1914, the German biologist Theodor Boveri published his avant-garde results in the treatise "Zur Frage der Entstehung Maligner Tumoren" (Concerning the Origin of Malignant Tumours). In his essay, he proposed that cancer cells can stem from abnormal mitosis as consequence of an excessive number of centrosomes. In fact, this condition leads to extra spindle poles and thus to an aberrant gain or loss of chromosomes (aneuploidy) in daughter cells. Even if a distinctive feature of a wide range of human cancers is represented by outstanding structural and numerical centrosome aberrations (Nigg & Raff, 2009; Godinho *et al*, 2014), Boveri's theory on the role of centrosome amplification in malignancy onset remained a controversial issue and cancer research focused almost exclusively on mutations of oncogenes and oncosuppressors as primary tumorigenesis drivers. In this context, the presence of extra centrosomes has long been considered as a mere consequence of oncogenesis (Fukasawa, 2007).

The last decades showed a systematic reassessment of centrosome role in carcinogenesis. In contrast to the vision of centrosome amplification as by-product of neoplastic transformation, it has been shown that this aberration is also found in early low grade and pre-neoplastic lesions (Lingle *et al*, 2002; Pihan *et al*, 2003; Segat *et al*, 2010;

Lopes *et al*, 2018). Moreover, experimentally induced centrosome amplification *in vivo* (obtained overexpressing the centriole duplication master regulator kinase SAK/PLK4) has been shown to increase the rate of spontaneous tumorigenesis, both in engineered flies and mice (Basto *et al*, 2008; Levine *et al*, 2017). Notably, it has been noticed how the karyotypical anomalies present in PLK4 overexpressing mice resemble the ones found in human tumour samples carrying supernumerary centrosomes (Levine *et al*, 2017).

Centrosome amplification could spontaneously occur *in vivo* as a consequence of four main causative events: centrosome cycle defects (e.g., overduplication during S-phase), *de novo* centriole biogenesis (i.e., biogenesis of centrioles without the need of a pre-existing template structure), cytokinesis failure (i.e., completion of mitosis without physical separation of daughter cells) or infection by fusogenic viruses. Cells which enter mitosis carrying centrosome amplification assemble, at least transiently, a multipolar spindle (Fig. 5). In this scenario, optimal microtubule-kinetochore interactions are not established, causing a sustained activation of the spindle assembly checkpoint (SAC). Prolonged SAC duration leads to an extended mitotic arrest, which can eventually result into death in mitosis when high cyclin B1 levels persist. If cells cannot sustain sufficient CDK1 activity, they can escape mitosis without proper chromosomal segregation (mitotic slippage), resulting into either a single cell with whole genome duplication (tetraploid cell) or multiple highly aneuploid cells (Andreassen & Margolis, 1994; Brito & Rieder, 2006). Usually, tetraploid cells either experience cell death during subsequent G_1 phase or enter a senescent state. Since high rates of aneuploidy are not well tolerated (Weaver *et al*, 2008), re-enter into cell division after experiencing a multipolar mitosis followed by cytokinesis is a rare event, as clearly showed by long-term live cell imaging experiments (Ganem *et al*, 2009). However, if cells circumvent these antiproliferative fates they can go through additional cell cycles, continue accumulating chromosomal aberrations and drive tumorigenesis (Fujiwara *et al*, 2005) (Fig. 5).

Taking this into account, it is unsurprising that cancer cells have evolved mechanisms to elude such catastrophic cell divisions and hence cell death. Some of these include centrosome inactivation (i.e., a drastic decrease in PCM levels associated to a centriole which results into a strong microtubule nucleation impairment), centrosome loss (an ill-defined phenomenon similar to inactivation but resulting into a loss of centriole integrity) or centrosome clustering. Centrosome clustering designates the ability of mitotic cells with centrosome amplification to gather extra centrosomes into two spindle poles, thereby achieving seemingly normal bipolar (pseudo-bipolar) divisions (Fig. 5).

However, centrosome clustering mechanisms are intrinsically error-prone, causing merotelic chromosome attachments (i.e., chromosomes simultaneously attached to microtubules emanating from the same spindle pole), events which can escape the robust block imposed by SAC (Cimini, 2008) and result in single chromosome losses/gains and genome instability (Ganem *et al*, 2009; Silkworth *et al*, 2009), accelerating tumoral transformation (Weaver *et al*, 2008).

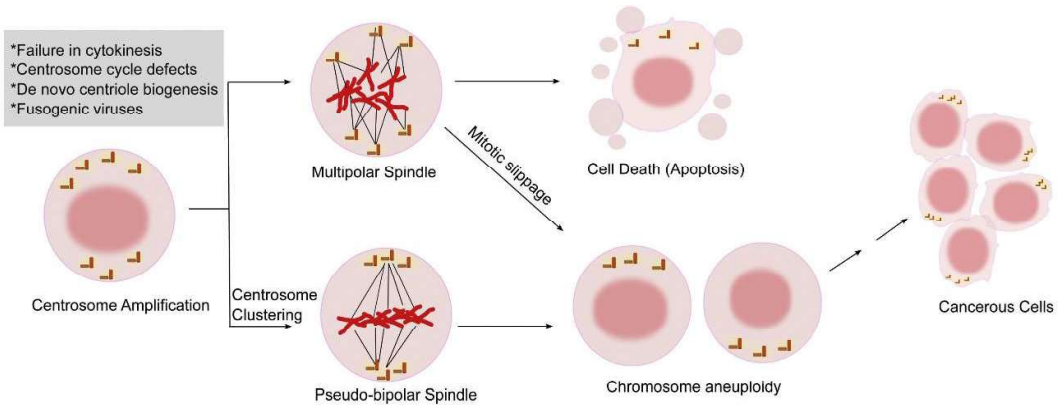

Figure 5. Centrosome amplification concurs in neoplastic transformation. Cells carrying supernumerary centrosomes can give rise to a multipolar spindle and either die before cell division completion or evade mitotic checkpoints through mitotic slippage. Alternatively, extra centrosomes can cluster in a pseudo-bipolar spindle. Independently from the spindle arrangement, mitosis of cells with centrosome amplification results in aneuploid daughter cells which can drive tumorigenesis. Image from (Jaiswal & Singh, 2020).

A characteristic repercussion of pseudo-bipolar mitoses is the generation of lagging chromosomes (Ganem *et al*, 2009; Silkworth *et al*, 2009). This term refers to the presence of chromatids which cannot timely migrate to the mass of already segregated chromosomes during anaphase. Lagging chromosomes have been shown to favour DNA damage in at least two ways. In fact, it has been shown that during cytokinesis they can be trapped into the cleavage furrow and experience double strand-breaks, which in turn can lead to translocations into daughter cells (Janssen *et al*, 2011). Moreover, significantly delayed chromosomes can be encapsulated by a nuclear envelope resulting into a micronucleus. DNA inside micronuclei accumulates extensive damage probably

because of nuclear membrane fragility and spilling of DNA into the cytoplasm (Zhang *et al*, 2015). In addition, DNA in micronuclei undergoes replication even during mitosis, although poorly (Crasta *et al*, 2012). This leads to the exposure of single strand DNA in the replicative forks, which is then fragmented by endonucleases and imperfectly resealed by DNA repair mechanisms, resulting into a single but catastrophic chromosomal rearrangement referred to as chromotripsis (Zhang *et al*, 2015), which can drive tumour transformation (Cortés-Ciriano *et al*, 2020).

In addition, extra centrosomes have also been shown to support tumour progression by promoting metastatization, both in a cell autonomous and non-cell autonomous way. In fact, Godinho and colleagues showed that centrosome amplification (obtained by PLK4 overexpression) in a three-dimensional culture system of breast cells leads to an increase in microtubule nucleation activity, which in turn results into elevated Rac1 signalling. Rac1 hyperactivation boosts actin polymerization and weakening of cell-cell adhesion, inducing the formation of invasive structures (invadopodia) (Godinho *et al*, 2014). Few years later, it has also been reported that centrosome amplification drives an invasive behaviour exploiting paracrine signalling: cells with extra centrosomes release a specific pro-invasive secretome (called extra centrosomes-associated secretory phenotype, ECASP) which promotes invadopodia formation in cells carrying a normal centrosome number (Arnandis *et al*, 2018).

Mechanisms of centrosome number control

It is now well established the notion that centrosomes are highly regulated by cell cycle cues. In fact, the same system of cyclins and cyclin-dependent kinases which regulates DNA replication and cell division has been also shown to coordinate timely duplication of these structures (Nigg, 2007). Conversely, only recently it has been shown how centrosomes can impact on the cell cycle by igniting signalling cascades. As an example, both an increase in centrosome number and loss of these structures result into a strong p53 activation and p21-dependent cell cycle arrest (Holland *et al*, 2012; Bazzi & Anderson, 2014; Lambrus *et al*, 2015). This underlies how centrosome aberrations are able to signal to the p53 tumour suppressor, igniting signalling cascades which concur to prevent proliferation of aberrant cells and thus tumorigenesis. Interestingly, centrosome

depletion and amplification have been shown to stabilize p53 relying on two genetically distinct pathways.

In 2016, three research groups independently performed a CRISPR screen for proteins able to overcome cell cycle arrest when knocked-out, upon centrosome depletion (obtained via PLK4 inactivation, genetically or pharmacologically) (Fong *et al*, 2016; Lambrus *et al*, 2016; Meitinger *et al*, 2016). Among their hits, they identified two proteins (53BP1 and USP28) which do not localize at the centrosome and act upstream of p53 to induce a p21-dependent arrest. The model for centrosome loss sensing (the so-called "mitotic surveillance pathway") suggests that in response to centriole depletion, 53BP1 brings together p53 and USP28, acting as a scaffold for USP28-mediated deubiquitination and subsequent stabilization of p53.

Even if it is plausible that the mitotic surveillance pathway could be evolved to prevent divisions with increased chances of mitotic errors, the sensor for centrosome loss remains elusive. So far, three hypothetical sensors have been suggested:

1) The mitotic surveillance pathway could be triggered at the level of microtubule-kinetochore interactions. During mitosis, 53BP1 has been reported to transiently localizes to kinetochores in the early stages of cell division and this event has no known function so far (Jullien *et al*, 2002). It has been proposed that 53BP1, even if it is not a component of the canonical SAC, could sense perturbations arising at the microtubule-kinetochore level due to centrosome loss.
2) Centrosome loss could be sensed by p53 itself (Contadini *et al*, 2019). In non-transformed human cells, p53 has been reported to transiently localize to the centrosomes of mitotic cells upon ATM-dependent phosphorylation. Specifically, ATM induces a phosphorylation event on discrete p53 cytoplasmic foci, which then move toward the centrosome following a microtubule-mediated movement and pericentrin-mediated docking (Ciciarello *et al*, 2001; Prodosmo *et al*, 2013). Once there, in unperturbed mitotic cells, p53 undergoes dephosphorylation, and it detaches to allow mitotic progression (Tritarelli *et al*, 2004; Oricchio *et al*, 2006). The functional meaning of ATM-p53-centrosome axis is still debated but it has been shown that if there are no centrosomes, phosphorylated p53 foci accumulate in the cytoplasm. These in turn recruit 53BP1 with consequent p53 stabilization and irreversible cell-cycle arrest, resembling the mitotic surveillance pathway.

This evidence could suggest that ATM-p53-centrosome might be a signalling axis involved in centrosome depletion sensing.

3) No counting mechanism exists. According to this hypothesis, the 53BP1-USP28-p53 axis would be evoked indirectly, in response to accumulation of stress arising from sequential prolonged prometaphases displayed by acentrosomal cells. This would be in line with the fact that prolonged mitotic timing per se is able to hinder the proliferative ability of daughter cells (Uetake & Sluder, 2010). In line with this, depletion of either 53BP1 or USP28 suppresses not only the G_1 block due to centrosome depletion but also the arrest due to prolonged metaphase block coming from other distinct mitotic stresses, independently of the SAC (Fong *et al*, 2016; Lambrus *et al*, 2016; Meitinger *et al*, 2016).

As already mentioned, not only centrosome loss is able to influence cell behavior. In fact, it has been shown that supernumerary centrosomes induce p53 (Holland *et al*, 2012; Lambrus *et al*, 2015; Wong *et al*, 2015). *In vivo* experiments in PLK4-overexpressing mouse models showed that p53-proficient tissues do not sustain supernumerary centrosomes propagation nor tumorigenesis (Coelho *et al*, 2015; Kulukian *et al*, 2015; Vitre *et al*, 2015; Serçin *et al*, 2016). A *Trp53*-null background instead has been seen to allow division of cells carrying extra centrosomes, facilitating error-prone mitosis and thus neoplastic transformation (Coelho *et al*, 2015).

It has been shown that cytokinesis failure is able to promote a p53-p21-dependent cell cycle arrest relying on LATS2 and Hippo pathway (Aylon *et al*, 2006; Ganem *et al*, 2014), only in part depending on extra centrosomes. This could be explained by the fact that LATS2 activation might be primarily evoked by some features of polyploid cells, such as an increment in nuclear DNA content or an altered surface to volume ratio, instead of by an increase in centrosome number. In 2017, Fava and colleagues filled the gap between centrosome amplification and p53 induction, showing that the presence of supernumerary centrosomes alone specifically triggers the activation of the PIDDosome, a multiprotein complex whose assembly invariably results into p53 stabilization (Fava *et al*, 2017).

The PIDDosome

The Caspase-2 PIDDosome is a high molecular weight multiprotein complex composed of PIDD1 (p53-inducible protein with death domain or LRDD), RAIDD (RIP-associated ICH1/CED3-homologous protein with death domain or CRADD) and Caspase-2 (or CASP2) (Tinel & Tschopp, 2004), represented with a 5:7:7 (or alternatively 7:7:7) stoichiometry. PIDD1 was first discovered as a novel gene regulated by p53. In fact, the presence of a non-canonical p53 responsive element in its promoter led to classify this protein as a putative regulator of the p53-dependent apoptosis pathway in the context of the DNA damage response (Lin *et al*, 2000). PIDD1 contains seven leucine-rich repeats (LRR) at its N-terminus, two ZU5 domains (domains present in ZO-1, Unc5-like netrin receptors and Ankyrins with unclear function), an UPA domain (uncharacterized domain conserved in UNC5, PIDD1 and Ankyrins) and a death domain (DD) at its carboxy-terminal. Interestingly, the full-length PIDD1 precursor undergoes autoprocessing events utilizing a poorly understood intein-like protein splicing mechanism that has been so far found exclusively in the nucleoporin Nup98 and the transmembrane receptor Unc5CL (Tinel *et al*, 2007; Heinz *et al*, 2012). PIDD1 autoproteolysis can occur at two sites, resulting in the coexistence of different PIDD1 protein species (Fig. 6):

1. PIDD1-FL, the full-length precursor of 910 amino acids,
2. PIDD1-N (amino acids 1–445), the N-terminal fragment resulting from cleavage at the first autoproteolytic site (Ser446),
3. PIDD1-C (amino acids 446–910), the C-terminal fragment resulting from the aforementioned cleavage site and
4. PIDD1-CC (amino acids 588–910), resulting from cleavage at the second autoproteolytic site (Ser588).

Seminal work by Tschopp and collaborators revealed that PIDD1 autoproteolytic fragments can assemble in different multiprotein complexes, thanks to their protein-protein interaction domains. PIDD1-C binds RIP1 and NEMO (NF-κB essential modulator) forming the so-called NEMO-PIDDosome, which promotes NEMO sumoylation and consequently NF-κB pathway activation (Janssens *et al*, 2005). PIDD-CC in turn, is responsible for assembling the Caspase-2-PIDDosome (hereinafter PIDDosome) together with RAIDD and Caspase-2 (Tinel & Tschopp, 2004; Janssens *et al*, 2005; Tinel *et al*, 2007). PIDD-N has not been found in specific macromolecular

complexes, but it has been hypothesized that this fragment could play a regulatory role, inhibiting NEMO-PIDDosome formation (Janssens *et al*, 2005; Tinel *et al*, 2011).

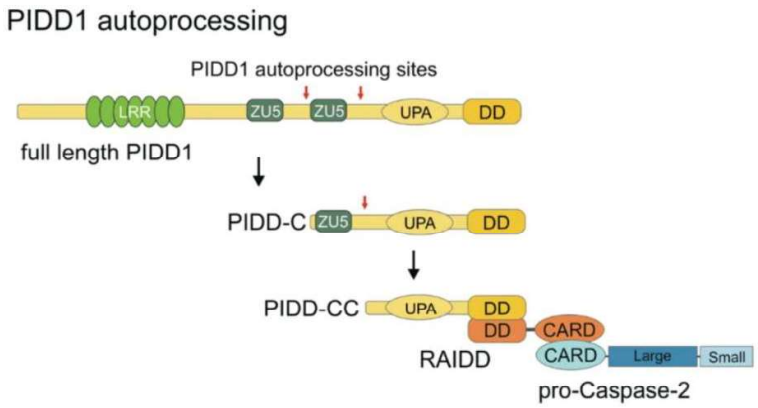

Figure 6. PIDD1 precursor undergoes autoprocessing. Autoproteolysis of full-length PIDD1 results into three different fragments: PIDD1-N (not shown), PIDD1-C and PIDD1-CC. The latter can interact with RAIDD through a homotypic DD:DD binding. The presence of a CARD domain in RAIDD allows its interaction with pro-Caspase-2. Red arrows show the two autocleavage sites. Image from (Sladky & Villunger, 2020).

RAIDD is a bipartite adaptor protein which is able to simultaneously bind PIDD1 through a homotypic DD:DD interaction and Caspase-2 through its CARD (caspase recruitment domain) domain. Thus, RAIDD works as a scaffold protein, recruiting PIDD1 and Caspase-2 inside the PIDDosome complex.

Caspase-2 is a cysteine-driven aspartate-directed endopeptidase (Lamkanfi *et al*, 2002). Despite being an evolutionarily conserved protein, its functions are still debated and its involvement in apoptotic pathways is controversial. Peculiarly, Caspase-2 is classified as an initiator caspase, even if it shares common features with effector caspases, presenting a substrate specificity which is nearly identical to that of Caspase-3 and Caspase-7. Caspase-2 is present in cells as an inactive zymogen and dimerization is the key event that leads to its initial activation. Once a dimer, it undergoes a trans-autocatalytic cleavage event, generating two subunits, large (p19) and small (p12), after which the enzyme acquires optimal catalytic activity (Baliga *et al*, 2004). Analogously to the death-inducing signalling complex (or DISC) for Caspase-8 and the apoptosome for Caspase-9, the PIDDosome is the activation platform for Caspase-2. In fact, a core complex of five (or seven) PIDD1 DDs and seven RAIDD DDs mediates the recruitment

of seven pro-Caspase-2 moieties, enabling their proximity-induced dimerization (Fig. 7) (Park *et al*, 2007).

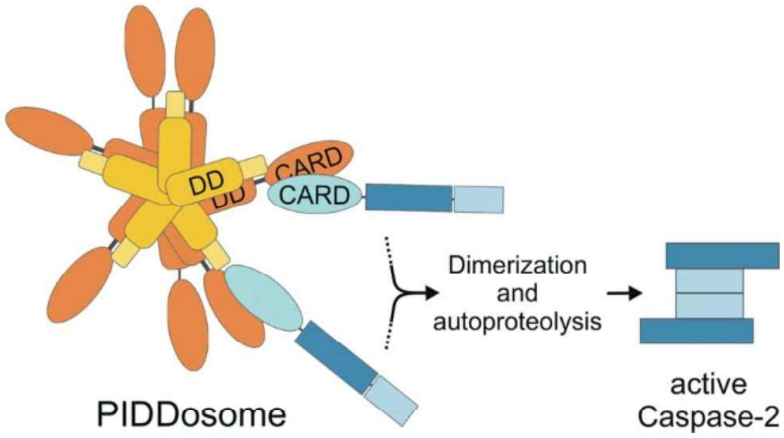

Figure 7. PIDDosome assembly leads to Caspase-2 activation. In the presence of PIDDosome-activating stimuli, PIDD1-CC establishes homotypic interactions with the adaptor protein RAIDD through their DDs. RAIDD in turn promotes pro-Caspase-2 recruitment through the CARD domain, leading to dimerization and autoproteolysis of the pro-caspase, eventually leading to its full activation. Image from (Sladky & Villunger, 2020).

Several substrates of this enzyme have been identified over the years, in the attempt to unravel Caspase-2 functions. Even if more than 200 substrates have been catalogued (Rawlings *et al*, 2018; Brown-Suedel & Bouchier-Hayes, 2020), a physiological validation of these hits is almost completely absent. Moreover, the largest high-throughput studies of Caspase-2 substrates performed through N-terminal degradomics (Wejda *et al*, 2012; Julien *et al*, 2016) failed to retrieve its best-known substrates (MDM2, BID and Golgin-160)(Oliver *et al*, 2011; Guo *et al*, 2002; Mancini *et al*, 2000), highlighting the limitation of this kind of *in vitro* approaches to study Caspase-2 specificity and corroborating the notion that Capase-2 involvement in cellular processes is still poorly understood.

The PIDDosome and centrosome counting

The early functional characterization of the PIDDosome provided evidence for a role of this complex in the regulation of apoptosis induced by genotoxic agents (Tinel & Tschopp, 2004). However, PIDDosome involvement in cell death modulation became puzzling as it was repeatedly demonstrated that mouse models lacking individual components of the complex failed to show precise phenotypes ascribable to defects in DNA damage response (O'Reilly *et al*, 2002; Berube *et al*, 2005; Manzl *et al*, 2009, 2012, 2013). Thus, it was clear that a precise stimulus responsible for PIDDosome activation was still missing.

In 2017, Fava and colleagues reasoned that all the stimuli which had been previously reported to feed into PIDDosome activation (e.g., anti-mitotic agents, genotoxic agents, inhibition of Aurora B kinase) (Dodson *et al*, 2004) (Ditchfield *et al*, 2003) had also a possible common effect: the potential to induce cytokinesis failure and hence centrosome amplification. Starting from this, they demonstrated that PIDDosome activation is the missing link between centrosome amplification and p53 stabilization, individuating supernumerary centrosomes as the most selective trigger for the activation of the complex (Fava *et al*, 2017).

From a mechanistic point of view, a mitosis which ends with cytokinesis failure results into a single tetraploid daughter cell carrying extra centrosomes. The presence of supernumerary centrosomes induces PIDDosome assembly, whose main downstream consequence is the activation of Caspase-2. Activated Caspase-2 is the enzyme responsible for the cleavage of the E3 ubiquitin ligase MDM2 at the level of the second aspartate residue in the conserved caspase cleavage motif Asp-Val-Pro-Asp (Pochampally *et al*, 1998; Oliver *et al*, 2011). MDM2 is the most studied regulator of p53, influencing both levels and stability of the tumour suppressor (Horn & Vousden, 2007). This proteolytic event results in the physical separation of the two main MDM2 domains: the N-terminal p53-binding domain and the C-terminal ubiquitin-conjugating RING finger domain (responsible for proteasome targeting).

Upon MDM2 cleavage, p53 can no longer undergo MDM2-mediated polyubiquitination and successive proteasomal degradation. In addition, p53 still retains the ability to bind the MDM2 N-terminal fragment (called "p60"), with a higher affinity in comparison to the uncleaved form. Binding of MDM2 p60 to p53 leads to p53 stabilization, accumulation, and transcriptional activation (Fig. 8). It has been proposed

that MDM2 p60 binding to p53 could affect its selectivity for target gene expression. In fact, in the context of PIDDosome activation, p53 activation mediates a p21-dependent cell cycle arrest programme paralleled by no significant up-regulation of pro-apoptotic genes (e.g. *BBC3*, which encodes for PUMA, and *BAX*) and no appreciable cell death induction (Oliver *et al*, 2011; Fava *et al*, 2017).

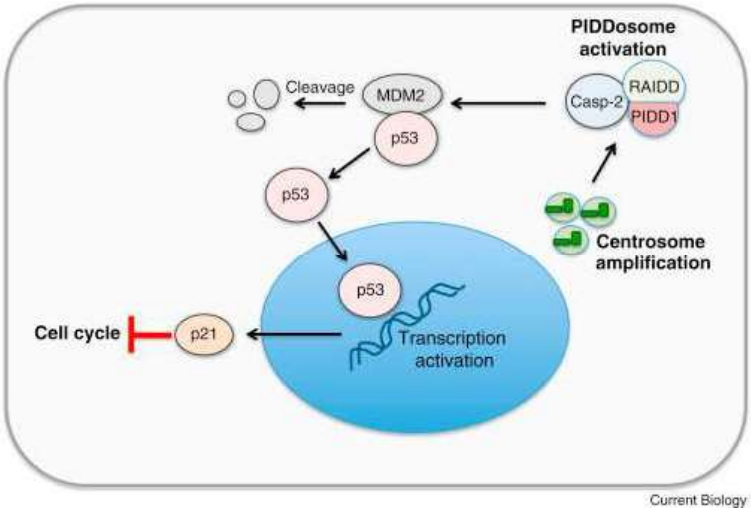

Figure 8. Supernumerary centrosomes induce a PIDDosome-dependent cell cycle arrest. The presence of extra centrosomes is the triggering event which induces PIDDosome assembly and Caspase-2 activation. Activated Caspase-2 cleaves MDM2, abolishing p53 degradation and thus promoting its stabilisation. Consequently, p53 enters the nucleus and activates the transcription of target genes, among which *CDKN1A* (which encodes p21), leading to cell cycle arrest. Image from (Godinho, 2017).

Therefore, PIDDosome activation seems to be the cellular pathway which senses the increase in centrosome number, preventing cells from entering additional error-prone mitoses. Interestingly, the core PIDDosome component PIDD1 has been shown to localize at the centrosome, and more specifically at the parent centriole only. Moreover, activation of the complex seems to respond specifically to supernumerary mature centrioles: in fact, when PLK4 is overexpressed, PIDDosome activation occurs only at a point in time when extra procentrioles have fully matured into extra parent centrioles (Fava *et al*, 2017). Even if these observations would suggest a direct role for PIDD1 in centrosome amplification sensing, the mechanistic aspects of PIDDosome activation and of a putative centrosome counting mechanism still remain obscure.

AIMS OF THE THESIS

The PIDDosome is a macromolecular complex containing PIDD1, RAIDD and Caspase-2. It has been previously demonstrated that cytokinesis failure is a potent PIDDosome activating event, resulting into a p53-dependent cell cycle arrest. Experimental evidence demonstrated that upon cytokinesis failure an increase in centrosome number rather than an increase in ploidy is responsible for PIDDosome activation (Fava *et al*, 2017). According to this, it has been speculated that cells have a mechanism in place to recognize the presence of supernumerary centrosomes, leading to PIDDosome assembly and eventually halting the cell cycle. Nevertheless, the mechanistic aspects which allow cells to sense centrosome amplification remained elusive.

Identification of the factor(s) recruiting PIDD1 at the centrosome

The PIDDosome core component PIDD1 has been reported to physically associate with centrosomes and specifically fully mature (parent) centrioles (Fava *et al*, 2017). Since the distinguishing feature between parent and daughter centrioles resides in the presence of specific proteinaceous structures (centriole appendages) which decorate the former, the first aim of this project was the molecular dissection of PIDD1 recruitment to the centrosome with a special focus on appendages. Answering this question enables a selective de-localization of PIDD1 from these structures to rigorously test its relevance for PIDDosome signalling.

Identification of the cues which induce PIDDosome activation

PIDD1 has been reported to constitutively localize at the centrosome, even in the absence of PIDDosome activating stimuli. In search for specific factors promoting PIDDosome assembly in activating conditions, putative key aspects of PIDD1 protein (e.g., its autoproteolysis, its turnover at the centrosome and its localization throughout cell cycle) have been investigated in this regard, dissecting their contribution to PIDDosome activation.

Investigation of PIDD1 centrosome localization role in DNA-damage induced PIDDosome activation

PIDDosome activation occurs not only in response to centrosome amplification but also in the context of the DNA damage response. Moreover, it has been recently highlighted how Caspase-2 mediated MDM2 proteolysis in irradiated cells contributes to halt continual cell cycling in the presence of DNA damage, proposing a role for PIDDosome activation in shaping p53 behaviour and thus cell fate (Tsabar et al, 2020). The last part of this project was aimed at investigating if PIDD1 centrosome localization plays a role in PIDDosome activation also during the DNA damage response, unveiling if different upstream triggers prime PIDDosome signalling by alternative means.

All the results presented in this thesis have been published in the paper: Burigotto M., Mattivi A., Migliorati D., et al. "Centriolar distal appendages activate the centrosome-PIDDosome-p53 signalling axis via ANKRD26". *EMBO J* 2021.

MATERIALS AND METHODS

Cell culture

A549 (ATCC® CCL-185) and HEK293T (gift by Dr. Ulrich Maurer, University of Freiburg) cell lines were cultured in DMEM (Corning, 15-017-CVR). hTERT-RPE1 cells (gift by Stephan Geley, Medical University of Innsbruck) were maintained in DMEM/F12 1:1 (Gibco, 21331-020). All media were supplemented with 10% fetal bovine serum (Gibco, 10270-106), 2 mM L-glutamine (Corning, 25-005-CI), 100 IU/mL penicillin, and 100 µg/mL streptomycin solution (Corning, 30-002-CI). Cells were incubated at 37°C with 5% CO_2 and regularly tested for mycoplasma contamination.

Drug treatments, ciliogenesis induction and synchronization procedures

The following compounds were used: ZM447439 2 µM (Selleck Chemicals, S1103), dihydrocytochalasin-B 4 µM (DHCB, Sigma-Aldrich, D1641), Camptothecin (CPT, APExBIO, A2877), Nutlin-3a (MedChemExpress, HY-10029). To all untreated controls solvent only was administered. To induce ciliogenesis, RPE1 cells were seeded on glass coverslips in 6-well plates. After 24h, cells were washed with PBS and exposed to serum-free medium for another 48h before fixation. Synchronization of RPE1 cells in Fig. 7 was performed by arresting cells with 2 mM thymidine (SigmaAldrich, T1895) for 24h, followed by release in fresh medium containing nocodazole 200 nM (BioTrend, BN0389) for 14h. Mitotic cells were then harvested by selective shake-off, washed four times and released into fresh medium. To dissociate centrosome clusters in telophase, nocodazole 1 µM was added 1.5h after the release.

Molecular cloning

Vectors for the generation of CRISPR/Cas9-mediated loss-of-function cell lines were produced using the Lenti-CRISPR-V2 backbone (gift from Feng Zhang; Addgene plasmid #52961). Oligonucleotides yielding small guide RNAs (sgRNAs) targeting the

genes of interest were designed using CRISPR Design (http://crispr.mit.edu). Lenti-CRISPR-V2 plasmid was digested with Esp3I (Thermo Scientific #ER0452) and gel purified. Equimolar quantities of complementary oligonucleotides were annealed in 10 mM Tris-HCl pH 7.5, 50 mM NaCl, 1 mM EDTA by heating to 95°C and then slowly ramping down to 25°C. Annealed oligonucleotides were diluted 1:100 in ddH2O and used to set up a ligation reaction with the previously digested backbone, using T4 DNA Ligase (Thermo Scientific #EL0012). All plasmids were verified by Sanger sequencing. A complete list of the sgRNAs used in this work is reported in Supplementary Table 1. Human cDNAs of ANKRD26 (transcript NM_014915) and SCLT1 (transcript NM_144643) were custom synthesized by Eurofins Genomics in the pEX-A258 and pUC57 backbone, respectively. The ANKRD26 synthetic cDNA contained a silent mutation to prevent recognition by sgRNA ANKRD26#2 and ANKRD26#4. pMSCV-Pidd1 T788A (Addgene plasmid #60529) was a gift from Trudy Oliver and Ala788 was back mutated to Thr (obtaining a sequence corresponding to the transcript NM_145886). The desired cDNAs were cloned into pcDNA5/FRT/TO (Invitrogen V652020) in order to generate the following constructs: pcDNA5/FRT/TO-myc-SCLT1, pcDNA5/FRT/TO-myc-ANKRD26 and pcDNA5/FRT/TO-PIDD1-V5. The cDNA of each construct was then subcloned into the lentiviral plasmid FUW-tetO-MCS+ (a modified version of Addgene plasmid #84008, gift by Dr. Alessio Zippo). The PIDD1 construct used for FRAP experiments was built cloning PIDD1L828E cDNA in a FUW-tetO-MCS+ plasmid already containing a mNeonGreen sequence. PIDD1 autoproteolytic fragments, PIDD1 truncating mutations and ANKRD26 mutants were generated by PCR using the primers reported in Supplementary Table 3. PCR products were cloned into FUW-tetO-MCS+ plasmid and all constructs were sequence-verified. Site-directed mutagenesis was performed as previously reported (Edelheit *et al*, 2009) with the primers listed in Supplementary Table 4. The insertion of the desired mutations was checked by Sanger sequencing.

Generation of lentiviral particles, titration and transduction

HEK293T cells were seeded in antibiotic-free medium and co-transfected with pCMV-VSV-G (a gift from Bob Weinberg, Addgene plasmid #8454), psPAX2 (a gift from Didier Trono, Addgene plasmid #12260) and the required transfer plasmid using

calcium phosphate. Supernatants were harvested 48h after transfection, filtered using 0.22 μm Primo® Syringe Filters (EuroClone, EPSPE2230) and stored at -20°C. The viral titre was estimated as described (Pizzato *et al*, 2009). Virions were diluted with fresh medium at a concentration of 0.2 reverse transcriptase units per mL (U/mL, for A549 cells) or 0.1 U/mL (for RPE1 cells), supplemented with 4 μg/mL hexadimethrine bromide (Sigma-Aldrich, H9268) and administered to cells for 24h. For lentiviral-mediated rescue experiments, the cDNA of the gene of interest was modified to introduce a silent mutation affecting the PAM sequence recognized by the sgRNA encoded by Lenti-CRISPR-V2 (a gift from Feng Zhang, Addgene plasmid #52961) used to generate the destination cell line, see Appendix and Table EV2. Generation of cell lines lacking DAPs expression by CRISPR/Cas9 Cells transduced with Lenti-CRISPR-V2 targeting coding exons of the genes of interest were selected with puromycin (InvivoGen, #ant-pr-1), 1 μg/mL on A549 and 10 μg/mL on RPE1 cells for 72h, and seeded at a density of 0.2 cells per well in 96-well plates and incubated for about three weeks. Single clones were further expanded and characterized.

CRISPR clone characterization

DNA was extracted from loss-of-function clones using the NucleoSpin Tissue kit (Macherey-Nagel, 740952) following the manufacturer's protocol. For each guide, PCR reactions employing Phusion DNA polymerase (Thermo Scientific, F530-L) were performed, using a primer pair (see Supplementary Table 2) designed to obtain amplicons spanning the cut site. PCR products were run on an agarose gel and purified using NucleoSpin Gel and PCR Clean-up kit (Macherey-Nagel, 740609), according to manufacturer's instructions. Each amplicon was then Sanger sequenced and the presence of frameshifting INDELs on all alleles was verified using Inference of CRISPR Edits (ICE) analysis thanks to Synthego Bioinformatics tool (https://ice.synthego.com) (Hsiau *et al*, 2019). For a comprehensive list of all clones used in this thesis and their characterization see Supplementary Fig. 1.

Immunofluorescence microscopy

Cells grown on glass coverslips (Marienfeld-Superior, 0117580) were washed in PBS and fixed following four different protocols depending on the antigens to be stained. Cells were: i) directly fixed and permeabilized with absolute ice-cold methanol for at least 20 min at −20°C in Fig. 9F (first and second row), 12B, 10A, 10C (second and third row), 10D and in Supplementary Fig. 2A, 2C and 6A; ii) pre-extracted for 2 min with PTEM buffer (0.2% Triton™ X-100, 20 mM PIPES at pH 6.8, 1 mM $MgCl_2$, 10 mM EGTA in ddH_2O) and then fixed with methanol as described above in Fig. 11B, 14C, 14F, 15D, 10C (first row), 13A (first row), 18B and Supplementary Fig. 4A; ; iii) pre-extracted for 2 min with PTEM buffer and then fixed with 4% v/v formaldehyde (Sigma-Aldrich, F8775) in PTEM for 10 min at room temperature in Fig. 9A, 9C, 9E, 9F (third row), 11E, 19F, 10C (fourth row), 13A (second row) and Supplementary Fig. 1C; iv) directly fixed and permeabilized with 4% v/v formaldehyde in PTEM for 12 min at room temperature in Fig. 17A and 17C. After fixation, cells were washed with PBS, blocked with 3% w/v BSA in PBS for 20 min and then stained for 1h at room temperature with the appropriate combination of primary antibodies diluted in blocking solution. The following antibodies were used:

Primary antibody	Host	Dilution	Company	Reference
γ-tubulin	mouse	1:1000	Thermo Fisher Scientific	MA1-19421
γ-tubulin AF488	mouse	1:100	SCBT	sc-17787
ANKRD26	rabbit	1:800	GeneTex	GTX128255
Arl13B	mouse	1:500	SCBT	sc-515784
centrin-1	rabbit	1:500	Protein Tech	12794-1-AP
CEP128	rabbit	1:500	Sigma Life Science	HPA001116
CEP164	mouse	1:500	SCBT	sc-515403
FBF1	rabbit	1:500	Sigma Life Science	HPA023677
myc-tag	mouse	1:500	Thermo Fisher Scientific	MA1-980
myc-tag	rabbit	1:500	CST	#2278
ODF2	rabbit	1:500	Sigma Life Science	HPA001874
PIDD1	mouse	1:500	Enzo Life Sciences	ALX-804-837
V5-tag	rabbit	1:500	CST	#13202

Cells were washed with PBS and incubated with the appropriate species-specific fluorescent secondary antibody together (excluding for Fig. 9A and 9E) with 1 µg/mL Hoechst 33342 (Invitrogen, H3570) for 45 min. The following antibodies were used:

Secondary antibody	Dilution	Company	Reference
Alexa Fluor 488 goat anti-mouse	1:1000	Invitrogen	A11029
Alexa Fluor 488 goat anti-rabbit	1:1000	Invitrogen	A11034
Alexa Fluor 555 goat anti-mouse	1:1000	Invitrogen	A21424
Alexa Fluor 555 goat anti-rabbit	1:1000	Invitrogen	A21429
Alexa Fluor 647 goat anti-mouse	1:1000	Invitrogen	A21236

After incubation, cells were washed with PBS and distilled water, and mounted in ProLong™ Diamond Antifade Reagent (Invitrogen, P36965) (Fig. 9A and 9E) or ProLong™ Gold Antifade Reagent (Invitrogen, P36934) (all other figures). All images were acquired on a spinning disk Eclipse Ti2 inverted microscope (Nikon Instruments Inc), equipped with Lumencor Spectra X Illuminator as LED light source, an X-Light V2 Confocal Imager and an Andor Zyla 4.2 PLUS sCMOS monochromatic camera using a plan apochromatic 100x/1.45 oil immersion objective. Images were deconvolved with Huygens Professional software (Scientific Volume Imaging, Hilversum, The Netherlands).

For 2D stimulated emission depletion (STED) microscopy (Fig. 9A and 9E), images were acquired on an SP8 gSTED microscope (Leica Microsystems, Wetzlar, Germany) equipped with an 80 MHz pulsed white light laser (WLL), a CW 592 nm STED depletion laser and a pulsed 775 nm STED depletion laser. For Fig. 9A the 592 nm STED depletion laser was used, whereas in Fig. 9D STED depletion was performed at 775 nm. 4-5 z-planes were acquired for each image to allow post-processing by deconvolution to boost lateral resolution. All STED images stacks were z-aligned and deconvolved with Huygens Professional software using the GMLE algorithm. All images were exported with Fiji to obtain maximum intensity projections of z-stacks and to adjust contrast and brightness, and further processed with Adobe Photoshop. For STED imaging, primary antibodies were used at 1:200 dilution and the following secondary antibodies were used:

Secondary antibody	Dilution	Company	Reference
Alexa Fluor 594 goat anti-mouse	1:120	Invitrogen	A11037
STAR RED goat anti-mouse	1:120	Abberior	2-0002-011-2
STAR 440SXP goat anti-rabbit	1:200	Abberior	2-0012-003-4
STAR 488 goat anti-mouse	1:200	Abberior	2-0002-006-8

Quantification of immunofluorescence images

Fluorescence intensities in circular regions of interest (ROIs) with a diameter of 20 pixels including the parent centriole(s) were calculated with Fiji from at least five independent images obtained by maximum intensity projections of z-stacks. For each specific ROI, the value of a background ROI (placed in proximity to the centrosome) was subtracted and fluorescence intensity was expressed either as absolute value or as the ratio between the fluorescence intensity of the protein of interest and the intensity of a centriolar reference marker. Co-localization analysis of STED micrographs was performed on deconvolved images and no further pre-processing was applied. Co-localization between PIDD1 and ODF2, PIDD1 and FBF1, and PIDD1 and ANKRD26 was evaluated using the automated 3D object-based co-localization analysis tool implemented in the DiAna v.1.47 plugin for ImageJ (Gilles *et al*, 2017). Threshold and size parameters used for the object segmentation step were optimized for each protein and kept constant for all the images. Data are shown as the ratio between the number of touching objects on the total number of objects. For ciliogenesis assays, the fraction of ciliated cells was determined by visual counting from immunofluorescence micrographs. Ciliary length was estimated by manually following the ciliary shape with a segmented line from the basal body (CEP128 signal) to the ciliary tip (opposite end of the ARL13B signal) on 2D maximum intensity projections using Fiji.

Cell lysis and immunoblotting

Cells were harvested by trypsinization and lysed in 50 mM Tris pH 7.4, 150 mM NaCl, 0.5% NP-40, 50 mM NaF, 1 mM Na3VO4, 1 mM PMSF, one tablet/10 mL Pierce™ Protease Inhibitors Mini Tablets, EDTA-free (Thermo Fisher Scientific, #A32955), 2 mM $MgCl_2$ and 0.2 mg/mL DNase I (Thermo Fisher Scientific, #89836). Protein concentration was determined by bicinchoninic acid assay (Pierce™ BCA Protein Assay Kit, Thermo Fisher Scientific, 23225) using a plate reader. For immunoblotting analysis, equal amounts of protein samples were resolved on polyacrylamide gels using self-made gels or pre-cast gels (Biorad 5678095). Proteins were electroblotted on nitrocellulose membranes (GE Healthcare RPN3032D) using wet transfer. 5% w/v non-fat milk in PBS-Tween 0.1% v/v was used as blocking solution and antibody diluent.

Membranes were incubated overnight at 4°C with primary antibodies, washed with PBS-Tween 0.1% and then incubated with HRP-conjugated secondary antibodies for 45 min at room temperature. Chemiluminescence signals were obtained incubating the membranes with Amersham™ ECL Select™ Western Blotting Detection Reagent (GE Healthcare, RPN2235) and visualized with an Alliance LD2 Imaging System (UVITEC Cambridge). The following antibodies were used:

Primary antibody	Host	Dilution	Company	Reference
ANKRD26	rabbit	1:500	GeneTex	GTX128255
CASP2	rat	1:1000	Enzo Life Sciences	ALX-804-356
CDC27	mouse	1:1000	BD Biosciences	610455
CEP83	rabbit	1:500	Sigma Life Science	HPA038161
HSP90	mouse	1:5000	SCBT	sc13119
MDM2	mouse	1:1000	Invitrogen	MA1-113
myc-tag	mouse	1:1000	Thermo Fisher Scientific	MA1-980
p53	rabbit	1:1000	Cell Signaling Technology	#9282
V5-tag	mouse	1:1000	Invitrogen	R96025

Secondary antibody	Dilution	Company	Reference
Goat anti-mouse IgG/HRP	1:5000	Dako	P0161
Goat anti-rabbit IgG/HRP	1:5000	Dako	P0448
Goat anti-rat IgG/HRP	1:5000	Thermo Fisher Scientific	31470

Time lapse video microscopy

RPE1 cells transduced with a pHR-SFFV-CETN1-EGFP lentivirus were seeded into Ibidi µ-Slide 8 Well dishes (Ibidi, 80826) and either treated with DMSO or DHCB. 6h before imaging, cells were washed with PBS and DMEM/F12 medium was replaced with supplemented Leibovitz-15 culture medium without phenol red (Thermo Fisher Scientific, 21083027), in the presence of 1 µM SiR-DNA (Spirochrome, SC007) to visualize the DNA. Movies were recorded every 4 min for the first hour and then every 10 min for up to 16h. Each field contained around 25 z-slices collected in 0.6 µm steps. Four-dimensional tracking of centrosomes Single particle tracking of centrosomes was performed on 3D (x,y,z) live-cell time-lapse movies using the semi-automatic plug-in of Fiji called TrackMate (Tinevez *et al*, 2017). Movie pre-processing before tracking

analysis only involved uniform denoising and background subtraction steps. TrackMate plug-in settings were optimized for successful detection and linking of the spot-like structures corresponding to the CETN1-GFP signal and have been kept constant for all the analysed movies. Gap-closing events were allowed for a maximum of 3 consecutive frames. From the x, y and z coordinates of each centrosome, provided by the plug-in over time, the reciprocal distance between the two centrosomes was calculated (one of the two centrioles of each pair was randomly selected for this calculation).

Measurement of centrosomal PIDD1 protein turnover by FRAP

12,000 PIDD1-deficient RPE1 cells transduced with a lentiviral vector expressing PIDD1- L828E-mNeonGreen were seeded for each well of a 24-well glass bottom dish (Ibidi). Cells were treated with either DMSO or DHCB for 16 hours before imaging on an Axio Observer Z1 microscope (Zeiss) equipped with a 3i Marianas spinning disk confocal system, a CSU-X1 confocal scanner unit (Yokogawa Electric Corporation), Plan-Apochromat 63x/1.4NA Oil Objectives (Zeiss), Orca Flash 4.0 sCMOS Camera (Hamamatsu) and a VectorTM High Speed FRAP module. Imaging was performed in CO_2 independent medium (Gibco, 18045054) supplemented with 10% fetal bovine serum (Clontech), 2 mM L-glutamine (PAN Biotech), 100 IU/mL penicillin, and 100 µg/mL streptomycin (GIBCO). Three independent experiments, for a total of 12 cells, were analysed for both conditions. FRAP analysis was carried out in the presence of either DMSO or DHCB as previously described (Overlack *et al*, 2017). Briefly, a region of interest (ROI) of 1.72 x 1.72 µm containing the centrosomes was bleached for 20 ms with a 488 nm laser line at 100% power. Images were binned 2x2 to increase signal-over-camera noise. At each time point, a z-stack consisting of 3 sections at 0.8 µm intervals was acquired. The mNeonGreen signal was imaged for 4 time-frames before photobleaching. After bleaching, a z-series was acquired every 1 s for a total duration of 2 min with an exposure time of 100 ms. Images were converted into maximal intensity projections and exported as 16-bit TIFF files for measurements of fluorescence intensity recovery rates using ImageJ. Apart from the bleached centrosome, a control non-bleached ROI from the same cell and a non-bleached ROI from outside of the cell (baseline) were also measured. The relative fluorescence intensity was calculated as RFI = (FROI(t)/FBG(t)) / (FROI(t0)/FBG(t0)), as described previously (Chen & Huang, 2001),

to correct for background intensity and for photobleaching that occurred during image acquisition. FROI(t) is the intensity of the bleached ROI containing the centrosome at different time points after bleaching, FBG(t) is the intensity of the control non-bleached ROI at the corresponding time points. FROI(t0) is the average intensity of the bleached ROI containing the centrosome for the 4 time-frames before photobleaching, FBG(t0) is the average intensity of the control non-bleached ROI before bleaching. A baseline value, calculated from the region outside the cell, was subtracted from all values. RFIs were then fitted to a double exponential curve using GraphPad Prism 6.0. Choice of the preferred fitting model was made with an extra sum-of-squares F test (selects the simpler model unless P is <0.05) in which both curves showed a P<0.0001.

Quantification of PIDD1 protein species using targeted PRM-LC-MS analysis

A549 cell samples were resuspended in lysis buffer (0.1 M ammonium bicarbonate, 8 M urea, 5 mM TCEP, and 10 mM chloroacetamide), and lysed with a Bioruptor sonicator (10 cycles, Bioruptor, Diagnode). Lysates were reduced and alkylated for 1h at 37°C followed by digestion overnight at 37°C with trypsin (1/50 w/w; Promega, Madison, Wisconsin). Peptides were purified using C18 reversed phase spin columns according to the manufacturer's instructions (Macrospin, Harvard Apparatus). Samples were dried under vacuum and stored at -80°C until further use. For targeted MS analysis, proteotypic peptides were selected from public repositories ProteomicsDB (www.proteomicsdb.org) and MaxQB (maxqb.biochem.mpg.de) to represent all PIDD1 fragments with unique and specific sequences. Peptides lacking missed cleavages, methionine and glutamine at the N-termini as well as peptides frequently observed were preferred. The final peptide list is illustrated in Fig. 16A. For these, synthetic heavy reference peptides were ordered (JPT Peptide Technologies) and pooled. In a first step, parallel reaction-monitoring (PRM) assays (Peterson et al, 2012) were generated from a mixture containing 100 fmol of each heavy reference peptide and shotgun data-dependent acquisition (DDA) LC-MS/MS analysis on a Thermo Orbitrap Fusion Lumos platform (Thermo Fisher Scientific). The setup of the µRPLC-MS system was as described previously (Ahrné *et al*, 2016). Chromatographic separation of peptides was carried out using an EASY nanoLC 1200 system (Thermo Fisher Scientific), equipped with a heated

RP-HPLC column (75 µm x 30 cm) packed in-house with 1.9 µm C18 resin (Reprosil-AQ Pur, Dr. Maisch). Peptides were analysed per LC-MS/MS run using a linear gradient ranging from 95% solvent A (0.1% formic acid) and 5% solvent B (99.9% acetonitrile, 0.1% formic acid) to 45% solvent B over 60 minutes at a flow rate of 200 nl/min. Mass spectrometry analysis was performed on Thermo Orbitrap Fusion Lumos mass spectrometer equipped with a nanoelectrospray ion source (both Thermo Fisher Scientific). Each MS1 scan was followed by high-collision-dissociation (HCD) of the 10 most abundant precursor ions with dynamic exclusion for 20 seconds. Total cycle time was approximately 1 s. For MS1, 1e6 ions were accumulated in the Orbitrap cell over a maximum time of 100 ms and scanned at a resolution of 120,000 FWHM (at 200 m/z). MS2 scans were acquired at a target setting of 1e5 ions, accumulation time of 50 ms and a resolution of 30,000 FWHM (at 200 m/z). Singly charged ions and ions with unassigned charge state were excluded from triggering MS2 events. The normalized collision energy was set to 30%, the mass isolation window was set to 1.4 m/z and one microscan was acquired for each spectrum. The acquired raw-files were database searched against a human database (Uniprot, download date: 2019/03/27, total of 34350 entries) by the MaxQuant software (Version 1.6.2.3). The search criteria were set as following: full tryptic specificity was required (cleavage after lysine or arginine residues); 3 missed cleavages were allowed; carbamidomethylation (C) was set as fixed modification; Arg10 (R), Lys8 (K) and oxidation (M) as variable modification. The mass tolerance was set to 10 ppm for precursor ions and 0.02 Da for fragment ions. The results were imported to Skyline (version 4.1) by generating a spectral library and manually selecting the peptides of interest and the best 6 transition thereof. Then, a scheduled (10 min windows) mass isolation lists containing all selected peptide ion masses were exported form Skyline and imported into the Lumos operating software PRM analysis using the following settings: the resolution of the orbitrap was set to 60k FWHM (at 200 m/z) and the fill time was set to 150 ms to reach a target value of 1e6 ions. Ion isolation window was set to 0.4 Th and the scan range was set to 150-1500 Th. A MS1 scan using the same setting as used for DDA above was included in each MS cycle. Each condition was analysed in biological triplicates. All raw-files were imported into Skyline for protein / peptide quantification. To control for variation in sample amounts, the total ion chromatogram (only comprising peptide ions with two or more charges) of each sample was determined by Progenesis QI (version 2.0, Waters). Here, the best peptide ions peak areas were normalized on total

MS1 signal (only considering doubly or higher charged peaks), and relative quantifications were calculated on the mean value of parental non-treated values.

RNA isolation and RT-qPCR

Total RNA was isolated using NucleoSpin RNA Plus kit (Macherey-Nagel 740984) and reverse transcribed using RevertAid First Strand cDNA Synthesis kit (Thermo Fisher Scientific K1622) and random hexamer primers, following manufacturer's protocol. PIDD1 gene expression was monitored via quantitative PCR using qPCRBIO Probe Mix (PCR Biosystems PB20.24) and the following probe sets were used: PIDD1 probe 1 (PCR amplicon spanning exon 5 and 6)(Hs.PT.58.1440761.g, IDT), PIDD1 probe 2 (PCR amplicon spanning exon 10 and 11)(Hs.PT.58.3199598.gs, IDT), β-actin (Hs.PT.39a.22214847, IDT) and RPLP0 (Hs.PT.39a.22214824, IDT). All probes were conjugated with a 6-FAM/ZEN/IBFQ dye/quencher mode. qPCR assays were performed on a CFX Touch Real-Time PCR Detection System (Biorad) and Ct values were extracted using a Bio-Rad CFX Manager software. Expression values were normalized to the geometric mean of β- actin and RPLP0 (Vandesompele *et al*, 2002) and the relative quantification is presented as linearized C_t values ($2^{-\Delta\Delta Ct}$), normalized to the wild type untreated reference values.

DNA content analysis by flow cytometry

Cells were harvested, washed with PBS, fixed with ice-cold 70% v/v ethanol in PBS for at least 20 min at -20°C and stored at −20°C until analysis. Fixed cells were centrifuged at 1000 g for 3 min, washed twice with PBS, and stained with 10 µg/mL propidium iodide (Invitrogen, P3566) for 30 min at 37°C in the presence of 100 µg/mL PureLink™ RNase A (Invitrogen, 12091-021). Cells were then analysed in a flow cytometer (FACSCanto, BD Bioscience). Data analysis and figure generation were performed using FlowJo software (FlowJo, LLC).

EdU incorporation assessment by flow cytometry

DNA replication was assessed via EdU incorporation by pulse labeling asynchronously growing cells. Cells were pulsed for 1h with 10 μM EdU, harvested and prepared for flow cytometry using the Click-iT™ EdU Alexa Fluor® Flow Cytometry Assay kit (Thermo Scientific, C10634), according to the instructions of the manufacturer. Briefly, cells were fixed and permeabilized with the provided solutions. Click-It reaction was performed using an Alexa-647 fluorophore. Eventually, samples were stained with propidium iodide as described above and analysed in a flow cytometer (FACSCanto, BD Bioscience). The percentage of induced tetraploid cells was calculated from values gated as in Appendix Fig. S3 as follows:

$$\%\ of\ cells \geq 4C\ (DHCB) - \%\ of\ cells\ \geq 4C\ (DMSO)$$

The percentage of proliferating tetraploid cells was calculated as follows:

$$\frac{\%\ of\ cells > 4C\ (release) - \%\ of\ cells\ > 4C\ (DMSO)}{induced\ tetraploid\ cells}$$

Yeast-two-hybrid analyses

The yeast-two-hybrid screens were performed by Hybrigenics Services, S.A.S., Evry, France. The coding sequence of PIDD1 1-758 S446A/S588A was PCR-amplified and cloned into pB66 as a C-terminal fusion to the Gal4 DNA-binding domain. The construct was used as bait to screen a random-primed Human Lung Cancer Cells cDNA library constructed into pP6. 51 million clones (5-fold the complexity of the library) were screened using a mating approach with YHGX13 (Y187 ade2- 101::loxP-kanMX-loxP, matα) and CG1945 (mata) yeast strains as previously described (Fromont-Racine *et al*, 1997). 180 His+ colonies were selected on a medium lacking tryptophan, leucine and histidine. Prey fragments of positive clones were amplified by PCR and sequenced at their 5' and 3' junctions. The resulting sequences were used to identify the corresponding interacting proteins in the GenBank database (NCBI) using a fully automated procedure. For the interaction domain mapping screen, the fragment containing amino acids 538-1204 of ANKRD26 (identified as prey in the previous Y2H screen) was enzymatically

fragmented. Fragments were dA-tailed, enriched by PCR and eventually cloned into the yeast prey vector pP9 using homologous recombination in yeast. The ANKRD26 fragment library had a size of 39,000 independent fragments. Amino acids 1-758 of PIDD1 (S446A, S588A) were cloned into pB27 as a C-terminal fusion to LexA (LexA-PIDD1). 1.3 million clones of the ANKRD26 fragment library were screened using a mating approach with YHGX13 (Y187 ade2-101::loxP-kanMX-loxP, matα) and L40DGal4 (mata) yeast strains as previously described (Fromont-Racine *et al*, 1997). His+ colonies were selected on a medium lacking tryptophan, leucine and histidine. Prey fragments of positive clones were amplified by PCR and sequenced at their 5' and 3' junctions. The sequences of 75 experimental ANKRD26 fragments were overlapped and their positions calculated relative to the full-length ANKRD26 protein. The minimal region that overlaps in all experimental ANKRD26 fragments represents the selected interacting domain.

Statistical analysis

Data are presented either as dot plot (mean in red ± s.e.m. in black) or as bar chart (mean ± s.e.m), unless differently specified in the corresponding figure legend. Normality of datasets was determined by Shapiro-Wilk test. Statistical differences were calculated by unpaired two-tailed Student's t-test or Mann-Whitney test (between two groups), and by one-way ANOVA or Kruskal-Wallis test (between multiple groups). Tukey's multiple comparison test was used as post hoc test when every mean was compared to every other mean, whereas Dunnett's multiple comparison test was used to compare every mean to a control mean. Statistical significance was annotated as: *$p<0.05$). Statistical analyses and graphs were produced using GraphPad Prism 8 (GraphPad, San Diego, CA, USA) software.

RESULTS

PIDD1 is a distal appendage protein whose localization relies on ANKRD26

We previously reported that PIDD1 decorates only centrioles positive for CEP164 (Fava *et al*, 2017), a known member of distal appendage proteins (DAPs) (Graser *et al*, 2007), demonstrating thereby that PIDD1 specifically localizes to parent centrioles. Taking into account that the clearest determinant of parent centrioles is the presence of DAs and SDAs, we wondered whether PIDD1 displays a preferential association with any of those structures. To address this question, we employed 2D stimulated emission depletion (STED) microscopy and co-stained PIDD1 with known members of SDA proteins (SDAPs) or DAPs, namely ODF2 and FBF1, respectively (Tanos *et al*, 2013; Mazo *et al*, 2016). Strikingly, PIDD1 STED signal displayed a 9-fold rotational symmetric arrangement that best co-localized with FBF1, suggesting that PIDD1 preferentially associates with DAs (Fig. 9A). To test whether PIDD1 is a bona fide DAP, we exploited the notion that despite abolishing ciliogenesis, preventing DA assembly allows cell proliferation in culture (Mazo *et al*, 2016). Thus, we utilized the CRISPR/Cas9 technology to deplete CEP83/CCDC41, a protein necessary for the assembly of DAs (Tanos *et al*, 2013) (Supplementary Fig. 1 reports a comprehensive validation of the CRISPR/Cas9 knock-out cell lines used in this work). Loss-of-function CEP83 derivatives were obtained from non-transformed retinal cells of the pigmented epithelium hTERT-RPE1 (hereafter referred to as RPE1) and from lung adenocarcinoma A549 cells. While CEP83 depletion was effective in perturbing DAs assembly (Supplementary Fig. 2A and B), SDAs recruitment appeared largely unaffected in both loss-of-function cell lines (Supplementary Fig. 2C and D). More importantly, CEP83 depletion drastically impinged on the PIDD1 recruitment to parent centrioles in both cell lines (Fig. 9B and C). Thus, super resolution microscopy and reverse genetics support the notion that PIDD1 is a DAP.

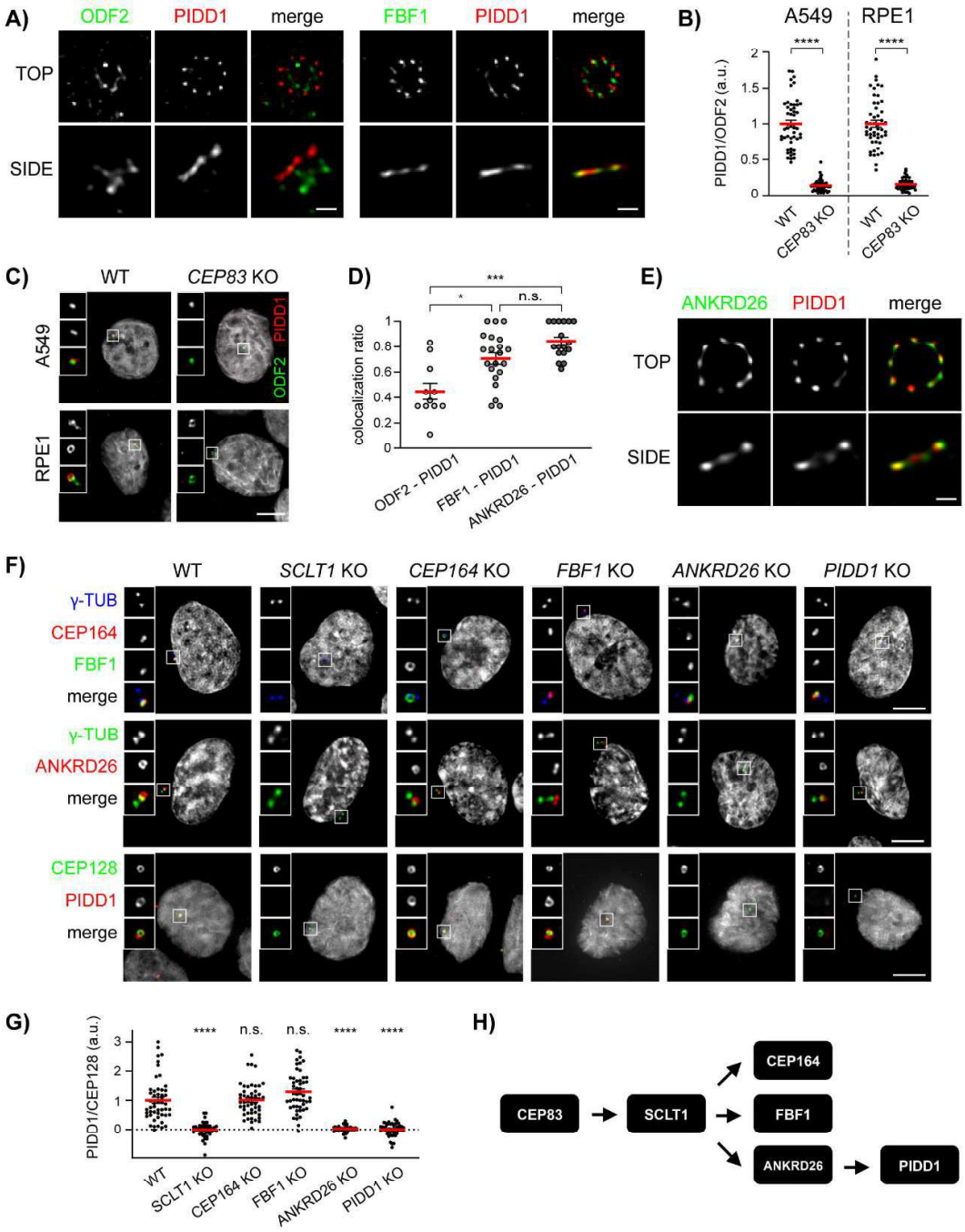

Figure 9. PIDD1 is a distal appendage protein whose localization relies on ANKRD26. (A) 2D STED micrographs of RPE1 cells co-stained with the indicated antibodies. Scale bar: 200 nm. (B) Dot plots showing the average pixel intensities at individual parent centrioles expressed as the PIDD1/ODF2 fluorescence ratio in the indicated cell lines and genotypes. Mean values (red lines) ± s.e.m. are reported. Data obtained from images as in (C). N ≥ 50 centrosomes were assessed for each condition, a.u. = arbitrary units. Unpaired Mann-Whitney test (****P < 0.0001). (C) Representative fluorescence micrographs from the indicated cell lines co-stained with the indicated antibodies. Blow-ups without Hoechst 33342 are

magnified 2.5X. Scale bar: 5 μm. (D) Co-localization between ODF2 and PIDD1 (n = 11), FBF1 and PIDD1 (n = 21), and ANKRD26 and PIDD1 (n = 17) assessed on images as in (A and E). The value represents the fraction PIDD1 objects touching either ODF2, FBF1 or ANKRD26 objects. Mean values (red lines) ± s.e.m. are reported. Kruskal-Wallis test (***P < 0.001; *P < 0.05; n.s. = non-significant). (E) 2D STED micrographs of RPE1 cells co-stained with the indicated antibodies, scale bar: 200 nm. (F) Representative fluorescence micrographs of RPE1 cells of the indicated genotypes co-stained with the indicated antibodies. Blow-ups without Hoechst 33342 are magnified 2.5X. Scale bar: 5 μm. (G) Dot plot showing the average pixel intensities at individual parent centrioles expressed as the PIDD1/CEP128 fluorescence ratio in RPE1 of the indicated genotypes. Mean values (red lines) ± s.e.m. are reported. Data obtained from images as in (F). N ≥ 50 centrosomes were assessed from as many individual cells for each condition, a.u. = arbitrary units. Statistical significance was assessed by KruskalWallis test, comparing each sample to the wild type (****P < 0.0001). (H) Scheme summarizing the epistatic interdependencies between DAPs emerging from work displayed in this figure.

Next, we aimed to better define the PIDD1 position in the physical and epistatic map of DAPs. To this end, we performed a yeast-two-hybrid screen using the PIDD1 1-758 (see below) fragment as bait against a cDNA library obtained from an equimolar mix of three different lung cancer cell lines (including A549). This screen retrieved only one centrosomal protein as prey: ANKRD26 (Jakobsen *et al*, 2011; Bowler *et al*, 2019) and particularly the portion comprised between amino acid 538 and 1204 (Supplementary Fig. 2E-F). Consistently, co-staining of PIDD1 with ANKRD26 in STED microscopy revealed the highest degree of co-localization among our super resolution analyses (Fig. 9D-E), strengthening the notion that PIDD1 and ANKRD26 directly interact at DAs in human cells.

The recent annotation of ANKRD26 as DAP was accompanied by detailed analysis of its localization at the outermost periphery of DAs (Bowler *et al*, 2019). However, the epistatic relationship between ANKRD26 and PIDD1 relative to other DAPs remained to be defined. To this end, we generated RPE1 derivatives lacking the expression of several individual known DAPs, namely SCLT1, CEP164 and FBF1 in addition to cells defective for ANKRD26 and PIDD1 themselves. Among these proteins, SCLT1 appeared as the most upstream factor in the epistatic tree, as all other proteins were delocalized by its depletion (Fig. 9F). CEP164, FBF1 and ANKRD26 appeared to be recruited to DAs independently from each other and downstream of SCLT1 (Fig. 9F). While PIDD1 deficiency did not display any notable effect on the recruitment of all the

other DAPs analysed, ANKRD26 deficiency, but not CEP164 or FBF1 depletion, abrogated PIDD1 recruitment to DAs (Fig. 9F-G). Hence, we defined the position of PIDD1 in the epistatic map of DAPs, demonstrating that it represents the most downstream member among those included in our analysis (Fig. 9H). Taken together, yeast-two-hybrid, epistatic studies and super resolution microscopy demonstrate that PIDD1 is a bona fide DAP and suggest a tight, likely direct, association between ANKRD26 and PIDD1 at the DA periphery.

Peripheral DAPs are dispensable for ciliogenesis

The presence of DAs on parent centrioles has been functionally linked to the centrosomes' capability to become basal bodies and to promote the formation of primary cilia (PC). Therefore, considering the fact that PIDD1 is a novel member of DAPs, we hypothesized that PIDD1 might contribute to ciliogenesis. To tackle this question, we took advantage of our set of RPE1 derivatives defective for individual DAPs and exposed them to serum-starvation in order to promote PC formation. Consistently with previous results (Tanos *et al*, 2013), SCLT1 and CEP164 deficiency completely abolished PC formation (Fig. 10A-B). Moreover, re-expressing SCLT1 with a lentiviral strategy in SCLT1-deficient RPE1 cells allowed us to restore the ciliogenesis process, demonstrating that the observed phenotype was dependent on SCLT1 protein depletion rather than on artefacts caused by CRISPR/Cas9 (Fig. 10C-D). In line with a less stringent requirement for FBF1 functionality to support ciliogenesis (Yang *et al*, 2018), FBF1 deficiency triggered a clear reduction of the average ciliary length, yet allowing the formation of shorter cilia in about 40% of serum-starved cells (Fig. 10A-B and E). ANKRD26 depletion instead resulted in a more nuanced phenotype, not impinging on the percentage of ciliated cells but leading to the generation of shorter PC, probably reflecting a role of this protein in ciliary gating (Yan *et al*, 2020) (Fig. 10A-B and E). Interestingly, PIDD1 deficiency did not interfere with ciliogenesis in any of the assays we performed (Fig. 10A-B and E). Taken together, our data demonstrate that the ANKRD26-dependent centrosome recruitment of PIDD1 appears dispensable for PC formation, revealing that DAs might also serve as scaffolds to promote cellular functions distinct from ciliogenesis (Fig. 10F).

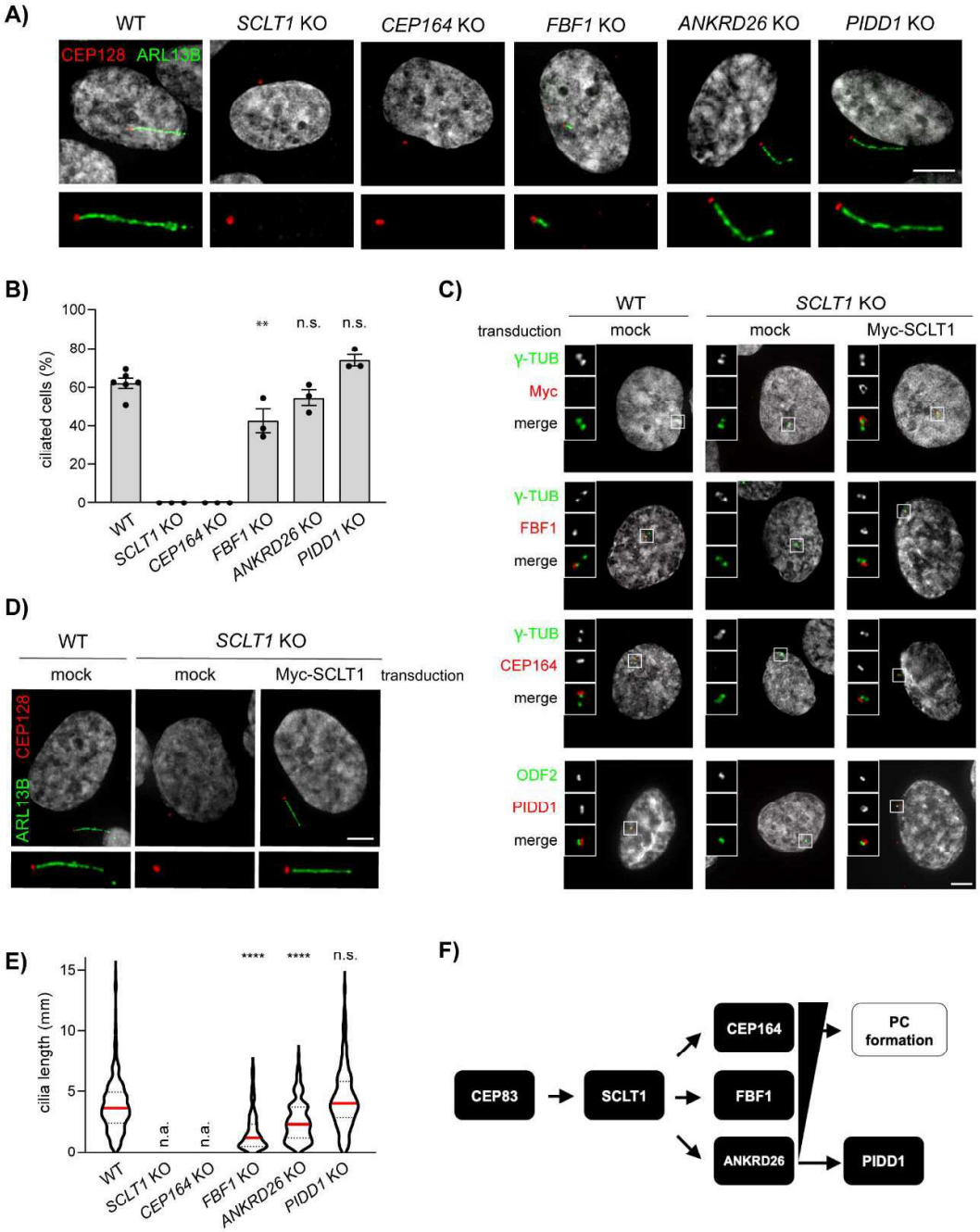

Figure 10. Peripheral DAPs are dispensable for ciliogenesis. (A) RPE1 cells of the indicated genotypes were subjected to serum-starvation followed by immunofluorescence with the indicated antibodies to visualize the PC. Representative micrographs are shown. Blow-ups without Hoechst 33342 are magnified 2X. Scale bar: 5 µm. (B) The percentage of ciliated cells was assessed by visual scoring of micrographs as in (A) across 3 biological replicates, with ≥ 50 cells per replicate. Individual values of biological replicates, their mean ± s.e.m. are reported. ANOVA test, comparing each sample to the wild type (**P < 0.01; n.s. = non-significant). (C) Fluorescence micrographs of RPE1 cells of the indicated genotypes, either left untransduced (mock) or transduced with a lentiviral vector expressing Myc-SCLT1, and co- stained with

the indicated antibodies. Blow-ups without Hoechst 33342 are magnified 2.5X. Scale bar: 5 μm. (D) RPE1 cells of the indicated genotypes were either left untransduced (mock) or transduced with a lentiviral vector expressing Myc-SCLT1 and subjected to serum starvation. Immunofluorescence with the indicated antibodies allowed visualization of the PC. Representative micrographs are shown, blow-ups without Hoechst 33342 are magnified 2X. Scale bar: 5 μm. (E) Ciliary length was measured from the same dataset described in (B), violin plots showing values for individual cilia obtained by pooling at least three biological replicates (≥ 150 cells); n.a. = not applicable due to absence of ciliated cells. Median values (red lines) and quartiles (black, dashed lines) are shown. Kruskal-Wallis test, comparing each sample to the wild type (****P < 0.0001; n.s. = non-significant). (F) Scheme summarizing the epistatic interdependencies between DAPs emerging from data displayed in Fig. 9 and the functional implications described in this figure. PC = primary cilium.

ANKRD26 directly recruits PIDD1 to DAs

With the aim to better define the minimal ANKRD26 fragment required for PIDD1 recruitment to DAs, we performed a follow-up yeast-two-hybrid screen. Briefly, we generated a deletion library of the previously identified ANKRD26 fragment (amino acids 538 – 1204). This new library was then screened against the same PIDD1 bait, eventually restricting the putative PIDD1 Minimal Interaction Domain (PMID) of ANKRD26 to the region between amino acid 911 and 1181 (overlapping with the annotated CCDC144C-like domain) (Fig. 11A).

In order to test the impact of ANKRD26' PMID on PIDD1 centrosomal localization, we cloned lentiviral constructs encoding a Myc-tagged version of ANKRD26 lacking the newly identified PMID (ANKRD26-ΔPMID) and the PMID alone (ANKRD26-PMID), together with a full-length form of ANKRD26 (ANKRD26 WT). Complementation studies in RPE1 derivatives deficient for ANKRD26 revealed that while ANKRD26-PMID alone was not sufficient for DA localization, ANKRD26-ΔPMID localized to DAs similarly to ANKRD26 WT (Fig. 11B-C). Furthermore, exogenously expressed ANKRD26 WT, but not ANKRD26-ΔPMID, was able to rescue the ability of PIDD1 to localize at DAs (Fig. 11D-E). Taken together, we refined the ANKRD26 region sustaining a direct interaction with PIDD1 and demonstrated that the same region, despite being dispensable for ANKRD26 localization, is necessary for PIDD1 docking at the centrosome.

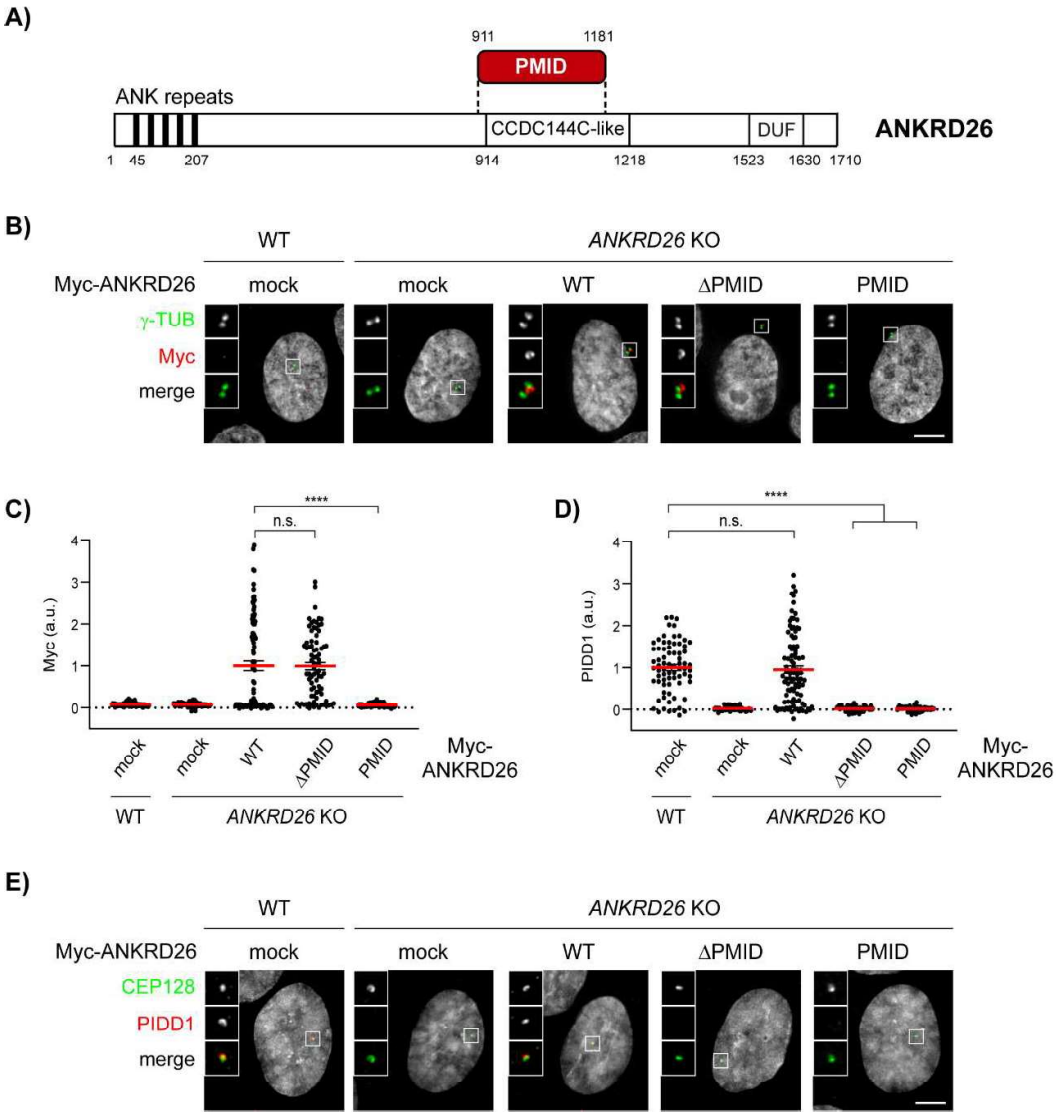

Figure 11. ANKRD26 directly interacts with PIDD1 at DAs. (A) Schematic of the ANKRD26 domain identified as PIDD1 interactor by yeast-two-hybrid screen. PMID = PIDD1 Minimal Interaction Domain; CCDC144C-like = Coiled-Coil Domain similar to CCDC144C; DUF: Domain of Unknown Function. (B) Representative fluorescent micrographs of RPE1 cells of the indicated genotypes, either transduced with the indicated lentiviral vectors or left untransduced (mock). Cells were co-stained with the indicated antibodies. Blow-ups without Hoechst 33342 are magnified 2.5X. Scale bar: 5 μm. (C) Dot plot showing the average pixel intensities of the Myc signal at individual parent centrioles in RPE1 cells of the indicated genotypes, either transduced with the indicated lentiviral vectors or left untransduced (mock). Mean values (red lines) ± s.e.m. are reported. N > 50 centrosomes were assessed for each condition in as many individual cells; a.u. = arbitrary units. Kruskal-Wallis test (****P < 0.0001; n.s. = non-significant). (D) Dot plot showing the average pixel intensities of the PIDD1 signal at individual parent centrioles in RPE1 cells of

the indicated genotypes, either transduced with the indicated lentiviral vectors or left untransduced (mock). Mean values (red lines) ± s.e.m. are reported. N > 50 centrosomes were assessed for each condition in as many individual cells; a.u. = arbitrary units. Kruskal-Wallis test (****P < 0.0001; n.s. = non-significant). (E) Representative fluorescent micrographs of RPE1 cells of the indicated genotypes, either transduced with the indicated lentiviral vectors or left untransduced (mock). Cells were co-stained with the indicated antibodies. Blow-ups without Hoechst 33342 are magnified 2.5X. Scale bar: 5 μm.

PIDD1 localization to DAs is necessary for PIDDosome activation

Defining the epistatic and physical position of PIDD1 in the context of DAs (Fig. 9 and 11) readily enabled us to test whether there is a link between PIDD1 localization to DAs and its functional output in terms of PIDDosome activation. As PIDD1 localizes to parent centrioles irrespectively of PIDDosome activation (Fava *et al*, 2017), we reasoned that DA localization might represent a prerequisite for PIDDosome activation mediated by supernumerary centrosomes. To test this hypothesis, we utilized RPE1 derivatives lacking the expression of several individual DAPs and assessed their ability to activate the PIDDosome by measuring the accumulation of MDM2 cleavage fragments in response to cytokinesis failure. The inhibition of actomyosin ring functionality upon dihydrocytochalasin-B (DHCB) treatment resulted in MDM2 cleavage in parental cells (Fig. 12A). Releasing the cells from DHCB into fresh medium did not revert the accumulation of MDM2 cleavage products, suggesting that this latter event depends on one of the consequences of failed cell division (i.e. extra centrosomes, Fig. 12B), rather than on the drug treatment itself (Fig. 12A). Cells lacking CEP164 or FBF1, two DAPs that were dispensable for PIDD1 localization to parent centrioles, behaved similarly to the parental line (Fig. 12A). In stark contrast, depletion of all the proteins required for PIDD1 recruitment to DAs, namely CEP83, SCLT1 and ANKRD26, in addition to PIDD1 deficiency itself, led to complete abrogation of PIDDosome activation upon cytokinesis failure (Fig. 12A). The extent of binucleation induced by DHCB in the various genotypes appeared comparable, thereby excluding the possibility that differences in PIDDosome activation depend on reduced proliferation rate (Fig. 12B-C). Consistently, no reduction in the rate of supernumerary centrosome acquisition upon DHCB treatment could be observed when comparing knock-out cell lines with parental cells (Fig. 12B and D). Importantly, lack of PIDDosome activation upon cytokinesis failure led to genome reduplication in all the experimental conditions analysed, as

assessed by EdU incorporation analysis upon DHCB treatment (Fig. 12E and Supplementary Fig. 3).

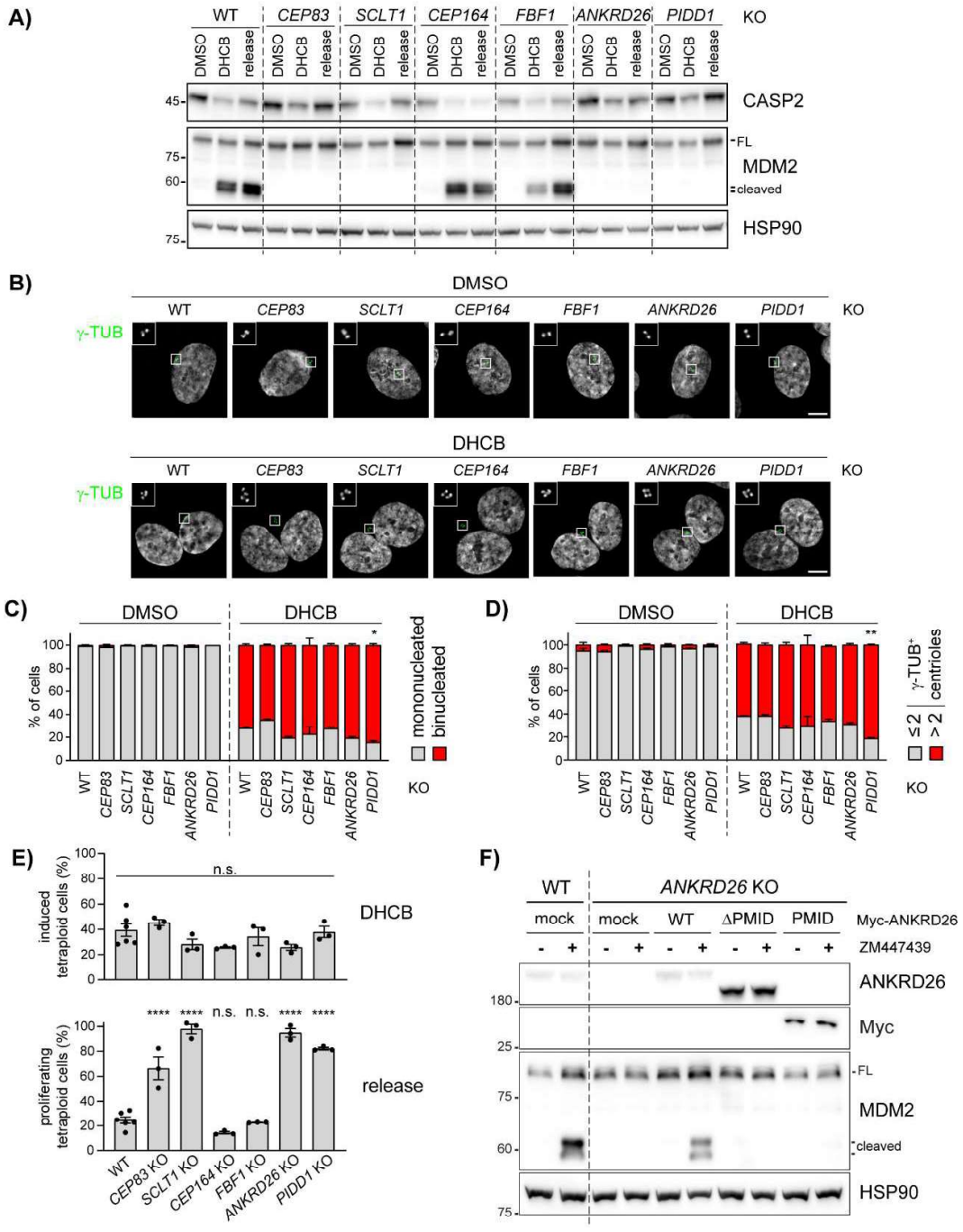

Figure 12. PIDD1 localization to DAs is necessary for PIDDosome activation. (A) RPE1 cells of the indicated genotypes were treated either with DMSO or with DHCB for 24h. A fraction of DHCB treated

cells were released into fresh medium for other 24h (release). Samples were subjected to immunoblotting; n = 3 independent experiments. (B) Fluorescence micrographs of RPE1 cells of the indicated genotypes, either treated for 24h with DHCB or with vehicle alone (DMSO). Blow-up without Hoechst 33342 is magnified 2.5X. Scale bar: 5 μm. (C) Immunofluorescence micrographs of RPE1 as in (B) were used to visually assess the percentage of cells presenting one or two nuclei. N = 3, ≥ 50 cells from each independent experiment. Mean values ± s.e.m. are reported. The increase in the number of binucleated cells between the wild type sample and all the other genotypes was assessed (ANOVA test; *P < 0.05). (D) Immunofluorescence micrographs of RPE1 as in (B) were used to visual score the number of centrosomes per cell by counting the number of γ-tubulin-positive centrioles. N = 3, ≥ 50 cells from each independent experiment. Mean values ± s.e.m. are reported. The increase in the number of cells with > 2 centrosomes between the wild type sample and all the other genotypes was assessed (ANOVA test; **P < 0.01). (E) Quantitative assessment of the fraction of RPE1 cells undergoing cytokinesis failure upon DHCB treatment, inferred on the basis of the increase of ploidies ≥ 4C (upper panel), and of the fraction of the abovementioned cells undergoing genome reduplication upon release after DHCB treatment (lower panel). Individual values of biological replicates, their mean and standard deviations are reported. ANOVA test, comparing each sample to the wild type (****P < 0.0001; n.s. = non-significant). (F) RPE1 cells were either left untransduced (mock) or transduced with lentiviral vectors expressing the indicated Myc-ANKRD26 constructs. Subsequently, cells were treated either with DMSO or ZM447439 for 24h and subjected to immunoblotting; n = 3 independent experiments.

Moreover, the abovementioned paradigm is not restricted to RPE1 cells, as SCLT1- deficient A549 cells displayed compromised PIDD1 recruitment to DAs, PIDDosome activation and cell cycle arrest in response to cell division failure, all of which could be rescued by exogenously expressing SCLT1 (Fig. 13). Finally, we assessed the ANKRD26-ΔPMID ability to sustain PIDDosome activation (Fig. 12F), demonstrating that surgical removal of the PMID leads not only to PIDD1 delocalization but also to defective PIDDosome activation. Thus, interfering with PIDD1 localization to DAs by different genetic means invariably compromised PIDDosome activation and the resulting cell cycle arrest in response to cytokinesis failure.

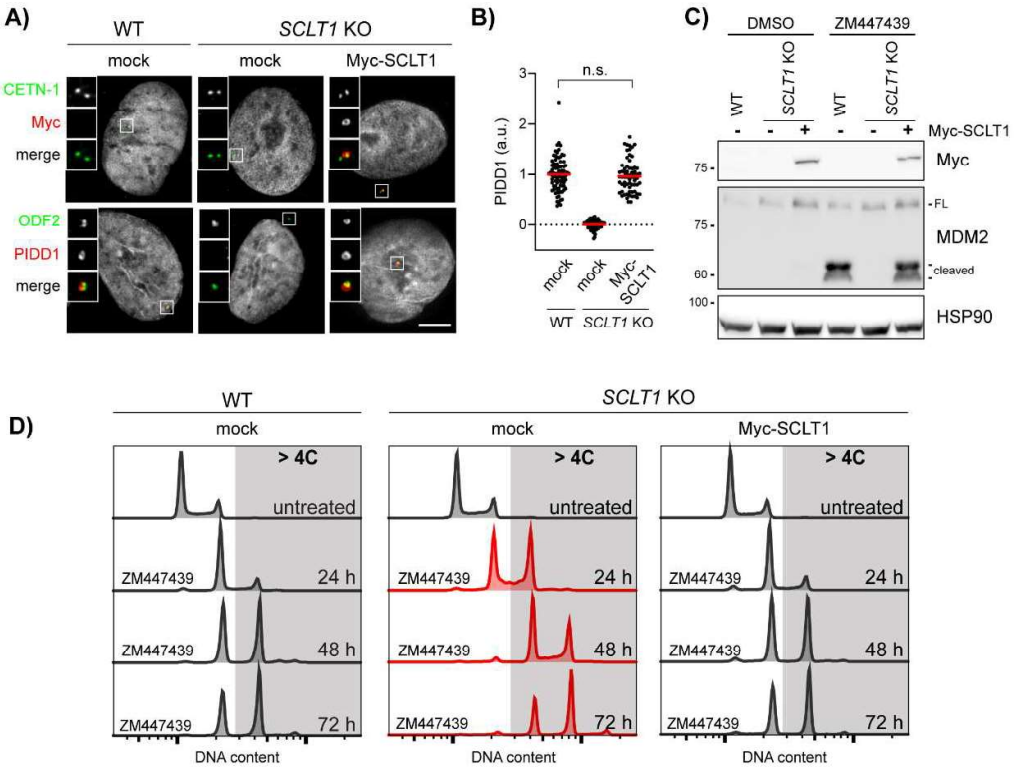

Figure 13. Complementation of SCLT1 in SCLT1 KO cells rescues PIDDosome activation also in A549 cells. (A) Fluorescence micrographs of A549 cells of the indicated genotypes. Cells were either left untransduced (mock) or transduced with a lentiviral vector expressing Myc41 SCLT1, and co-stained with the indicated antibodies. Blow-ups without Hoechst 33342 are magnified 2.5X. Scale bar: 5 μm. (B) Dot plot showing the average pixel intensities of PIDD1 at individual parent centrioles in A549 cells of the indicated genotypes, treated as in (A). Mean values (red lines) ± s.e.m. are reported. N > 50 centrosomes were assessed for each condition in as many individual cells; a.u. = arbitrary units. Mann-Whitney test (n.s. = non-significant). (C) A549 cells of the indicated genotypes were either left untransduced (-) or transduced with a lentiviral vector expressing Myc-SCLT1 (+). Cells were treated either with DMSO or with ZM447439 for 24h and subjected to immunoblotting; n = 3 independent experiments. (D) DNA content analysis of A549 cells of the indicated genotypes. Cells were either left untransduced (mock) or transduced with a lentiviral vector expressing Myc- SCLT1, treated with ZM447439 for up to 72h and processed for DNA content analysis.

Only the PIDD1 precursor is capable of localizing to centriole DAs.

Once established that ANKRD26 concurs to form the centrosomal receptor for PIDD1, we set out to look for the PIDD1 portion sustaining its localization. Of note, PIDD1 has been previously shown to undergo autoprocessing following a proteolytic

mechanism displayed also by the nucleoprotein Nup98 and the transmembrane receptor Unc5CL (Heinz et al, 2012; Tinel et al, 2007). PIDD1 autoproteolysis can occur at two sites, resulting in the coexistence of different PIDD1 protein species: i) PIDD1-FL, the Full-Length precursor of 910 amino acids, ii) PIDD1-N (amino acids 1- 445), the N-terminal fragment resulting from cleavage at the first autoproteolytic site, iii) PIDD1-C (amino acids 446-910), the C-terminal fragment resulting from the aforementioned cleavage site, and iv) PIDD1-CC (amino acids 588-910), resulting from cleavage at the second autoproteolytic site (Fig. 14A). Notably, three of these PIDD1 species (i.e. PIDD1-FL, PIDD1-C and PIDD1-CC, but not PIDD1-N) contain the death domain (DD), essential for PIDDosome activation (Park et al, 2007). To address our question, we established a lentiviral strategy allowing to re-express V5-epitope tagged PIDD1 fragments in A549 derivatives deficient for PIDD1. Strikingly, while exogenously expressed wild type PIDD1 localized to the centrosome, neither PIDD1-N, PIDD1-C (carrying the S588A mutation that prevents further cleavage into PIDD1-CC) nor PIDD1-CC displayed any detectable recruitment to the centrosome, despite being expressed at levels comparable to those obtained via autoproteolysis of the wild type precursor (Fig. 14B-D). The lack of centrosomal localization of PIDD1 autoproteolytic fragments was also verified in presence of supernumerary centrosomes, excluding the possibility that PIDD1 fragments selectively acquire competence to localize at the centrosome in PIDDosome activating conditions (Supplementary Fig. 4A). Consistently, the expression of a PIDD1 version defective in autoproteolysis ($PIDD1^{S446A\text{-}S588A}$), leading thereby to the production of the sole PIDD1-FL precursor, displayed proficiency in localizing at the centrosome (Fig. 14E-F). Furthermore, deletion mutants of $PIDD1^{S446A\text{-}S588A}$ identified the 1-758 portion of PIDD1 as the minimal PIDD1 precursor fragment displaying DA recruitment (Fig. 14E-F and Supplementary Fig. 4B). Thus, our data demonstrate that only the PIDD1 noncleaved precursor can localize to centrosomes and that several PIDD1 domains concur to PIDD1 recruitment to DAs.

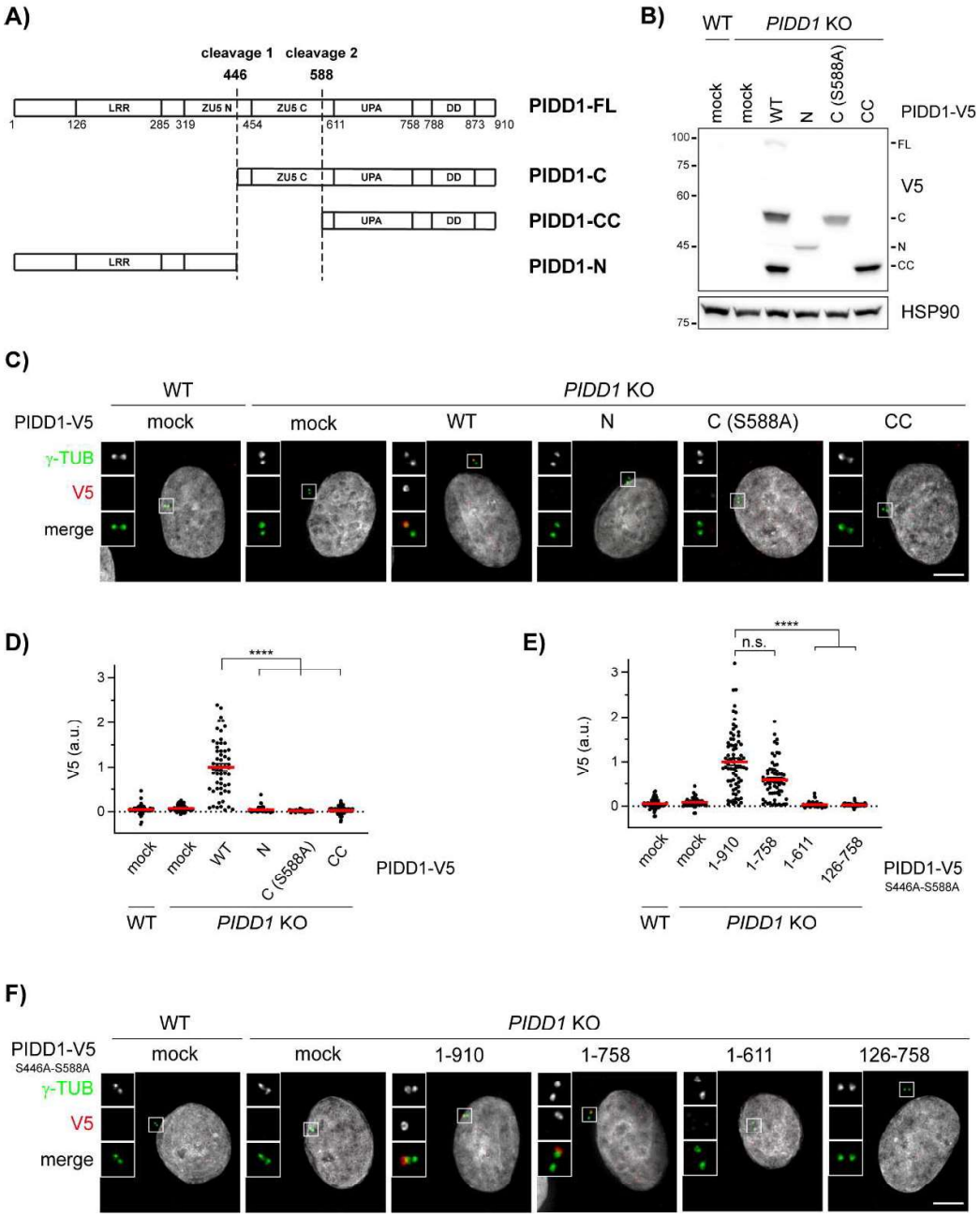

Figure 14. Only the PIDD1 non cleaved precursor is capable of localizing to centriole DAs. (A) Schematic of the PIDD1 domain structure and of the different PIDD1 species generated by autoproteolysis. LRR = Leucin Rich Repeat Domain; ZU5 (N and C) domains = Domain present in ZO-1, Unc5-like netrin receptors and in ankyrins; UPA domain = conserved in UNC5, PIDD, and Ankyrins; DD = death domain. (B) A549 cells of the indicated genotypes were either left untransduced (mock) or transduced with lentiviral vectors expressing the indicated PIDD1-V5 derivatives and subjected to immunoblotting. N = 2 independent experiments. (C) Fluorescence micrographs of A549 cells of the indicated genotypes either left untransduced (mock), or transduced with PIDD1-V5 lentiviral vectors as in (B), and co- stained with

the indicated antibodies. Blow-ups without Hoechst 33342 are magnified 2.5X. Scale bar: 5 μm. (D) Dot plot showing the average V5 pixel intensities at individual parent centrioles in A549 cells of the indicated genotypes, either transduced with the indicated lentiviral vectors or left untransduced (mock). Mean values (red lines) ± s.e.m. are reported. Data obtained from images as in (C). N > 50 centrosomes were assessed for each condition in as many individual cells; a.u. = arbitrary units. Kruskal-Wallis test (****P < 0.0001). (E) Dot plot showing the average V5 pixel intensities at individual parent centrioles in A549 cells of the indicated genotypes, either transduced with the indicated lentiviral vectors or left untransduced (mock). Mean values (red lines) ± s.e.m. are reported. Data obtained from images as in (F). N > 50 centrosomes were assessed for each condition in as many individual cells; a.u. = arbitrary units. Kruskal-Wallis test (****P < 0.0001; n.s. = non-significant). (F) Representative fluorescence micrographs of A549 cells of the indicated genotypes. Cells were either left untransduced (mock) or transduced with PIDD1-V5 lentiviral vectors expressing the PIDD1 non-cleavable derivative (PIDD1S446A-S588A) or truncations thereof. Blow-ups without Hoechst 33342 are magnified 2.5X. Scale bar: 5 μm.

PIDD1 autoproteolysis is constitutive and occurs independently of its centrosomal localization

The analysis of the functional relevance of PIDD1 autoproteolytic products has been so far confined to the assessment of Caspase-2 activation induced by the ectopic overexpression of PIDD1 species in HEK293T cells, revealing that PIDD1-CC is the only DD-containing species capable of supporting Caspase-2 activation in this assay (Tinel et al, 2007). The importance of the centrosomal localization of the PIDD1 precursor shown here suggested us in turn that PIDD1 recruitment at DAs might be necessary to sustain its autoproteolysis. Given our inability to reliably detect endogenous PIDD1 species by immunoblotting with the available antibodies, we decided to tackle this issue with two independent experimental approaches. Firstly, we exploited our lentiviral complementation strategy: V5-tagged PIDD1 underwent constitutive autoproteolysis when re-expressed in PIDD1-deficient cells and sustained Caspase-2 activation in response to cytokinesis failure (Fig. 15A). Strikingly, CEP83-, SCLT1- and ANKRD26-deficient cells exposed to the same titre of PIDD1 lentiviral vectors maintained their ability to promote PIDD1 autoprocessing, despite losing the potential to activate the PIDDosome (Fig. 15A). Secondly, in collaboration with Dr. Alexander Schmidt (Proteomics Core Facility, Biozentrum, University of Basel, Switzerland) we developed a mass spectrometric assay relying on high resolution and precision parallel reaction monitoring (PRM) to assess endogenous PIDD1 abundance (Peterson *et al*, 2012),

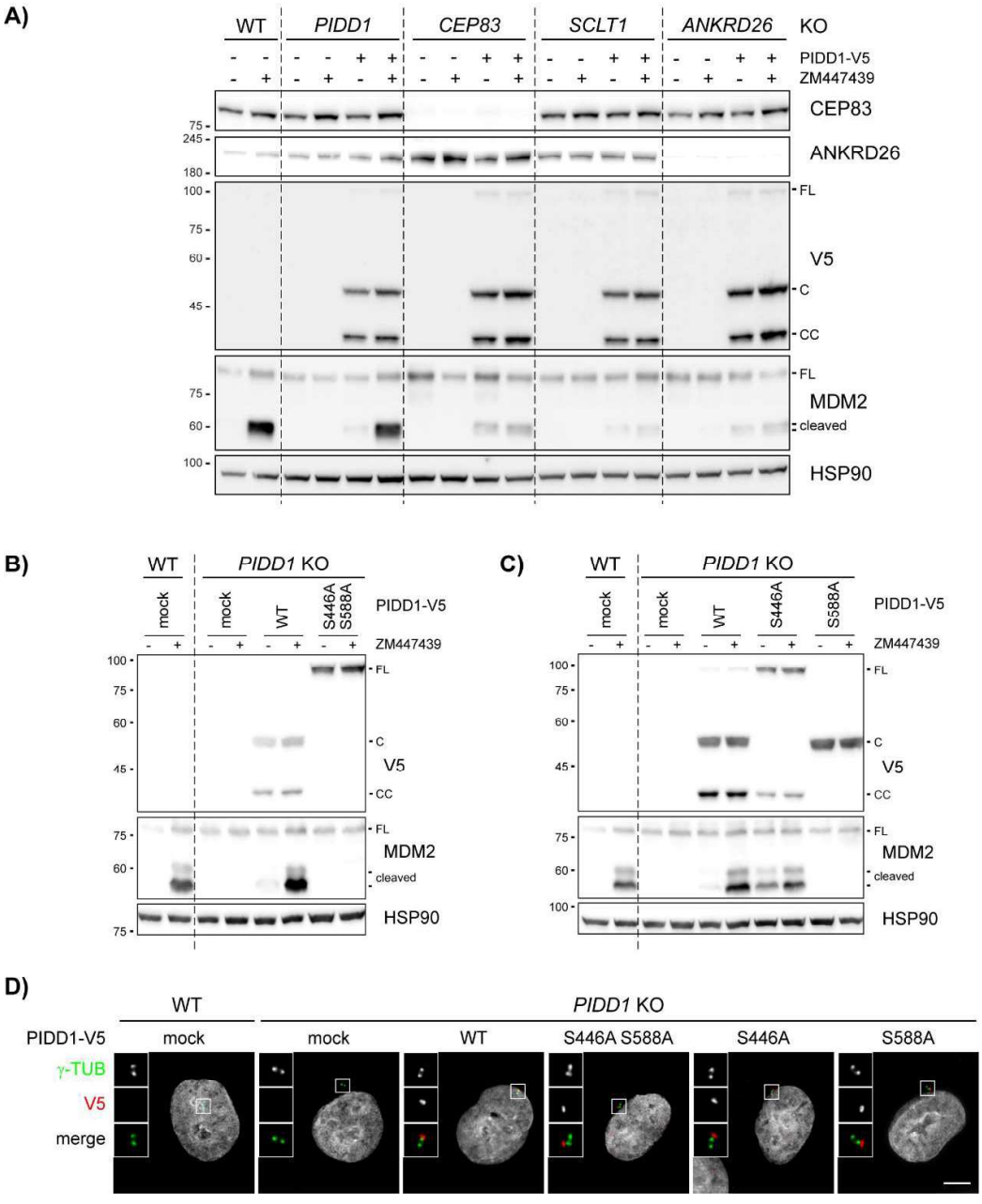

Figure 15. PIDD1 autoproteolysis is constitutive, occurs independently of DAs localization but is necessary for PIDDosome activation. (A) A549 cells of the indicated genotypes were either left untransduced or transduced with a lentiviral vector expressing PIDD1-V5 in its wild type form. Cells were treated either with DMSO or with ZM447439 for 24h and subjected to immunoblotting. N = 2 independent experiments. (B,C) A549 cells of the indicated genotypes were either left untransduced (mock), or transduced with lentiviral vectors expressing PIDD1-V5 in its wild type form or carrying the indicated point mutations. Cells were treated either with DMSO or with ZM447439 for 24h and subjected to immunoblotting. N = 2 independent experiments. (D) Fluorescence micrographs of A549 cells of the

indicated genotypes. Cells were either left untransduced (mock) or transduced with PIDD1-V5 lentiviral vectors carrying the indicated point mutations, and stained with the indicated antibodies. Blow-ups without Hoechst 33342 are magnified 2.5X. Scale bar: 5 μm.

focusing on four different reference peptides spanning the different autoproteolytic species (Fig. 16A). PRM analyses demonstrated that neither cell division failure nor delocalization of PIDD1 from DAs (achieved by SCLT1 deficiency) had any impact on the abundance of the four endogenous peptides (Fig. 16B). Taken together, our data demonstrate that PIDD1 localization to DAs is a requirement for PIDD1 function, yet it does not influence PIDD1 proteostasis.

A)

PRM PIDD1 reference peptides

Peptide #	Residues	Sequence	Contained in
1	183-198	LQTLPPALGALSTLQR	FL, N
2	491-497	VSMQVVR	FL, C
3	616-623	VNLIALQR	FL, C, CC
4	871-877	AVLELGR	FL, C, CC

B)

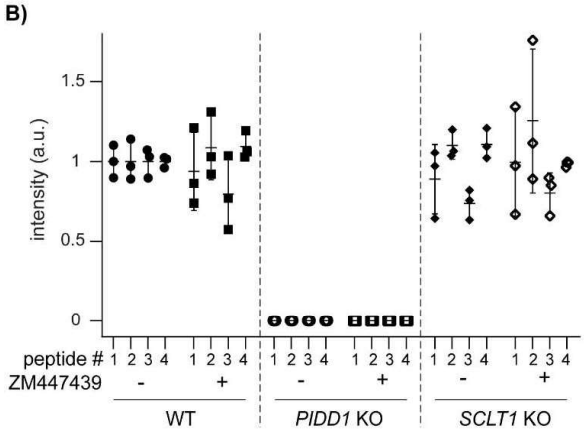

Figure 16. Endogenous PIDD1 localization to DAs does not influence its proteostasis. (A) Table reporting features of the reference (isotopically labelled) synthetic peptides that served as internal references for the quantification of the corresponding endogenous PIDD1 peptides. (B) Quantification across a biological triplicate of four different PIDD1 peptides (described in A) in A549 cells of the indicated genotypes treated either with DMSO (-) or with ZM447439 (+) by means of parallel reaction monitoring. Mean values ± standard deviations are reported.

Autoproteolytic generation of PIDD1-CC is necessary for PIDDosome activation by supernumerary centrosomes

Bearing in mind that PIDD1 autoproteolysis occurs independently of PIDD1 localization and of PIDDosome activation, the importance of PIDD1 autoprocessing in this context appears unclear. Yet, our complementation strategy afforded a unique opportunity to investigate the relationship between PIDD1 autoproteolysis and PIDDosome function in a physiologically relevant context, namely PIDDosome activation in response to extra centrosomes. Clearly, an autoproteolytically defective version of PIDD1 (PIDD1S446A-S588A) could not restore endogenous PIDD1 function (Fig. 15B). The utilization of mutants selectively impinging on one of the two cleavage sites (PIDD1S446A and PIDD1S588A) revealed that the production of PIDD1-CC (and not PIDD1-C) is crucial to activate the PIDDosome (Fig. 15C). Nonetheless, all PIDD1 mutants impinging on autoproteolytic events could equally localize to the centrosome (Fig. 15D and Supplementary Fig. 4C). Taken together, our data show that the ability of the PIDD1 precursor to autoprocess into PIDD1-CC appears indispensable for PIDDosome activation. However, autoproteolysis seems not sufficient, since the PIDD1-CC fragment is constitutively produced in the absence of an active PIDDosome and independently of PIDD1 ability to localize to the centrosome.

Extra centrosomes generate clusters

To further unveil the mechanism by which extra centrosomes instruct PIDDosome activation, we decided to characterize the PIDD1 centrosomal localization across an unperturbed cell cycle as well as upon cytokinesis failure in RPE1 cells. Previous work highlighted that while the DAP CEP83/CCDC41 retained association with parent centrioles throughout the cell cycle, including the mitotic cell division, more peripheral DAPs such as CEP164 and ANKRD26 appeared to dissociate from parent centrioles during mitosis, demonstrating thereby that DAs undergo an important reorganization while traversing mitosis (Bowler *et al*, 2019). Similarly, endogenous PIDD1 dissociates from parent centrioles only at mitosis onset (Fig. 17A-B). During the late stages of mitosis, one centriole for each spindle pole becomes increasingly competent for PIDD1 localization to DAs. Eventually, both G1 daughter cells display one PIDD1-positive centriole (Fig. 17A-B).

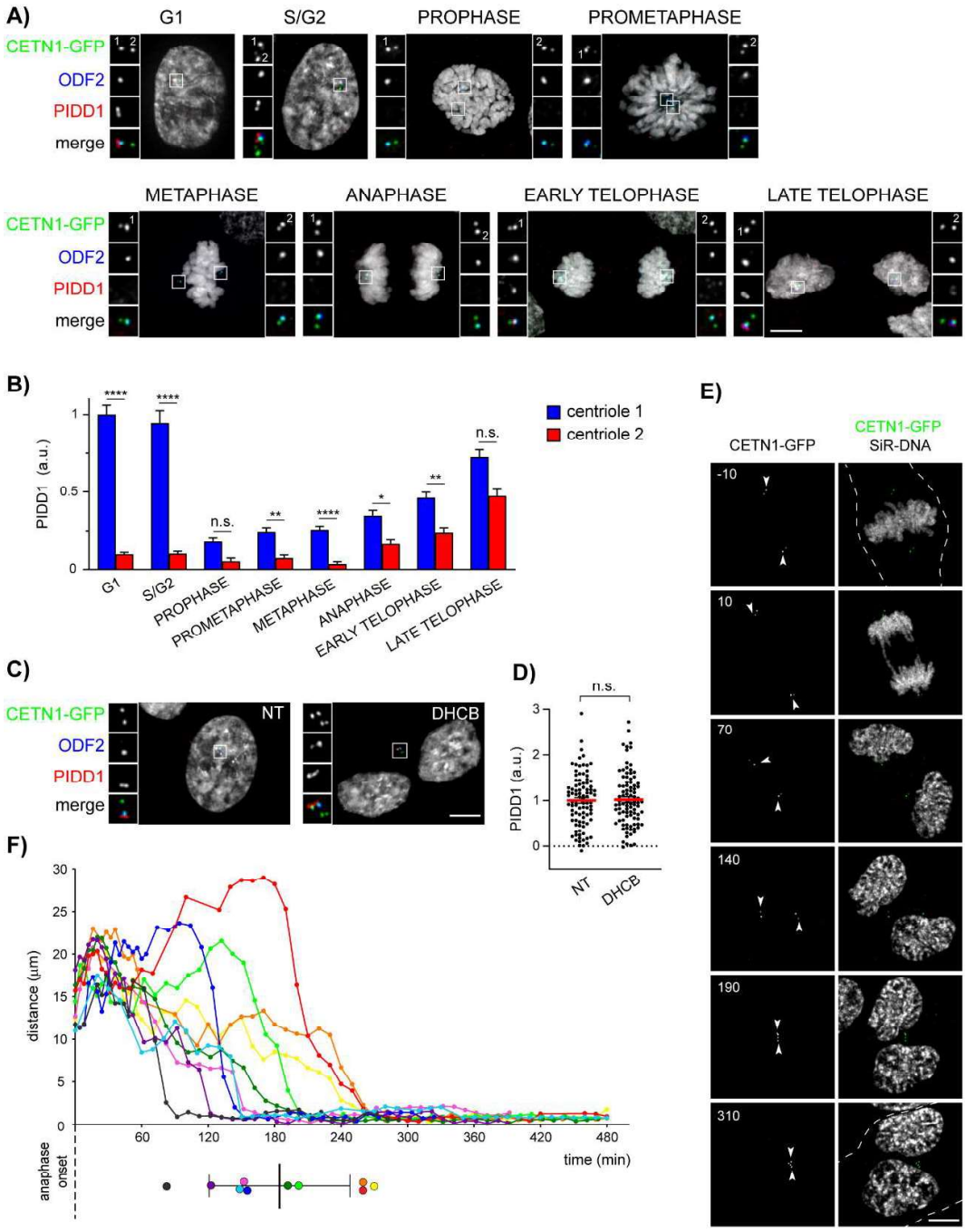

Figure 17. Extra PIDD1-positive centrosomes generate clusters. (A) Representative fluorescence micrographs across the indicated cell cycle phases from RPE1 cells stably expressing CETN1-GFP. Centrosomal antigens were stained with the indicated antibodies. Blow-ups without Hoechst 33342 are magnified 2.5X. Scale bar: 5 µm. The centrioles subjected to fluorescence intensity measurement in (B) are labelled with numbers. (B) Quantification of the PIDD1 average pixel intensity at individual centrioles across the indicated cell cycle phases of RPE1 cells stained as in (A). Mean values ± s.e.m. are reported. N > 50 centrioles were assessed for each phase, a.u. = arbitrary units. Kruskal-Wallis test (****P < 0.0001;

**P < 0.01; *P < 0.05; n.s. = non-significant). (C) Fluorescence micrographs of RPE1 cells stably expressing CETN1-GFP treated either with DMSO or with DHCB for 24h. Blow-ups without Hoechst 33342 are magnified 2.5X. Scale bar: 5 μm. (D) Dot plot showing PIDD1 average pixel intensities at individual parent centrioles calculated from images as in (C). Mean values (red lines) ± s.e.m. are reported. N > 50 centrosomes were assessed for each condition, a.u. = arbitrary units. Unpaired Student's t-test, two tails (n.s. = non-significant). (E) Movie stills of a representative RPE1 cell stably expressing CETN1-GFP treated with DHCB and subjected to time-lapse video microscopy in the presence of SiR-DNA. Time is expressed in minutes, relative to anaphase onset. The dashed line indicates the plasma membrane of the cell of interest, arrowheads indicate the centrosomes' position. Scale bar: 5 μm. (F) Centrosomal distance over time in RPE1 cells stably expressing CETN1-GFP and treated with DHCB. Time zero corresponds to the frame preceding anaphase onset. Coloured dots (lower panel) summarize the clustering time for each cell, mean ± 38 standard deviation in black. Data calculated from four-dimensional imaging as in (E). N = 10 cells.

Strikingly, in cells that failed cytokinesis, extra centrosomes appeared invariably clustered and, intriguingly, PIDD1-positive parent centrioles appeared to organize in closed proximity to each other within the clusters (Fig. 17C). Moreover, the amount of PIDD1 at individual centrioles within the clusters did not vary if compared to untreated cells in interphase, suggesting that no major changes in the protein recruitment to DAs occur upon cytokinesis failure (Fig. 17D). Live imaging of RPE1 cells expressing Centrin1-GFP and treated with the cytokinesis inhibitor DHCB demonstrated that 12 centrosome clusters form 184 ± 61 min after anaphase onset (average ± standard deviation, n = 10) and that, once clusters are formed, they remain stably associated (Fig. 17E-F and Supplementary Fig. 5).

Despite the fact that the overall PIDD1 levels at individual centrosomes did not vary upon cytokinesis failure, we reasoned that a differential exchange rate between the centrosomal and the cytoplasmic pool of PIDD1 might account for PIDDosome activation. In fact, an increased exchange rate at the centrosome, selectively recruiting the PIDD1 uncleaved precursor, might concur to locally elevate the concentration of the active PIDD1-CC fragment, necessary for PIDDosome activation. Thus, in collaboration with Dr. Stefano Maffini (Department of Mechanistic Cell Biology, Max Planck Institute of Molecular Physiology, Dortmund, Germany) we performed Fluorescence Recovery After Photobleaching (FRAP) analysis on PIDD1-deficient RPE1 cells stably expressing PIDD1L828E-mNeonGreen. This mutant retains both autoproteolysis and centrosomal

recruitment, while preventing PIDDosome activation (Park *et al*, 2007; Fava *et al*, 2017) (Fig. 18A-C), thereby allowing us to analyse PIDD1 dynamics uncoupled from the cell cycle consequences of PIDDosome activation. Our FRAP analysis showed recovery rates that were best described by a double exponential fitting curve (Fig. 18D-E). Nearly 60% of PIDD1L828E-mNeonGreen molecules showed a rapid recovery halftime of 1.7 s, while the slower component turned over with a halftime of 13.8 s. These values highlight how the centrosomal PIDD1 pool displays a high turnover, when compared to other centriolar proteins, e.g. CEP89: ~ 1 min; CEP120: ~ 2 min; Ninein: ~ 2.5 min (Sillibourne *et al*, 2013; Mahjoub *et al*, 2010; Moss *et al*, 2007). To our surprise, DHCB treated cells exhibit only a slight decrease in PIDD1 recovery (3.0 s for the fast component and 28.1 s for the slow component, Fig. 18D-E), a variation that appears unlikely to account for PIDDosome activation.

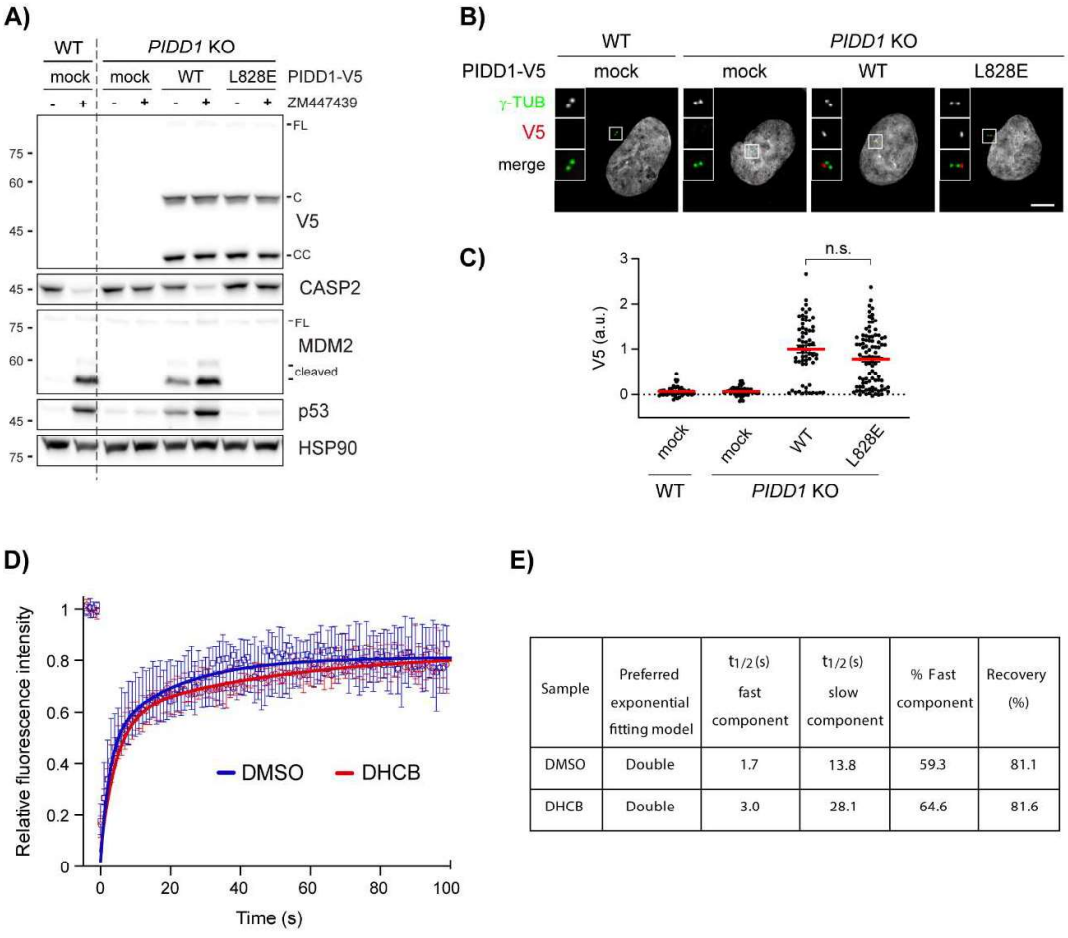

Sample	Preferred exponential fitting model	$t_{1/2}$ (s) fast component	$t_{1/2}$ (s) slow component	% Fast component	Recovery (%)
DMSO	Double	1.7	13.8	59.3	81.1
DHCB	Double	3.0	28.1	64.6	81.6

Figure 18. PIDD1 displays a rapid exchange rate between the centrosomal and cytoplasmic pool. (A) A549 cells of the indicated genotypes were either left untransduced (mock), or transduced with lentiviral vectors expressing PIDD1-V5 in its wild type form or carrying the L828E mutation. Cells were treated

either with DMSO or with ZM447439 for 24h and subjected to immunoblotting; n = 2 independent experiments. (B) Fluorescence micrographs of A549 cells of the indicated genotypes, treated as in (A) and co- stained with the indicated antibodies. Blow-ups without Hoechst 33342 are magnified 2.5X. Scale bar: 5 μm. (C) Dot plot showing the average pixel intensities of V5-tag at individual parent centrioles in A549 cells, measured from micrographs as in (B). Mean values (red lines) ± s.e.m. are reported. N > 50 centrosomes were assessed for each condition in as many individual cells; a.u. = arbitrary units. Mann-Whitney test (n.s. = nonsignificant). (D) FRAP analyses of centrosomal PIDD1L828E-mNeonGreen turnover in PIDD1-deficient RPE1 cells treated with either DMSO or DHCB. Graph shows the median with interquartile range (N = 12 cells per condition). FRAP curves for both experimental conditions were best fitted with a double exponential curve. (E) Relevant recovery parameters of FRAP experiments.

Centrosome clustering is necessary for PIDDosome activation

Considering that a rapid exchange rate between the centrosomal and cytoplasmic pool of PIDD1 is an intrinsic property of the centrosome, we reasoned that the physical proximity between two structures rapidly turning over the PIDD1 uncleaved precursor might locally augment the concentration of PIDD1-CC, thereby promoting PIDDosome activation. As microtubules had been shown to contribute generating cohesive forces between centrosomes (Panic *et al*, 2015), we speculated that microtubule depolymerisation could prevent centrosome clustering and hence PIDDosome activation. To test this hypothesis, we titrated nocodazole in conditions which lead both to cytokinesis failure (via Aurora B kinase inhibition) and a rapid mitotic traverse irrespectively of the presence of the microtubule poison (via Mps1 kinase inhibition) (Santaguida *et al*, 2010) in A549 cells. Increasing concentrations of nocodazole progressively led to i) an effective de-clustering of parent centrioles (measured as an increase in the distance between PIDD1-positive centrioles, Fig. 19A), without impinging on the simultaneous presence of two PIDD1-positive centrosomes in the same cell (Appendix Fig. 6A); ii) a decline in PIDDosome activation, which was completely abolished when cells were treated with 1 μM nocodazole (Fig. 19B); and iii) a dose-dependent propensity to genome reduplication (Fig. 19C) following cytokinesis failure.

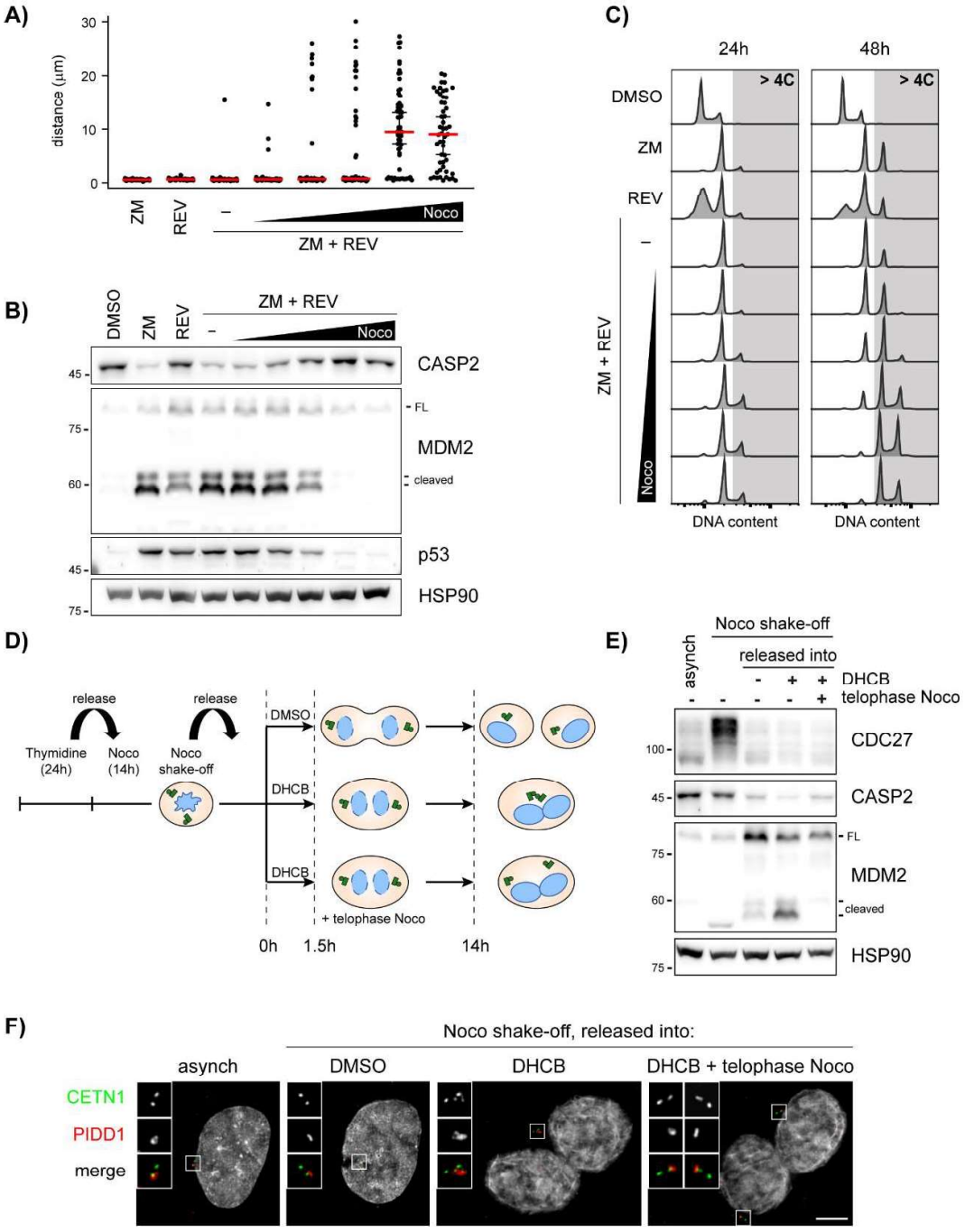

Figure 19. Centrosome clustering is necessary for PIDDosome activation. (A) Dot plot showing the distance between parent centrioles pairs in A549 cells following the indicated treatments (ZM = ZM447439; REV = reversine). Nocodazole concentrations are 0.03 µM, 0.1 µM, 0.33 µM, 1 µM, 3.3 µM. Median (red) and 95% confidence interval thereof (black) are shown. N > 50 cells were analysed. (B) Immunoblot of A549 cells subjected to the indicated treatments for 24h as in (A). N = 3 independent experiments. (C) DNA content analysis of A549 cells subjected to the indicated treatments as in (A) either for 24h (left

panels) or 48h (right panels). N = 2 independent experiments. (D) Schematic of the experimental conditions utilized to synchronize RPE1 cells and to specifically interfere with centrosome clustering after telophase. (E) Immunoblots of RPE1 cells synchronized as in (D). N = 3 independent experiments. (F) Representative fluorescence micrographs of RPE1 cells synchronized as in (D). Centrosomal antigens were stained with the indicated antibodies. Blow-ups without Hoechst 33342 are magnified 2X. Scale bar: 5 μm.

These data support the notion that clustering of supernumerary centrosomes is required to promote PIDDosome activation, which is in turn essential to halt the cell cycle progression. Importantly, nocodazole did not perturb PIDDosome activation in response to another trigger (camptothecin or CPT, see below and Supplementary Fig. 6B) nor PIDD1 recruitment to the centrosome (Supplementary Fig. 6C). While the possibility that nocodazole perturbs PIDDosome activation independently of its declustering activity cannot be presently ruled out, our data demonstrate that the nocodazole effect shown here did not depend on direct PIDDosome inhibition or on altered centriolar competency to sustain PIDDosome activation. Declustering centrosomes using a protocol to specifically depolymerize microtubules in cells synchronized in telophase, i.e. right before centrosome clustering, allowed to recapitulate the reported findings also in RPE1 cells (Fig. 19D-F and Supplementary Fig. 6D). Taken together, our data support the notion that centrosome clustering is key for enabling PIDDosome activation.

PIDD1 localization to DAs is required for PIDDosome activation in response to DNA damage

The longest-known PIDDosome activating cue is represented by genotoxic stress (Tinel & Tschopp, 2004; Sladky *et al*, 2017). As it has been reported that i) PIDD1 gene can be transactivated by the p53 protein, leading to its increased expression upon DNA damage (Lin *et al*, 2000) and that ii) DNA damage can promote the formation of extra centrosomes by multiple means (Mullee & Morrison, 2016), we reasoned that perturbing the centrosome-PIDDosome signalling axis could afford a way to genetically dissect the contribution of extra centrosomes to PIDDosome activation in response to DNA damage. With this aim, we treated A549 derivatives defective for SCLT1 or ANKRD26 with CPT, a topoisomerase I inhibitor, previously shown to induce robust PIDDosome activation (Ando *et al*, 2017). Immunoblot analysis revealed that PIDDosome activation upon CPT

was entirely dependent on PIDD1 recruitment to the centrosome, as both SCLT1 and ANKRD26 knock-out cell lines displayed no activation (Fig. 20A). To our great surprise, this activation was not resulting from an increase in centrosome number, as CPT treatment did not impinge on centrosome abundance in our experimental conditions (Fig. 20B), nor on PIDD1 levels at the centrosome (Fig. 21A). Furthermore, this phenomenon was not restricted to A549 cells, as RPE1 derivatives exhibited a similar behaviour (Fig. 21B-D).

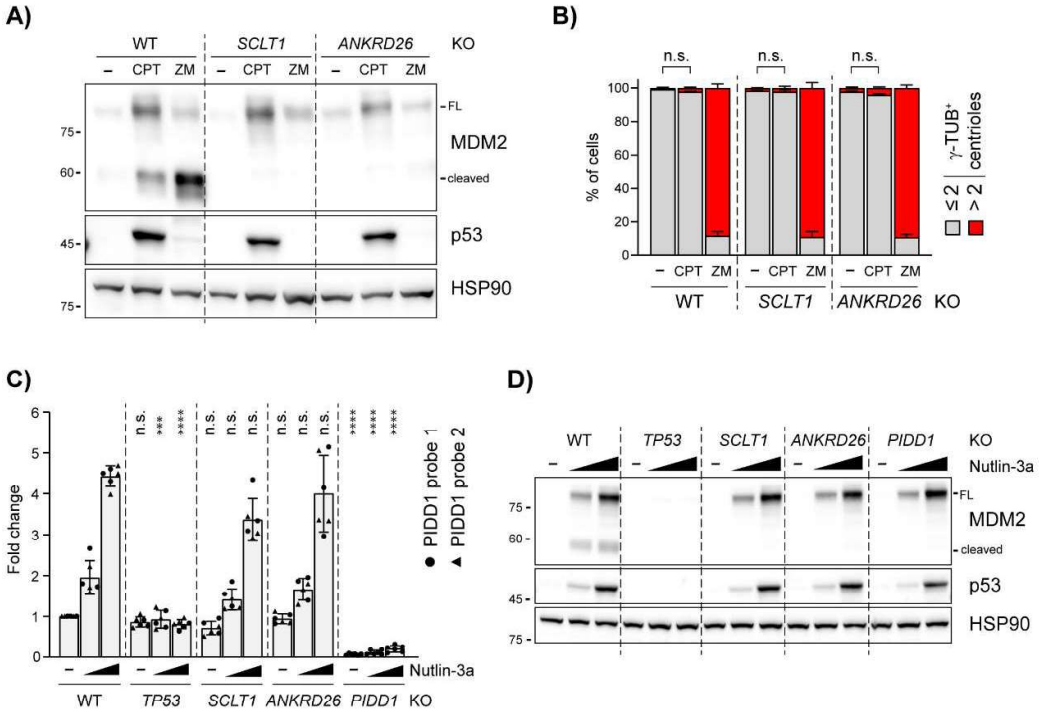

Figure 20. PIDD1 localization to DAs is required for PIDDosome activation in response to DNA damage. (A) A549 cells of the indicated genotypes were treated for 24h as indicated (CPT = camptothecin, ZM = ZM447439). Samples were subjected to immunoblotting; n = 3 independent experiments. (B) A549 cells treated as in (A) were subjected to fluorescence microscopy and centrosome abundance was assessed by visually scoring γ-tubulin-positive centrioles per cell. Mean values ± s.e.m. are reported. N = 3, ≥ 50 cells from each independent experiment. ANOVA test (n.s. = non-significant). (C) RT-qPCR analysis of PIDD1 mRNA expression in A549 cells upon treatment with increasing doses of Nutlin 3a (i.e. 3.3 μM or 10 μM) using two independent probes. The average fold of induction ± standard deviation is shown. N = 3 biological replicates with two technical replicates each. Comparisons were performed between treatments of every genotype and the corresponding treatment of wild type (WT) cells, ANOVA test (****P < 0.0001; ***P < 0.001; n.s. = non-significant). (D) Immunoblot analysis of samples treated as in (C). N = 3 independent experiments.

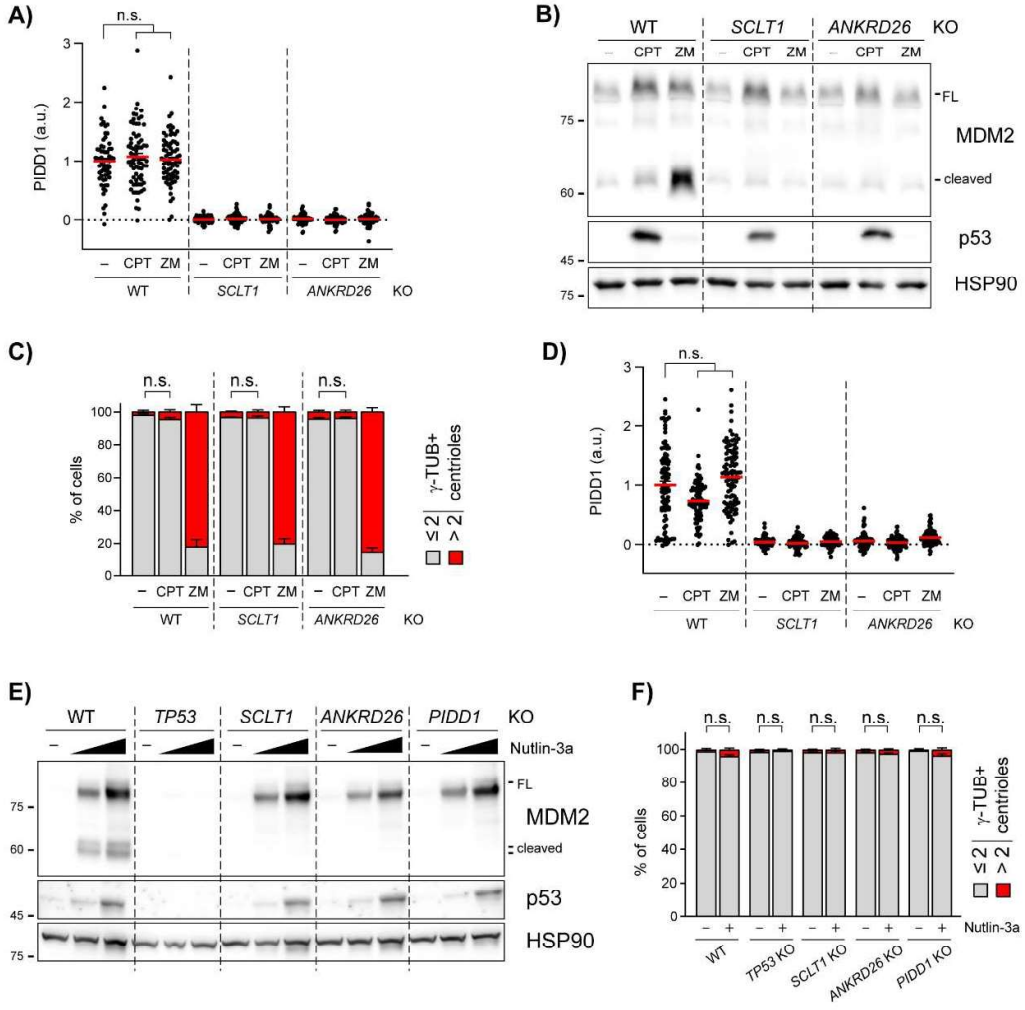

Figure 21. PIDD1 localization to DAs is required for PIDDosome activation in response to DNA damage also in RPE1 cells. (A) Dot plot showing the average pixel intensities of PIDD1 at individual parent centrioles in A549 cells of the indicated genotypes and treatments (CPT = camptothecin, ZM = ZM447439). Mean values (red lines) ± s.e.m. are reported. N > 50 centrosomes were assessed for each condition in as many individual cells; a.u. = arbitrary units. Kruskal-Wallis test (n.s. = non-significant). (B) RPE1 cells of the indicated genotypes were treated either with CPT or ZM or DMSO for 24h. Samples were subjected to immunoblotting; n = 3 independent experiments. (C) RPE1 cells treated as in (B) were subjected to fluorescence microscopy and centrosome abundance was assessed by counting the number of γ-tubulin-positive centrioles per cell across different genotypes and treatments. Mean values ± s.e.m. are reported. N = 3, ≥ 50 cells from each independent experiment. ANOVA test (n.s. = non-significant). (D) Dot plot showing the average pixel intensities of PIDD1 at individual parent centrioles in RPE1 of the indicated genotypes and treatments. Mean values (red lines) ± s.e.m. are reported. N > 50 centrosomes were assessed for each condition in as many individual cells; a.u. = arbitrary units. Kruskal-Wallis test (n.s. = nonsignificant). (E) RPE1 cells of the indicated genotypes were either left untreated or treated with Nutlin-3a (3.3 μM or 10 μM). Cells were subjected to immunoblotting; n = 3 independent experiments. (F) A549 cells were either treated with 10 μM Nutlin-3a for 24h or left untreated. Cells were subjected to fluorescence

microscopy and centrosome abundance was assessed by counting the number of γ-tubulin-positive centrioles per cell across different genotypes and treatments. Mean values ± s.e.m. are reported. N = 3, ≥ 50 cells from each independent experiment. ANOVA test (n.s. = non-significant).

As our data with CPT were obtained in two p53-proficient cell lines, we reasoned that p53-dependent *PIDD1* transactivation (Lin *et al*, 2000) could be responsible of centrosome-dependent PIDDosome activation in response to DNA damage. To test this notion, we induced non-genotoxic p53 activation using the small molecule MDM2 inhibitor Nutlin-3a (Vassilev *et al*, 2004), which led to a p53- and dose- dependent elevation of PIDD1 mRNA (Fig. 20C). Conceivably, this p53- dependent phenomenon did not require the presence of intact DAs. Strikingly, however, p53 stabilization was accompanied by the appearance of MDM2 cleavage fragments only in wild type cells, while DAP knock-out cell lines completely blunted Nutlin-3a-dependent PIDDosome activation (Fig. 20D). Similar results were obtained for RPE1 cells, excluding the possibility of cell line dependent artifacts (Fig. 21E). Furthermore, no significant increase in centrosome number was detected upon Nutlin-3a treatment, ruling out the possibility of PIDDosome activation was due to this event (Fig. 21F). Taken together, our results demonstrate that while an elevation of PIDD1 expression, such as during the DNA damage response, is sufficient to bypass the requirement for extra centrosomes to promote PIDDosome activation, it still requires the concomitant local accumulation of the PIDD1 precursor in the vicinity of the centrosome's DAs.

DISCUSSION

In healthy cells, centrosome number is accurately controlled, as this organelle exerts a crucial role for correct and timely chromosome segregation. Thus, continuous cell proliferation preventing centrosome amplification or depletion is assured by several mechanisms, among which a regulated centriole duplication, tightly coupled with the cell division cycle, and a faithful distribution between daughter cells at the end of cell division. Since centrosome abnormalities can lead to the assembly of abnormal mitotic spindles and, consequently, to aneuploidy and oncogenesis, cells have evolved specific signalling cascades which sense these defects and induce cell cycle arrest, mainly relying on p53 activation.

It has been previously reported that the multiprotein complex PIDDosome is specifically activated upon cytokinesis failure, acting as an essential and nonredundant p53 activator, engaged as a surveillance mechanism responsive to supernumerary centrosomes (Fava *et al*, 2017). Even if the PIDDosome component PIDD1 has been reported to localize at the centrosome, numerous mechanistic aspects of how cells sense extra centrosomes remained unanswered.

Here, starting from a super resolution microscopy approach, PIDD1 protein localization at the periphery of DAs has been precisely shown. In addition, yeast-two-hybrid established a direct interaction between PIDD1 and ANKRD26, a protein recently annotated as peripheral component of DAs (Bowler *et al*, 2019). Furthermore, we defined the ANKRD26 fragment interacting with PIDD1: the PMID (PIDD1 Minimal Interaction Domain, amino acids 911-1181). Importantly, the ANKRD26' PMID appeared dispensable for its recruitment to DAs, yet necessary for PIDD1 localization, validating the physiological relevance of the yeast-two-hybrid interaction. Taking into consideration the high exchange rate displayed between PIDD1 centrosomal and cytoplasmic fractions measured by FRAP (Fig. 18), it is not surprising that PIDD1 has never been identified in centrosomal protein inventories relying on biochemical isolation of centrosomes followed by shotgun proteomics (Jakobsen *et al*, 2011). Reverse genetics instead readily circumstantiated the notion that PIDD1 is a novel bona fide DAP whose localization depends on ANKRD26 (Fig. 9 and Fig. 11). Moreover, DAP-deficient cellular derivatives allowed us to solidly establish a direct link between PIDD1 centrosomal localization and its ability to sustain PIDDosome activation (Fig. 12). Furthermore, PIDDosome

activation and PC formation appeared as genetically separable determinants of DAPs (Fig. 10). This did not only allow to avoid confounding effects in our analyses but could also clearly establish that DAs bear novel functions that had not been appreciated to date, namely activating the PIDDosome to signal to p53.

The potential implications of this work on human pathophysiology go beyond tumour suppression. The *ANKRD26* locus has been in fact associated to autosomal dominant thrombocytopenia, a bleeding disorder caused by platelet depletion (Noris *et al*, 2011). The megakaryocyte, the platelets' cellular precursor, physiologically reaches a hyperploid state via consecutive rounds of endomitosis, thereby carrying supernumerary centrosomes (Nagata *et al*, 1997). Thus, megakaryocytes must naturally prevent PIDDosome activation. Intriguingly, one study has demonstrated that *ANKRD26* becomes normally silenced during late stages of healthy megakaryopoiesis and that *ANKRD26* mutations found in thrombocytopenic patients compromise the abovementioned repression (Bluteau *et al*, 2014). Taken together, the findings presented in this Thesis contribute to explain how megakaryocytes can tolerate supernumerary centrosomes and, on the other hand, suggest that pharmacologically inhibiting the PIDDosome, e.g. via available Caspase-2 inhibitors (Poreba *et al*, 2019), might have beneficial effects on thrombocytopenic patients carrying *ANKRD26* mutations.

The structural determinants of PIDD1 autoproteolysis were defined in a rigorous way (Tinel *et al*, 2007). However, such analysis preceded the discovery of the dependency of PIDDosome activation on centrosomes (Fava et al, 2017). Thus, the physiological relevance of PIDD1 autoproteolytic fragments has remained elusive. Clearly, the generation of the shortest C-terminal fragment, PIDD1-CC, appears necessary for PIDDosome activation by extra centrosomes (Fig. 15). Lack of ANKRD26 and more upstream DAPs impinged on PIDD1 function independently of its protein stability and of its autoproteolytic processing, highlighting that PIDDosome activation requires both PIDD1 localization and autoproteolysis, two elements that are not interdependent (Fig. 15 and 16). Moreover, the fact that centrosomes selectively recruit the PIDD1 precursor clearly allows to temporally order the events: PIDDosome activation is preceded by i) recruitment of the PIDD1 precursor to DAs downstream of ANKRD26 and subsequently by ii) PIDD1 autoproteolysis into PIDD1-CC. While the quick turnover of PIDD1 at the centrosomes readily supports the model according to which the centrosome primes autoproteolytic PIDD1-CC fragments for PIDDosome activation, the molecular nature of this priming remains unclear. The simplest model predicts that PIDD1 might require local

autoproteolysis in the proximity of the centrosome, yet alternative models, suggesting for example proteolysis of the PIDD1 precursor in the cytoplasm after acquisition of a post-translational modification at the centrosome, cannot be excluded.

PIDD1 localization at DAs and PIDD1 precursor autoproteolysis appear necessary for PIDDosome activation, yet they are not sufficient as they all occur constitutively. How can the system discriminate between the presence of a single parent centriole and the simultaneous presence of two parent centrioles? The maturation of the youngest centrosome is accompanied by the acquisition of appendages on its oldest centriole and requires the mitotic traverse (Kong *et al*, 2014). During mitosis, and thus during the centrosome maturation process, PIDD1 appears to dissociate from the centrosome itself (Fig. 17A-B). During telophase, one of the two centrosomes (likely to be the oldest) becomes decorated by PIDD1 and, only eventually, the second centrosome recruits PIDD1 (Fig. 17A-B). Thus, in an unperturbed cell cycle, the only temporal window (i.e. telophase) in which two PIDD1-positive centrioles coexist in the same cell is characterized by maximal distance between those structures. Cytokinesis failure instead yields to the simultaneous presence of two juxtaposed PIDD1-positive structures (Fig. 17C), as short after cell division failure extra centrosomes show rapid directional movement towards each other (Fig. 17E-F). Importantly, perturbing the spatial arrangement of extra centrosomes uncouples the presence of two PIDD1-positive parent centrioles from PIDDosome activation (Fig. 19). Taken together, this evidence suggests that the presence of the physical proximity of two parent centrioles, a condition that is promoted by the microtubule network and maintained over time, can give rise to PIDDosome activation (Fig. 19).

Considering that the exact cellular cue leading to PIDDosome activation had remained mysterious, the data presented here demonstrate that the overall cellular availability of the PIDD1-CC species is not the only discriminant for PIDDosome activation. However, it can be speculated that the selective centrosome affinity for the PIDD1 precursor, together with the constitutively fast exchange rate of this species with the cytoplasmic PIDD1 pool, grants a higher local concentration of PIDD1-CC autoproteolytic product in the vicinity of the centrosome (Fig. 22). We propose that the simultaneous presence of two adjacent sources of PIDD1-CC, such as the clustered parent centrioles generated by cell division failure, critically contributes to surpass a concentration threshold, tipping the balance towards PIDDosome activation.

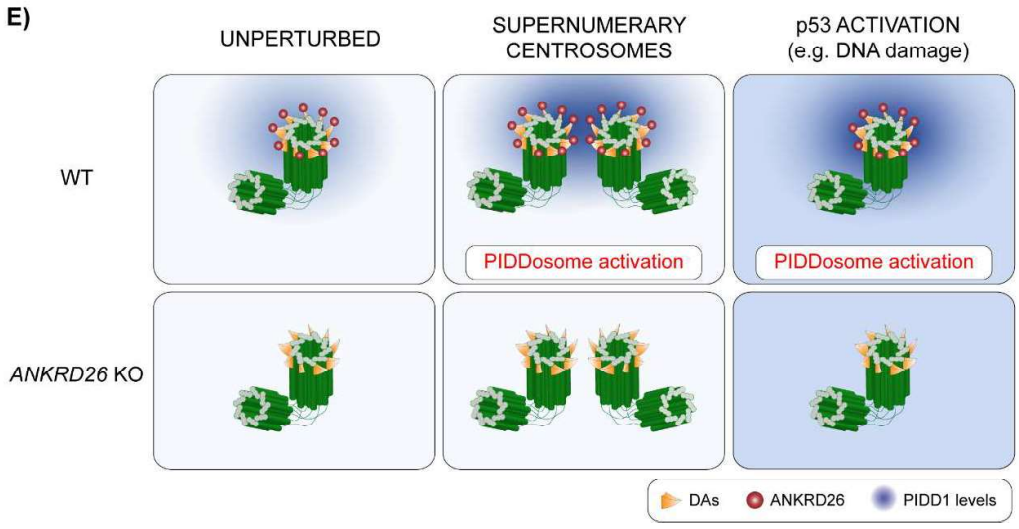

Figure 22. Proposed model for the centrosome-dependent PIDDosome activation upon different stimuli. The centrosome constitutively acts as PIDD1 centralizer. A local increase in PIDD1 concentration (achieved either by centrosome clustering or upon p53 activation) triggers PIDDosome activation. In ANKRD26-deficient cells, the inability of the centrosome to generate a local increase in PIDD1 concentration hinders the activation of the complex in response to both stimuli.

Additional work is needed to directly test the proposed model. In particular, it would be interesting to investigate whether artificially tethering PIDD1 to a cellular compartment other than the centrosome in cells devoid of this organelle could lead to PIDDosome activation as well. This experiment would address whether a high local concentration of PIDD1 active species is sufficient for PIDDosome activation or if additional centrosome-based cues are needed. Moreover, another aspect which should be clarified is the role of interphase centrosome clustering upon cytokinesis failure. The model hypothesized in this thesis suggests that centrosome clustering is a crucial event for PIDDosome activation. Nevertheless, it has not been determined whether sustained clustering is needed to promote the assembly of the complex or whether a transient clustering is sufficient to ignite the process. Clarifying these aspects would not only elucidate additional aspects of centrosome contribution to PIDDosome activation but also reveal whether p53 activation in this context is irreversible or whether an additional regulatory layer is present and carried out at the centrosome level.

Following the model proposed in this thesis, the ability of the centrosome to act as a PIDD1 centralizer could explain how PIDDosome activation is induced not only by supernumerary centrosomes but also in the context of the DNA damage response, leading it back to a single mechanism. In fact, the elevation of the overall PIDD1 levels promoted by p53-dependent *PIDD1* transactivation was shown to readily bypass PIDDosome activation requirement for extra centrosomes (Fig. 20) yet maintaining the dependency on PIDD1 precursor recruitment to the centrosome. While it cannot be excluded that the PIDDosome still assembles in the absence of PIDD1 recruitment to the centrosome and that the regulation of its activity towards MDM2 is exerted more downstream, the simplest model predicts that the centrosome directly contributes to the assembly of the complex. Furthermore, the data presented in this work clearly demonstrate that the centrosome is not only involved in generating a cell cycle inhibitory signal in response to mitotic malfunctions, but also contributes to shaping the DNA damage response. In fact, recent work has established that the PIDDosome is of paramount importance for dictating the p53 dynamic in response to ionizing radiation, with clear implications in determining the type of p53 response (Tsabar *et al*, 2020). Surprisingly, we demonstrate that i) the PIDDosome activation following DNA damage requires PIDD1 docking to the centrosome and that ii) this phenomenon does not necessarily rely on accumulation of extra centrosomes, e.g. via passage through a faulty mitosis. Nonetheless, the presence of supernumerary centrosomes might contribute rewiring cellular signalling triggered by DNA damage, e.g. synergizing on p53 activation.

In summary, this thesis offers new insights into the regulation of PIDDosome activation, proposing a model which is able not only to explain some mechanistic aspects of the cell response to supernumerary centrosomes but also to reconcile several seemingly unrelated or contradictory observations in the field. Firstly, it clarifies that PIDDosome assembly can indeed occur following DNA damage, as a consequence of p53-dependent *PIDD1* transactivation. Secondly, it explains why DNA damage triggers a robust PIDDosome activation in p53-defective cells only when they are forced into mitosis (e.g., through CHK1 inhibition) (Sidi *et al*, 2008). Conceivably, in this context PIDDosome assembly cannot rely on the p53-dependent elevation of PIDD1 levels but rather relies on the presence of supernumerary centrosomes, a common outcome of faulty mitoses arising in this experimental condition. Thirdly, it explains how the PIDDosome can be activated both upstream and downstream of p53. In the first scenario, PIDDosome assembly is triggered by the presence of extra centrosomes and results into p53 stabilization due to

Caspase-2-dependent MDM2 inactivation. On the contrary, in the context of DNA damage, the PIDDosome is engaged at a later stage, subsequently to p53 activation. Importantly, when the DNA damage response alone has failed to elicit a p53 output sufficient to halt cell division, PIDDosome activation becomes particularly prominent, imparting measurable changes to the dynamics of p53 accumulation (Tsabar *et al*, 2020). Considering that p53 dynamic is important to define the cellular fate upon DNA damage, it appears that the PIDDosome can act as an important fail-safe mechanism when the canonical DNA damage response signalling proves uncapable to effectively stop the cell division cycle (Fig. 23).

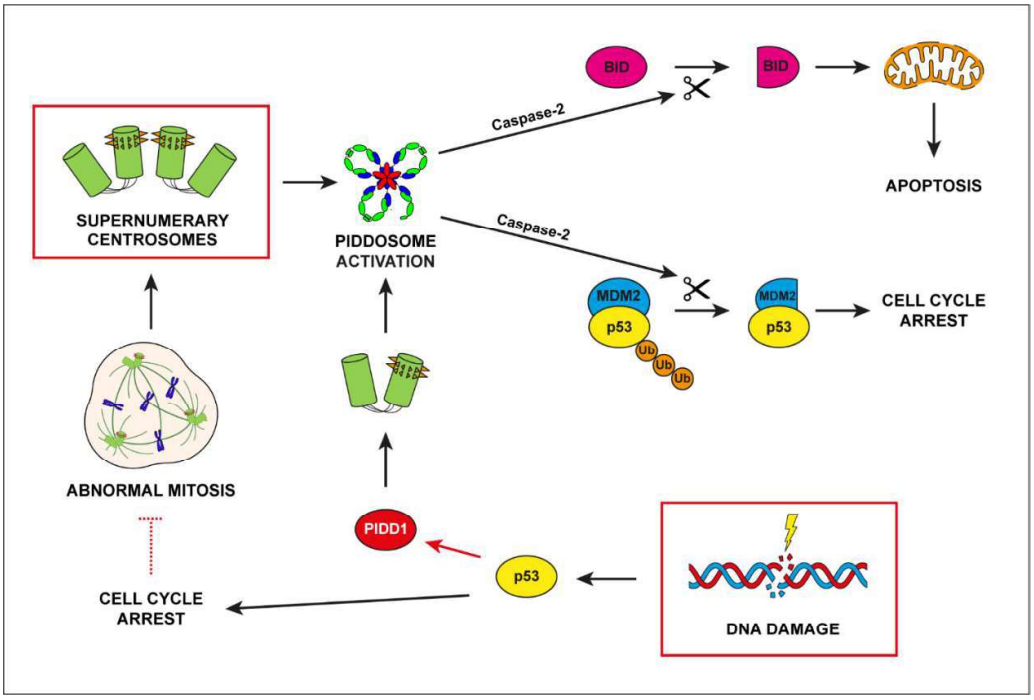

Figure 23. Sources and consequences of PIDDosome activation. Supernumerary centrosomes lead to Caspase-2 activation via the PIDDosome, resulting into either p53-dependent cell cycle arrest or apoptosis. DNA damage can induce PIDDosome activation following two different paradigms. In the first one, p53 stabilization transactivates *PIDD1*, resulting in a global increase in its cellular levels (red arrow). The centrosome, locally concentrating PIDD1 active moieties, leads to PIDDosome assembly. In the second scenario, cells which halted their cell cycle during DNA damage response can escape this proliferative block and re-enter mitosis (red dashed inhibitory arrow). Proliferation in the presence of unrepaired DNA damage or an under-replicated genome frequently leads to abnormal cell division and accumulation of supernumerary centrosomes, which eventually drive PIDDosome assembly. Caspase-2 activation promotes the proteolytic cleavage of its two main substrates, MDM2 and BID, culminating in cell cycle arrest or apoptosis, respectively.

Taken together, we speculate that the most physiological trigger for PIDDosome activation is the lack of cytokinesis, always resulting into the acquisition of supernumerary mature centrosomes. Yet, it appears that DNA damage alone or in combination with a faulty mitosis can trigger different degrees of PIDDosome activation, invariably relying on the centrosome as activatory scaffold to kickstart PIDDosome assembly (Fig. 23). The proposed model, however, does not clarify the contribution of p53-independent DNA damage response events in defining PIDDosome activation. It has been previously shown that PIDD1 death domain becomes phosphorylated at Thr788 in an ATM-dependent manner, promoting RAIDD binding and Caspase-2 autocatalytic activation (Ando *et al*, 2012). It will be interesting to investigate whether this and other posttranslational modifications can concur to set the threshold for PIDDosome activation capacity also in the context of a centrosome driven response, representing a general shared feature. Furthermore, an additional aspect that still remains elusive is what defines the output of PIDDosome activation. In fact, while in our experimental conditions the primary consequence of PIDDosome activation is a p53-dependent cell cycle arrest, Caspase-2 has also been shown to promote apoptosis in different settings. One might speculate that specific subcellular compartments possess peculiar PIDDosome regulators, as shown for NPM1 scaffolding activity towards PIDD1 in the nucleolus (Ando *et al*, 2017), thereby compartmentalizing Caspase-2 activity and concurring to promote distinct fates. Moreover, different cellular cues could be responsible for a distinctive posttranslational modification profile of PIDDosome components, ultimately resulting into differential proteolytic activities. Eventually, since cell cycle blockade depends on MDM2 cleavage whereas apoptosis relies additionally on the proteolytic processing of the proapoptotic BCL-2 family member BID (Guo *et al*, 2002; López-García *et al*, 2017), it could be speculated that PIDDosome-dependent cell fate determination could be shaped by the relative abundance of Caspase-2 key substrates at its primary activation site.

In conclusion, we have started to uncover how the centrosome can generate signals able to modulate cellular signalling and thus influence the cellular behaviour. Considering that several other crucial mediators of the DNA damage response, such as BRCA1, BRCA2 and p53 itself have been shown to physically localize at the centrosome (Contadini *et al*, 2019; Hsu & White, 1998; Nakanishi *et al*, 2007), future investigations will unveil how the centrosome can contribute to the coordination of signalling events across different subcellular compartments, namely the nucleus and the cytoplasm, thereby providing a molecular understanding of the carcinogenic role of extra centrosomes.

REFERENCES

Ahrné E, Glatter T, Viganò C, Schubert C von, Nigg EA & Schmidt A (2016) Evaluation and Improvement of Quantification Accuracy in Isobaric Mass Tag-Based Protein Quantification Experiments. *J Proteome Res* 15: 2537–2547

Andersen JS, Wilkinson CJ, Mayor T, Mortensen P, Nigg EA & Mann M (2003) Proteomic characterization of the human centrosome by protein correlation profiling. *Nature* 426: 570–574

Ando K, Kernan JL, Liu PH, Sanda T, Logette E, Tschopp J, Look AT, Wang J, Bouchier-Hayes L & Sidi S (2012) PIDD death-domain phosphorylation by ATM controls prodeath versus prosurvival PIDDosome signaling. *Mol Cell* 47: 681–693

Ando K, Parsons MJ, Shah RB, Charendoff CI, Paris SL, Liu PH, Fassio SR, Rohrman BA, Thompson R, Oberst A, *et al* (2017) NPM1 directs PIDDosome-dependent caspase-2 activation in the nucleolus. *J Cell Biol* 216: 1795–1810

Andreassen PR & Margolis RL (1994) Microtubule dependency of p34cdc2 inactivation and mitotic exit in mammalian cells. *J Cell Biol* 127: 789–802

Arnandis T, Monteiro P, Adams SD, Bridgeman VL, Rajeeve V, Gadaleta E, Marzec J, Chelala C, Malanchi I, Cutillas PR, *et al* (2018) Oxidative Stress in Cells with Extra Centrosomes Drives Non-Cell-Autonomous Invasion. *Dev Cell* 47: 409-424.e9

Aylon Y, Michael D, Shmueli A, Yabuta N, Nojima H & Oren M (2006) A positive feedback loop between the p53 and Lats2 tumor suppressors prevents tetraploidization. *Genes Dev* 20: 2687–2700

Bahe S, Stierhof Y-D, Wilkinson CJ, Leiss F & Nigg EA (2005) Rootletin forms centriole-associated filaments and functions in centrosome cohesion. *J Cell Biol* 171: 27–33

Baliga BC, Read SH & Kumar S (2004) The biochemical mechanism of caspase-2 activation. *Cell Death Differ* 11: 1234–1241

Basto R, Brunk K, Vinadogrova T, Peel N, Franz A, Khodjakov A & Raff JW (2008) Centrosome amplification can initiate tumorigenesis in flies. *Cell* 133: 1032–1042

Basto R, Lau J, Vinogradova T, Gardiol A, Woods CG, Khodjakov A & Raff JW (2006) Flies without centrioles. *Cell* 125: 1375–1386

Bazzi H & Anderson KV (2014) Acentriolar mitosis activates a p53-dependent apoptosis pathway in the mouse embryo. *Proc Natl Acad Sci U S A* 111: E1491-1500

Berube C, Boucher L-M, Ma W, Wakeham A, Salmena L, Hakem R, Yeh W-C, Mak TW & Benchimol S (2005) Apoptosis caused by p53-induced protein with death domain (PIDD) depends on the death adapter protein RAIDD. *Proc Natl Acad Sci U S A* 102: 14314–14320

Bettencourt-Dias M, Rodrigues-Martins A, Carpenter L, Riparbelli M, Lehmann L, Gatt MK, Carmo N, Balloux F, Callaini G & Glover DM (2005) SAK/PLK4 Is Required for Centriole Duplication and Flagella Development. *Current Biology* 15: 2199–2207

Blangy A, Lane HA, d'Hérin P, Harper M, Kress M & Nigg EA (1995) Phosphorylation by p34cdc2 regulates spindle association of human Eg5, a kinesin-related motor essential for bipolar spindle formation in vivo. *Cell* 83: 1159–1169

Bluteau D, Balduini A, Balayn N, Currao M, Nurden P, Deswarte C, Leverger G, Noris P, Perrotta S, Solary E, *et al* (2014) Thrombocytopenia-associated mutations in the ANKRD26 regulatory region induce MAPK hyperactivation. *J Clin Invest* 124: 580–591

Bobinnec Y, Moudjou M, Fouquet JP, Desbruyères E, Eddé B & Bornens M (1998) Glutamylation of centriole and cytoplasmic tubulin in proliferating non-neuronal cells. *Cell Motil Cytoskeleton* 39: 223–232

Bowler M, Kong D, Sun S, Nanjundappa R, Evans L, Farmer V, Holland A, Mahjoub MR, Sui H & Loncarek J (2019) High-resolution characterization of centriole distal appendage morphology and dynamics by correlative STORM and electron microscopy. *Nat Commun* 10: 993

Brito DA & Rieder CL (2006) Mitotic checkpoint slippage in humans occurs via cyclin B destruction in the presence of an active checkpoint. *Curr Biol* 16: 1194–1200

Brown-Suedel AN & Bouchier-Hayes L (2020) Caspase-2 Substrates: To Apoptosis, Cell Cycle Control, and Beyond. *Front Cell Dev Biol* 8

Chen D & Huang S (2001) Nucleolar components involved in ribosome biogenesis cycle between the nucleolus and nucleoplasm in interphase cells. *J Cell Biol* 153: 169–176

Chong WM, Wang W-J, Lo C-H, Chiu T-Y, Chang T-J, Liu Y-P, Tanos B, Mazo G, Tsou M-FB, Jane W-N, *et al* (2020) Super-resolution microscopy reveals coupling between mammalian centriole subdistal appendages and distal appendages. *Elife* 9

Ciciarello M, Mangiacasale R, Casenghi M, Zaira Limongi M, D'Angelo M, Soddu S, Lavia P & Cundari E (2001) p53 displacement from centrosomes and p53-mediated G1 arrest following transient inhibition of the mitotic spindle. *J Biol Chem* 276: 19205–19213

Cimini D (2008) Merotelic kinetochore orientation, aneuploidy, and cancer. *Biochim Biophys Acta* 1786: 32–40

Clare DK, Magescas J, Piolot T, Dumoux M, Vesque C, Pichard E, Dang T, Duvauchelle B, Poirier F & Delacour D (2014) Basal foot MTOC organizes pillar MTs required for coordination of beating cilia. *Nat Commun* 5: 4888

Coelho PA, Bury L, Shahbazi MN, Liakath-Ali K, Tate PH, Wormald S, Hindley CJ, Huch M, Archer J, Skarnes WC, *et al* (2015) Over-expression of Plk4 induces centrosome amplification, loss of primary cilia and associated tissue hyperplasia in the mouse. *Open Biol* 5: 150209

Contadini C, Monteonofrio L, Virdia I, Prodosmo A, Valente D, Chessa L, Musio A, Fava LL, Rinaldo C, Di Rocco G, *et al* (2019) p53 mitotic centrosome localization preserves centrosome integrity and works as sensor for the mitotic surveillance pathway. *Cell Death Dis* 10: 850

Cortés-Ciriano I, Lee JJ-K, Xi R, Jain D, Jung YL, Yang L, Gordenin D, Klimczak LJ, Zhang C-Z, Pellman DS, *et al* (2020) Comprehensive analysis of chromothripsis in 2,658 human cancers using whole-genome sequencing. *Nat Genet* 52: 331–341

Crasta K, Ganem NJ, Dagher R, Lantermann AB, Ivanova EV, Pan Y, Nezi L, Protopopov A, Chowdhury D & Pellman D (2012) DNA breaks and chromosome pulverization from errors in mitosis. *Nature* 482: 53–58

Danielsson F, Mahdessian D, Axelsson U, Sullivan D, Uhlén M, Andersen JS, Thul PJ & Lundberg E (2020) Spatial Characterization of the Human Centrosome Proteome Opens Up New Horizons for a Small but Versatile Organelle. *Proteomics*: e1900361

Debec A, Sullivan W & Bettencourt-Dias M (2010) Centrioles: active players or passengers during mitosis? *Cell Mol Life Sci* 67: 2173–2194

Ditchfield C, Johnson VL, Tighe A, Ellston R, Haworth C, Johnson T, Mortlock A, Keen N & Taylor SS (2003) Aurora B couples chromosome alignment with anaphase by targeting BubR1, Mad2, and Cenp-E to kinetochores. *J Cell Biol* 161: 267–280

Dodson H, Bourke E, Jeffers LJ, Vagnarelli P, Sonoda E, Takeda S, Earnshaw WC, Merdes A & Morrison C (2004) Centrosome amplification induced by DNA damage occurs during a prolonged G2 phase and involves ATM. *EMBO J* 23: 3864–3873

Doxsey S, Zimmerman W & Mikule K (2005) Centrosome control of the cell cycle. *Trends in Cell Biology* 15: 303–311

Edelheit O, Hanukoglu A & Hanukoglu I (2009) Simple and efficient site-directed mutagenesis using two single-primer reactions in parallel to generate mutants for protein structure-function studies. *BMC Biotechnol* 9: 61

Farina F, Gaillard J, Guérin C, Couté Y, Sillibourne J, Blanchoin L & Théry M (2016) The centrosome is an actin-organizing centre. *Nat Cell Biol* 18: 65–75

Fava LL, Schuler F, Sladky V, Haschka MD, Soratroi C, Eiterer L, Demetz E, Weiss G, Geley S, Nigg EA, *et al* (2017) The PIDDosome activates p53 in response to supernumerary centrosomes. *Genes Dev* 31: 34–45

Filippova N, Yang X, King P & Nabors LB (2012) Phosphoregulation of the RNA-binding protein Hu antigen R (HuR) by Cdk5 affects centrosome function. *J Biol Chem* 287: 32277–32287

Fliegauf M, Benzing T & Omran H (2007) When cilia go bad: cilia defects and ciliopathies. *Nature Reviews Molecular Cell Biology* 8: 880–893

Fong CS, Mazo G, Das T, Goodman J, Kim M, O'Rourke BP, Izquierdo D & Tsou M-FB (2016) 53BP1 and USP28 mediate p53-dependent cell cycle arrest in response to centrosome loss and prolonged mitosis. *Elife* 5

Freed E, Lacey KR, Huie P, Lyapina SA, Deshaies RJ, Stearns T & Jackson PK (1999) Components of an SCF ubiquitin ligase localize to the centrosome and regulate the centrosome duplication cycle. *Genes Dev* 13: 2242–2257

Fromont-Racine M, Rain JC & Legrain P (1997) Toward a functional analysis of the yeast genome through exhaustive two-hybrid screens. *Nat Genet* 16: 277–282

Fry AM (2002) The Nek2 protein kinase: a novel regulator of centrosome structure. *Oncogene* 21: 6184–6194

Fujiwara T, Bandi M, Nitta M, Ivanova EV, Bronson RT & Pellman D (2005) Cytokinesis failure generating tetraploids promotes tumorigenesis in p53-null cells. *Nature* 437: 1043–1047

Fukasawa K (2007) Oncogenes and tumour suppressors take on centrosomes. *Nat Rev Cancer* 7: 911–924

Ganem NJ, Cornils H, Chiu S-Y, O'Rourke KP, Arnaud J, Yimlamai D, Théry M, Camargo FD & Pellman D (2014) Cytokinesis failure triggers hippo tumor suppressor pathway activation. *Cell* 158: 833–848

Ganem NJ, Godinho SA & Pellman D (2009) A mechanism linking extra centrosomes to chromosomal instability. *Nature* 460: 278–282

Gilles J-F, Dos Santos M, Boudier T, Bolte S & Heck N (2017) DiAna, an ImageJ tool for object-based 3D co-localization and distance analysis. *Methods* 115: 55–64

Godinho S (2017) Centrosomes: PIDDosome Joins the Counting Game. *Curr Biol* 27: R237–R239

Godinho SA, Picone R, Burute M, Dagher R, Su Y, Leung CT, Polyak K, Brugge JS, Théry M & Pellman D (2014) Oncogene-like induction of cellular invasion from centrosome amplification. *Nature* 510: 167–171

Gönczy P (2012) Towards a molecular architecture of centriole assembly. *Nat Rev Mol Cell Biol* 13: 425–435

Gönczy P & Hatzopoulos GN (2019) Centriole assembly at a glance. *J Cell Sci* 132

Graser S, Stierhof Y-D, Lavoie SB, Gassner OS, Lamla S, Le Clech M & Nigg EA (2007) Cep164, a novel centriole appendage protein required for primary cilium formation. *J Cell Biol* 179: 321–330

Guarguaglini G, Duncan PI, Stierhof YD, Holmström T, Duensing S & Nigg EA (2005) The forkhead-associated domain protein Cep170 interacts with Polo-like kinase 1 and serves as a marker for mature centrioles. *Mol Biol Cell* 16: 1095–1107

Gundersen GG & Bulinski JC (1986) Microtubule arrays in differentiated cells contain elevated levels of a post-translationally modified form of tubulin. *Eur J Cell Biol* 42: 288–294

Guo Y, Srinivasula SM, Druilhe A, Fernandes-Alnemri T & Alnemri ES (2002) Caspase-2 induces apoptosis by releasing proapoptotic proteins from mitochondria. *J Biol Chem* 277: 13430–13437

Habedanck R, Stierhof Y-D, Wilkinson CJ & Nigg EA (2005) The Polo kinase Plk4 functions in centriole duplication. *Nat Cell Biol* 7: 1140–1146

Hardy T, Lee M, Hames RS, Prosser SL, Cheary D-M, Samant MD, Schultz F, Baxter JE, Rhee K & Fry AM (2014) Multisite phosphorylation of C-Nap1 releases it from Cep135 to trigger centrosome disjunction. *J Cell Sci* 127: 2493–2506

Heinz LX, Rebsamen M, Rossi DC, Staehli F, Schroder K, Quadroni M, Gross O, Schneider P & Tschopp J (2012) The death domain-containing protein Unc5CL is a novel MyD88-independent activator of the pro-inflammatory IRAK signaling cascade. *Cell Death Differ* 19: 722–731

Hinchcliffe EH, Miller FJ, Cham M, Khodjakov A & Sluder G (2001) Requirement of a centrosomal activity for cell cycle progression through G1 into S phase. *Science* 291: 1547–1550

Holland AJ, Fachinetti D, Zhu Q, Bauer M, Verma IM, Nigg EA & Cleveland DW (2012) The autoregulated instability of Polo-like kinase 4 limits centrosome duplication to once per cell cycle. *Genes Dev* 26: 2684–2689

Hori A & Toda T (2017) Regulation of centriolar satellite integrity and its physiology. *Cell Mol Life Sci* 74: 213–229

Horn HF & Vousden KH (2007) Coping with stress: multiple ways to activate p53. *Oncogene* 26: 1306–1316

Hsiau T, Conant D, Rossi N, Maures T, Waite K, Yang J, Joshi S, Kelso R, Holden K, Enzmann BL, *et al* (2019) Inference of CRISPR Edits from Sanger Trace Data. *bioRxiv*: 251082

Hsu LC & White RL (1998) BRCA1 is associated with the centrosome during mitosis. *Proc Natl Acad Sci U S A* 95: 12983–12988

Iaconis D, Monti M, Renda M, van Koppen A, Tammaro R, Chiaravalli M, Cozzolino F, Pignata P, Crina C, Pucci P, *et al* (2017) The centrosomal OFD1 protein interacts with the translation machinery and regulates the synthesis of specific targets. *Sci Rep* 7: 1224

Ishikawa H & Marshall WF (2011) Ciliogenesis: building the cell's antenna. *Nature Reviews Molecular Cell Biology* 12: 222–234

Jaiswal S & Singh P (2020) Centrosome dysfunction in human diseases. *Semin Cell Dev Biol*

Jakobsen L, Vanselow K, Skogs M, Toyoda Y, Lundberg E, Poser I, Falkenby LG, Bennetzen M, Westendorf J, Nigg EA, *et al* (2011) Novel asymmetrically localizing components of human centrosomes identified by complementary proteomics methods. *EMBO J* 30: 1520–1535

Janssen A, van der Burg M, Szuhai K, Kops GJPL & Medema RH (2011) Chromosome segregation errors as a cause of DNA damage and structural chromosome aberrations. *Science* 333: 1895–1898

Janssens S, Tinel A, Lippens S & Tschopp J (2005) PIDD mediates NF-kappaB activation in response to DNA damage. *Cell* 123: 1079–1092

Joachim J, Razi M, Judith D, Wirth M, Calamita E, Encheva V, Dynlacht BD, Snijders AP, O'Reilly N, Jefferies HBJ, *et al* (2017) Centriolar Satellites Control GABARAP Ubiquitination and GABARAP-Mediated Autophagy. *Curr Biol* 27: 2123-2136.e7

Julien O, Zhuang M, Wiita AP, O'Donoghue AJ, Knudsen GM, Craik CS & Wells JA (2016) Quantitative MS-based enzymology of caspases reveals distinct protein substrate specificities, hierarchies, and cellular roles. *PNAS* 113: E2001–E2010

Jullien D, Vagnarelli P, Earnshaw WC & Adachi Y (2002) Kinetochore localisation of the DNA damage response component 53BP1 during mitosis. *J Cell Sci* 115: 71–79

Khodjakov A, Cole RW, Oakley BR & Rieder CL (2000) Centrosome-independent mitotic spindle formation in vertebrates. *Curr Biol* 10: 59–67

Khodjakov A & Rieder CL (2001) Centrosomes enhance the fidelity of cytokinesis in vertebrates and are required for cell cycle progression. *J Cell Biol* 153: 237–242

Kim M, O'Rourke BP, Soni RK, Jallepalli PV, Hendrickson RC & Tsou M-FB (2016) Promotion and Suppression of Centriole Duplication Are Catalytically Coupled through PLK4 to Ensure Centriole Homeostasis. *Cell Reports* 16: 1195–1203

Kleylein-Sohn J, Westendorf J, Le Clech M, Habedanck R, Stierhof Y-D & Nigg EA (2007) Plk4-induced centriole biogenesis in human cells. *Dev Cell* 13: 190–202

Kong D, Farmer V, Shukla A, James J, Gruskin R, Kiriyama S & Loncarek J (2014) Centriole maturation requires regulated Plk1 activity during two consecutive cell cycles. *J Cell Biol* 206: 855–865

Kulukian A, Holland AJ, Vitre B, Naik S, Cleveland DW & Fuchs E (2015) Epidermal development, growth control, and homeostasis in the face of centrosome amplification. *Proc Natl Acad Sci U S A* 112: E6311-6320

Kunimoto K, Yamazaki Y, Nishida T, Shinohara K, Ishikawa H, Hasegawa T, Okanoue T, Hamada H, Noda T, Tamura A, *et al* (2012) Coordinated ciliary beating requires Odf2-mediated polarization of basal bodies via basal feet. *Cell* 148: 189–200

Lambrus BG, Daggubati V, Uetake Y, Scott PM, Clutario KM, Sluder G & Holland AJ (2016) A USP28-53BP1-p53-p21 signaling axis arrests growth after centrosome loss or prolonged mitosis. *J Cell Biol* 214: 143–153

Lambrus BG, Uetake Y, Clutario KM, Daggubati V, Snyder M, Sluder G & Holland AJ (2015) p53 protects against genome instability following centriole duplication failure. *J Cell Biol* 210: 63–77

Lamkanfi M, Declercq W, Kalai M, Saelens X & Vandenabeele P (2002) Alice in caspase land. A phylogenetic analysis of caspases from worm to man. *Cell Death Differ* 9: 358–361

Lee CM, Aizawa K, Jiang J, Kung SKP & Jain R (2019) JLP-centrosome is essential for the microtubule-mediated nucleocytoplasmic transport induced by extracellular stimuli. *Sci Adv* 5: eaav0318

Lee JY & Stearns T (2013) FOP is a centriolar satellite protein involved in ciliogenesis. *PLoS One* 8: e58589

Levine MS, Bakker B, Boeckx B, Moyett J, Lu J, Vitre B, Spierings DC, Lansdorp PM, Cleveland DW, Lambrechts D, *et al* (2017) Centrosome Amplification Is Sufficient to Promote Spontaneous Tumorigenesis in Mammals. *Dev Cell* 40: 313-322.e5

Lin Y, Ma W & Benchimol S (2000) Pidd, a new death-domain-containing protein, is induced by p53 and promotes apoptosis. *Nat Genet* 26: 122–127

Lingle WL, Barrett SL, Negron VC, D'Assoro AB, Boeneman K, Liu W, Whitehead CM, Reynolds C & Salisbury JL (2002) Centrosome amplification drives chromosomal instability in breast tumor development. *Proc Natl Acad Sci U S A* 99: 1978–1983

Lopes CAM, Mesquita M, Cunha AI, Cardoso J, Carapeta S, Laranjeira C, Pinto AE, Pereira-Leal JB, Dias-Pereira A, Bettencourt-Dias M, *et al* (2018) Centrosome amplification arises before neoplasia and increases upon p53 loss in tumorigenesis. *J Cell Biol* 217: 2353–2363

López-García C, Sansregret L, Domingo E, McGranahan N, Hobor S, Birkbak NJ, Horswell S, Grönroos E, Favero F, Rowan AJ, *et al* (2017) BCL9L Dysfunction Impairs Caspase-2 Expression Permitting Aneuploidy Tolerance in Colorectal Cancer. *Cancer Cell* 31: 79–93

Mahjoub MR, Xie Z & Stearns T (2010) Cep120 is asymmetrically localized to the daughter centriole and is essential for centriole assembly. *J Cell Biol* 191: 331–346

Mancini M, Machamer CE, Roy S, Nicholson DW, Thornberry NA, Casciola-Rosen LA & Rosen A (2000) Caspase-2 is localized at the Golgi complex and cleaves golgin-160 during apoptosis. *J Cell Biol* 149: 603–612

Manzl C, Fava LL, Krumschnabel G, Peintner L, Tanzer MC, Soratroi C, Bock FJ, Schuler F, Luef B, Geley S, *et al* (2013) Death of p53-defective cells triggered by forced mitotic entry in the presence of DNA damage is not uniquely dependent on Caspase-2 or the PIDDosome. *Cell Death Dis* 4: e942

Manzl C, Krumschnabel G, Bock F, Sohm B, Labi V, Baumgartner F, Logette E, Tschopp J & Villunger A (2009) Caspase-2 activation in the absence of PIDDosome formation. *J Cell Biol* 185: 291–303

Manzl C, Peintner L, Krumschnabel G, Bock F, Labi V, Drach M, Newbold A, Johnstone R & Villunger A (2012) PIDDosome-independent tumor suppression by Caspase-2. *Cell Death Differ* 19: 1722–1732

Marshall WF (2009) Centriole Evolution. *Curr Opin Cell Biol* 21: 14–19

Mazo G, Soplop N, Wang W-J, Uryu K & Tsou MFB (2016) Spatial Control of Primary Ciliogenesis by Subdistal Appendages Alters Sensation-Associated Properties of Cilia. *Dev Cell* 39: 424–437

Meitinger F, Anzola JV, Kaulich M, Richardson A, Stender JD, Benner C, Glass CK, Dowdy SF, Desai A, Shiau AK, *et al* (2016) 53BP1 and USP28 mediate p53 activation and G1 arrest after centrosome loss or extended mitotic duration. *J Cell Biol* 214: 155–166

Meraldi P (2016) Centrosomes in spindle organization and chromosome segregation: a mechanistic view. *Chromosome Res* 24: 19–34

Merdes A, Heald R, Samejima K, Earnshaw WC & Cleveland DW (2000) Formation of Spindle Poles by Dynein/Dynactin-Dependent Transport of Numa. *J Cell Biol* 149: 851–862

Mogensen MM, Malik A, Piel M, Bouckson-Castaing V & Bornens M (2000) Microtubule minus-end anchorage at centrosomal and non-centrosomal sites: the role of ninein. *J Cell Sci* 113 (Pt 17): 3013–3023

Morleo M, Brillante S, Formisano U, Ferrante L, Carbone F, Iaconis D, Palma A, Buonomo V, Maione AS, Grumati P, *et al* (2020) Regulation of autophagosome biogenesis by OFD1-mediated selective autophagy. *EMBO J*: e105120

Moser SC, Bensaddek D, Ortmann B, Maure J-F, Mudie S, Blow JJ, Lamond AI, Swedlow JR & Rocha S (2013) PHD1 links cell-cycle progression to oxygen sensing through hydroxylation of the centrosomal protein Cep192. *Dev Cell* 26: 381–392

Moss DK, Bellett G, Carter JM, Liovic M, Keynton J, Prescott AR, Lane EB & Mogensen MM (2007) Ninein is released from the centrosome and moves bi-directionally along microtubules. *J Cell Sci* 120: 3064–3074

Moyer TC & Holland AJ (2019) PLK4 promotes centriole duplication by phosphorylating STIL to link the procentriole cartwheel to the microtubule wall. *eLife* 8: e46054

Mullee LI & Morrison CG (2016) Centrosomes in the DNA damage response--the hub outside the centre. *Chromosome Res* 24: 35–51

Nagata Y, Muro Y & Todokoro K (1997) Thrombopoietin-induced polyploidization of bone marrow megakaryocytes is due to a unique regulatory mechanism in late mitosis. *J Cell Biol* 139: 449–457

Nakanishi A, Han X, Saito H, Taguchi K, Ohta Y, Imajoh-Ohmi S & Miki Y (2007) Interference with BRCA2, which localizes to the centrosome during S and early M phase, leads to abnormal nuclear division. *Biochem Biophys Res Commun* 355: 34–40

Narita K & Takeda S (2015) Cilia in the choroid plexus: their roles in hydrocephalus and beyond. *Front Cell Neurosci* 9: 39

Nigg EA (2007) Centrosome duplication: of rules and licenses. *Trends Cell Biol* 17: 215–221

Nigg EA & Holland AJ (2018) Once and only once: mechanisms of centriole duplication and their deregulation in disease. *Nat Rev Mol Cell Biol* 19: 297–312

Nigg EA & Raff JW (2009) Centrioles, centrosomes, and cilia in health and disease. *Cell* 139: 663–678

Nigg EA & Stearns T (2011) The centrosome cycle: Centriole biogenesis, duplication and inherent asymmetries. *Nat Cell Biol* 13: 1154–1160

Noris P, Perrotta S, Seri M, Pecci A, Gnan C, Loffredo G, Pujol-Moix N, Zecca M, Scognamiglio F, De Rocco D, *et al* (2011) Mutations in ANKRD26 are responsible for a frequent form of inherited thrombocytopenia: analysis of 78 patients from 21 families. *Blood* 117: 6673–6680

Oliver TG, Meylan E, Chang GP, Xue W, Burke JR, Humpton TJ, Hubbard D, Bhutkar A & Jacks T (2011) Caspase-2-mediated cleavage of Mdm2 creates a p53-induced positive feedback loop. *Mol Cell* 43: 57–71

O'Reilly LA, Ekert P, Harvey N, Marsden V, Cullen L, Vaux DL, Hacker G, Magnusson C, Pakusch M, Cecconi F, *et al* (2002) Caspase-2 is not required for thymocyte or neuronal apoptosis even though cleavage of caspase-2 is dependent on both Apaf-1 and caspase-9. *Cell Death Differ* 9: 832–841

Oricchio E, Saladino C, Iacovelli S, Soddu S & Cundari E (2006) ATM is activated by default in mitosis, localizes at centrosomes and monitors mitotic spindle integrity. *Cell Cycle* 5: 88–92

Overlack K, Bange T, Weissmann F, Faesen AC, Maffini S, Primorac I, Müller F, Peters J-M & Musacchio A (2017) BubR1 Promotes Bub3-Dependent APC/C Inhibition during Spindle Assembly Checkpoint Signaling. *Curr Biol* 27: 2915-2927.e7

Panic M, Hata S, Neuner A & Schiebel E (2015) The centrosomal linker and microtubules provide dual levels of spatial coordination of centrosomes. *PLoS Genet* 11: e1005243

Park HH, Logette E, Raunser S, Cuenin S, Walz T, Tschopp J & Wu H (2007) Death domain assembly mechanism revealed by crystal structure of the oligomeric PIDDosome core complex. *Cell* 128: 533–546

Peterson AC, Russell JD, Bailey DJ, Westphall MS & Coon JJ (2012) Parallel reaction monitoring for high resolution and high mass accuracy quantitative, targeted proteomics. *Mol Cell Proteomics* 11: 1475–1488

Piel M, Nordberg J, Euteneuer U & Bornens M (2001) Centrosome-dependent exit of cytokinesis in animal cells. *Science* 291: 1550–1553

Pihan GA, Wallace J, Zhou Y & Doxsey SJ (2003) Centrosome abnormalities and chromosome instability occur together in pre-invasive carcinomas. *Cancer Res* 63: 1398–1404

Pimenta-Marques A & Bettencourt-Dias M (2020) Pericentriolar material. *Curr Biol* 30: R687–R689

Piperno G & Fuller MT (1985) Monoclonal antibodies specific for an acetylated form of alpha-tubulin recognize the antigen in cilia and flagella from a variety of organisms. *J Cell Biol* 101: 2085–2094

Pizzato M, Erlwein O, Bonsall D, Kaye S, Muir D & McClure MO (2009) A one-step SYBR Green I-based product-enhanced reverse transcriptase assay for the quantitation of retroviruses in cell culture supernatants. *J Virol Methods* 156: 1–7

Pochampally R, Fodera B, Chen L, Shao W, Levine EA & Chen J (1998) A 60 kd MDM2 isoform is produced by caspase cleavage in non-apoptotic tumor cells. *Oncogene* 17: 2629–2636

Poreba M, Rut W, Groborz K, Snipas SJ, Salvesen GS & Drag M (2019) Potent and selective caspase-2 inhibitor prevents MDM-2 cleavage in reversine-treated colon cancer cells. *Cell Death & Differentiation* 26: 2695–2709

Prodosmo A, De Amicis A, Nisticò C, Gabriele M, Di Rocco G, Monteonofrio L, Piane M, Cundari E, Chessa L & Soddu S (2013) p53 centrosomal localization diagnoses ataxia-telangiectasia homozygotes and heterozygotes. *J Clin Invest* 123: 1335–1342

Rawlings ND, Barrett AJ, Thomas PD, Huang X, Bateman A & Finn RD (2018) The MEROPS database of proteolytic enzymes, their substrates and inhibitors in 2017 and a comparison with peptidases in the PANTHER database. *Nucleic Acids Res* 46: D624–D632

Remo A, Li X, Schiebel E & Pancione M (2020) The Centrosome Linker and Its Role in Cancer and Genetic Disorders. *Trends Mol Med* 26: 380–393

Ryder PV, Fang J & Lerit DA (2020) centrocortin RNA localization to centrosomes is regulated by FMRP and facilitates error-free mitosis. *J Cell Biol* 219

Santaguida S, Tighe A, D'Alise AM, Taylor SS & Musacchio A (2010) Dissecting the role of MPS1 in chromosome biorientation and the spindle checkpoint through the small molecule inhibitor reversine. *J Cell Biol* 190: 73–87

Schmit A-C (2002) Acentrosomal microtubule nucleation in higher plants. *Int Rev Cytol* 220: 257–289

Segat D, Cassaro M, Dazzo E, Cavallini L, Romualdi C, Salvador R, Vitale MP, Vitiello L, Fassan M, Rugge M, *et al* (2010) Pericentriolar material analyses in normal esophageal mucosa, Barrett's metaplasia and adenocarcinoma. *Histol Histopathol* 25: 551–560

Serçin Ö, Larsimont J-C, Karambelas AE, Marthiens V, Moers V, Boeckx B, Le Mercier M, Lambrechts D, Basto R & Blanpain C (2016) Transient PLK4 overexpression accelerates tumorigenesis in p53-deficient epidermis. *Nat Cell Biol* 18: 100–110

Sidi S, Sanda T, Kennedy RD, Hagen AT, Jette CA, Hoffmans R, Pascual J, Imamura S, Kishi S, Amatruda JF, *et al* (2008) Chk1 suppresses a caspase-2 apoptotic response to DNA damage that bypasses p53, Bcl-2, and caspase-3. *Cell* 133: 864–877

Silkworth WT, Nardi IK, Scholl LM & Cimini D (2009) Multipolar spindle pole coalescence is a major source of kinetochore mis-attachment and chromosome mis-segregation in cancer cells. *PLoS One* 4: e6564

Sillibourne JE & Bornens M (2010) Polo-like kinase 4: the odd one out of the family. *Cell Div* 5: 25

Sillibourne JE, Hurbain I, Grand-Perret T, Goud B, Tran P & Bornens M (2013) Primary ciliogenesis requires the distal appendage component Cep123. *Biol Open* 2: 535–545

Singla V (2006) The Primary Cilium as the Cell's Antenna: Signaling at a Sensory Organelle. *Science* 313: 629–633

Sir J-H, Pütz M, Daly O, Morrison CG, Dunning M, Kilmartin JV & Gergely F (2013) Loss of centrioles causes chromosomal instability in vertebrate somatic cells. *J Cell Biol* 203: 747–756

Sladky V, Schuler F, Fava LL & Villunger A (2017) The resurrection of the PIDDosome - emerging roles in the DNA-damage response and centrosome surveillance. *J Cell Sci* 130: 3779–3787

Sladky VC & Villunger A (2020) Uncovering the PIDDosome and caspase-2 as regulators of organogenesis and cellular differentiation. *Cell Death Differ* 27: 2037–2047

Staples CJ, Myers KN, Beveridge RDD, Patil AA, Lee AJX, Swanton C, Howell M, Boulton SJ & Collis SJ (2012) The centriolar satellite protein Cep131 is important for genome stability. *J Cell Sci* 125: 4770–4779

Stinchcombe JC, Majorovits E, Bossi G, Fuller S & Griffiths GM (2006) Centrosome polarization delivers secretory granules to the immunological synapse. *Nature* 443: 462–465

Sullenberger C, Vasquez-Limeta A, Kong D & Loncarek J (2020) With Age Comes Maturity: Biochemical and Structural Transformation of a Human Centriole in the Making. *Cells* 9

Takeda Y, Kuroki K, Chinen T & Kitagawa D (2020) Centrosomal and Non-centrosomal Functions Emerged through Eliminating Centrosomes. *Cell Struct Funct* 45: 57–64

Tanos BE, Yang H-J, Soni R, Wang W-J, Macaluso FP, Asara JM & Tsou M-FB (2013) Centriole distal appendages promote membrane docking, leading to cilia initiation. *Genes Dev* 27: 163–168

Tayeh Z, Stegmann K, Kleeberg A, Friedrich M, Choo JAMY, Wollnik B & Dobbelstein M (2020) Centrosome impairment causes DNA replication stress through MLK3/MK2 signaling and R-loop formation. *bioRxiv*: 2020.01.09.898684

Tinel A, Eckert MJ, Logette E, Lippens S, Janssens S, Jaccard B, Quadroni M & Tschopp J (2011) Regulation of PIDD auto-proteolysis and activity by the molecular chaperone Hsp90. *Cell Death Differ* 18: 506–515

Tinel A, Janssens S, Lippens S, Cuenin S, Logette E, Jaccard B, Quadroni M & Tschopp J (2007) Autoproteolysis of PIDD marks the bifurcation between pro-death caspase-2 and pro-survival NF-kappaB pathway. *EMBO J* 26: 197–208

Tinel A & Tschopp J (2004) The PIDDosome, a protein complex implicated in activation of caspase-2 in response to genotoxic stress. *Science* 304: 843–846

Tinevez J-Y, Perry N, Schindelin J, Hoopes GM, Reynolds GD, Laplantine E, Bednarek SY, Shorte SL & Eliceiri KW (2017) TrackMate: An open and extensible platform for single-particle tracking. *Methods* 115: 80–90

Tischer J, Carden S & Gergely F (2020) Accessorizing the centrosome: new insights into centriolar appendages and satellites. *Curr Opin Struct Biol* 66: 148–155

Tollenaere MAX, Mailand N & Bekker-Jensen S (2015) Centriolar satellites: key mediators of centrosome functions. *Cell Mol Life Sci* 72: 11–23

Tritarelli A, Oricchio E, Ciciarello M, Mangiacasale R, Palena A, Lavia P, Soddu S & Cundari E (2004) p53 localization at centrosomes during mitosis and postmitotic checkpoint are ATM-dependent and require serine 15 phosphorylation. *Mol Biol Cell* 15: 3751–3757

Tsabar M, Mock CS, Venkatachalam V, Reyes J, Karhohs KW, Oliver TG, Regev A, Jambhekar A & Lahav G (2020) A Switch in p53 Dynamics Marks Cells That Escape from DSB-Induced Cell Cycle Arrest. *Cell Rep* 33: 108392

Uetake Y, Loncarek J, Nordberg JJ, English CN, La Terra S, Khodjakov A & Sluder G (2007) Cell cycle progression and de novo centriole assembly after centrosomal removal in untransformed human cells. *J Cell Biol* 176: 173–182

Uetake Y & Sluder G (2010) Prolonged prometaphase blocks daughter cell proliferation despite normal completion of mitosis. *Curr Biol* 20: 1666–1671

Uzbekov R & Alieva I (2018) Who are you, subdistal appendages of centriole? *Open Biol* 8

Vandesompele J, De Preter K, Pattyn F, Poppe B, Van Roy N, De Paepe A & Speleman F (2002) Accurate normalization of real-time quantitative RT-PCR data by geometric averaging of multiple internal control genes. *Genome Biol* 3: RESEARCH0034

Vassilev LT, Vu BT, Graves B, Carvajal D, Podlaski F, Filipovic Z, Kong N, Kammlott U, Lukacs C, Klein C, *et al* (2004) In vivo activation of the p53 pathway by small-molecule antagonists of MDM2. *Science* 303: 844–848

Villumsen BH, Danielsen JR, Povlsen L, Sylvestersen KB, Merdes A, Beli P, Yang Y-G, Choudhary C, Nielsen ML, Mailand N, *et al* (2013) A new cellular stress response that triggers centriolar satellite reorganization and ciliogenesis. *EMBO J* 32: 3029–3040

Vitre B, Holland AJ, Kulukian A, Shoshani O, Hirai M, Wang Y, Maldonado M, Cho T, Boubaker J, Swing DA, *et al* (2015) Chronic centrosome amplification without tumorigenesis. *Proc Natl Acad Sci U S A* 112: E6321-6330

Vora SM & Phillips BT (2016) The benefits of local depletion: The centrosome as a scaffold for ubiquitin-proteasome-mediated degradation. *Cell Cycle* 15: 2124–2134

Wang J, Li T, Wang J-L, Xu Z, Meng W & Wu Q-F (2020) Talpid3-Mediated Centrosome Integrity Restrains Neural Progenitor Delamination to Sustain Neurogenesis by Stabilizing Adherens Junctions. *Cell Rep* 33: 108495

Wang L, Failler M, Fu W & Dynlacht BD (2018) A distal centriolar protein network controls organelle maturation and asymmetry. *Nat Commun* 9: 3938

Wang W-J, Soni RK, Uryu K & Tsou M-FB (2011) The conversion of centrioles to centrosomes: essential coupling of duplication with segregation. *J Cell Biol* 193: 727–739

Weaver BAA, Silk AD & Cleveland DW (2008) Low rates of aneuploidy promote tumorigenesis while high rates of aneuploidy cause cell death and tumor suppression. *Cell Oncol* 30: 453

Wejda M, Impens F, Takahashi N, Van Damme P, Gevaert K & Vandenabeele P (2012) Degradomics reveals that cleavage specificity profiles of caspase-2 and effector caspases are alike. *J Biol Chem* 287: 33983–33995

Wigley WC, Fabunmi RP, Lee MG, Marino CR, Muallem S, DeMartino GN & Thomas PJ (1999) Dynamic association of proteasomal machinery with the centrosome. *J Cell Biol* 145: 481–490

Wong YL, Anzola JV, Davis RL, Yoon M, Motamedi A, Kroll A, Seo CP, Hsia JE, Kim SK, Mitchell JW, *et al* (2015) Cell biology. Reversible centriole depletion with an inhibitor of Polo-like kinase 4. *Science* 348: 1155–1160

Yan H, Chen C, Chen H, Hong H, Huang Y, Ling K, Hu J & Wei Q (2020) TALPID3 and ANKRD26 selectively orchestrate FBF1 localization and cilia gating. *Nat Commun* 11: 2196

Yang TT, Chong WM, Wang W-J, Mazo G, Tanos B, Chen Z, Tran TMN, Chen Y-D, Weng RR, Huang C-E, *et al* (2018) Super-resolution architecture of mammalian centriole distal appendages reveals distinct blade and matrix functional components. *Nat Commun* 9: 2023

Ye X, Zeng H, Ning G, Reiter JF & Liu A (2014) C2cd3 is critical for centriolar distal appendage assembly and ciliary vesicle docking in mammals. *Proc Natl Acad Sci U S A* 111: 2164–2169

Zhang C-Z, Spektor A, Cornils H, Francis JM, Jackson EK, Liu S, Meyerson M & Pellman D (2015) Chromothripsis from DNA damage in micronuclei. *Nature* 522: 179–184

Zhang X, Chen MH, Wu X, Kodani A, Fan J, Doan R, Ozawa M, Ma J, Yoshida N, Reiter JF, *et al* (2016) Cell-Type-Specific Alternative Splicing Governs Cell Fate in the Developing Cerebral Cortex. *Cell* 166: 1147-1162.e15

SUPPLEMENTARY FIGURES

A)

Clone Name	Cell line	gRNA sequence	Type of INDEL	ICE KO score	Immunoblot characterization	MDM2 cleavage proficiency
CEP83 3#4	A549	AAGAATACAGGTGCGGCAGT	+1	99	Yes (App. Fig. S1B)	No
CEP83 4#2	A549	GGCTGAAGTAGCGGAATTAA	-344	n.a.	Yes (App. Fig. S1B)	No
CEP83 3#A3	RPE1	AAGAATACAGGTGCGGCAGT	-7, -11	94	Yes (App. Fig. S1B)	No
CEP83 3#A5	RPE1	AAGAATACAGGTGCGGCAGT	-7	99	Yes (App. Fig. S1B)	No
SCLT1 2#D1	A549	GGGCCTCAGTCATATGTTCC	-2, -8	97	n.a.	No
SCLT1 2#1	RPE1	GGGCCTCAGTCATATGTTCC	+1	99	n.a.	No
ANKRD26 2#22	A549	GCTCCTCTGCCGCCGCGCGA	-7, -2	94	Yes (Fig. 5A)	No
ANKRD26 4#28	RPE1	ATGTCTGTGACAACGAAAAC	+1	99	Yes (Fig. 3F)	No
PIDD1 2#10	A549	GCCGATAGCGGATGGTGATG	+1	99	n.a.	No
PIDD1 2#5	RPE1	GCCGATAGCGGATGGTGATG	n.a.	n.a.	n.a.	No
PIDD1 4#10	RPE1	GGCCCGGCGCTGCCGTGAAG	-10	99	n.a.	No
FBF1 1#3	RPE1	TATCAGCATCCATGCCGTCC	+1	99	n.a.	Yes
CEP164 2#25	RPE1	CTGATGTGGCTGGCGCGAGA	-2	100	n.a.	Yes
TP53 4#1	A549	TCCATTGCTTGGGACGGCAA	-218	n.a.	Yes (App. Fig. S1E)	n.a.
TP53 4#9	RPE1	TCCATTGCTTGGGACGGCAA	-725	n.a.	Yes (App. Fig. S1E)	n.a.

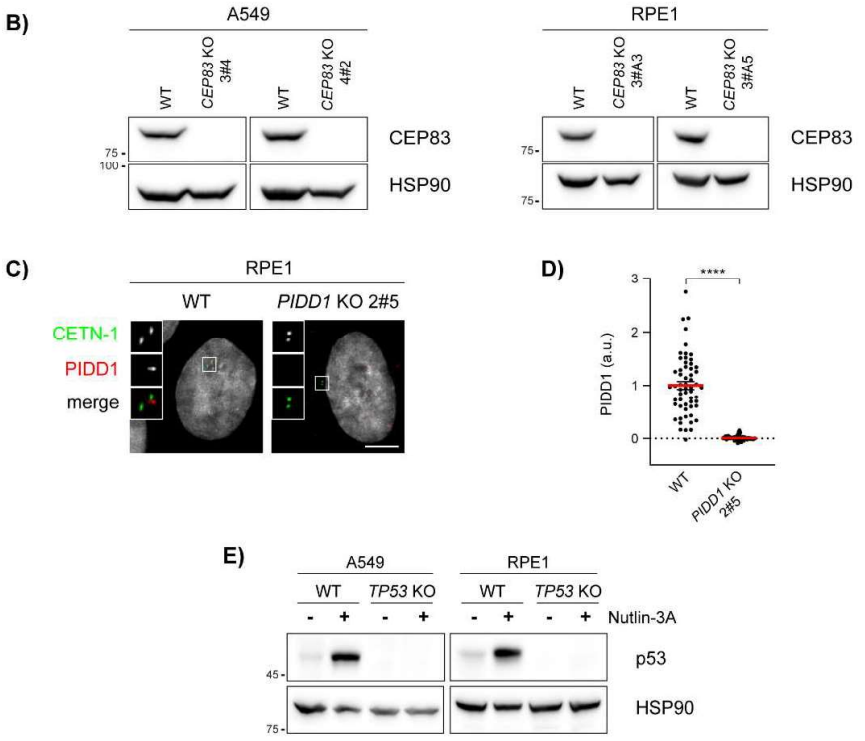

Supplementary Figure 1. Characterization of knock-out cell lines generated in this study. (A) Comprehensive list of CRISPR/Cas9 knock-out clones used in this study and their molecular/functional characterization; n.a. = not applicable. (B) A549 and RPE1 cells of the indicated genotype were subjected to immunoblot. (C) Representative immunofluorescence micrograph from the indicated cell lines co-stained with the indicated antibodies. Blow-ups without Hoechst 33342 are magnified 2.5X. Scale bar: 5 μm. (D) Dot plot showing the PIDD1 average pixel intensity at individual centrioles. Data obtained from images as in (C). N ≥ 50 centrosomes were assessed for each condition in as many individual cells, a.u. = arbitrary units. Mann-Whitney test. (E) A549 and RPE1 cell lines of the indicated genotypes were either left untreated or treated with 10 μM Nultin-3a for 24h and subjected to immunoblot.

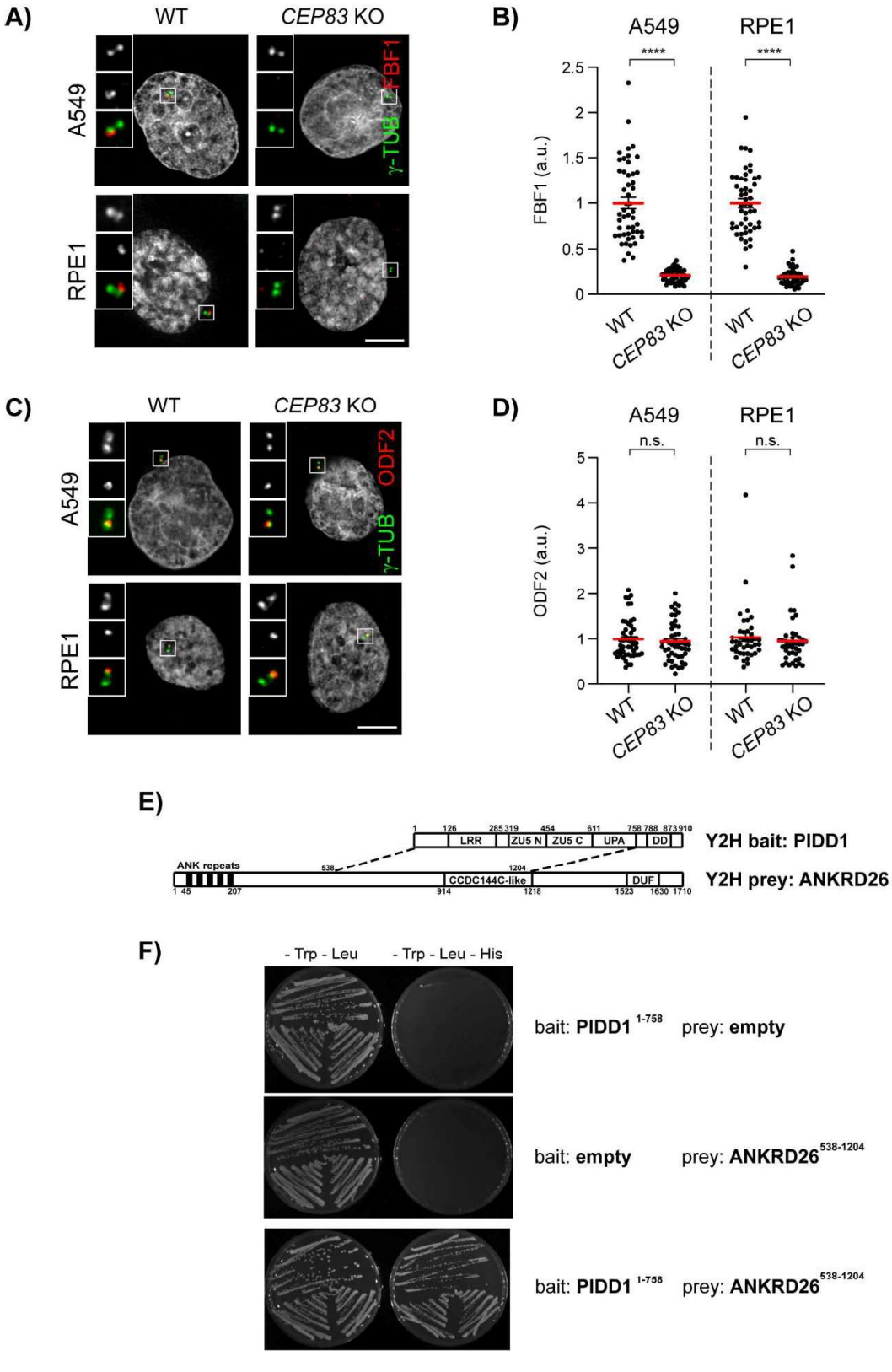
A)
WT
CEP83 KO
A549
RPE1
γ-TUB
FBF1
B)
A549
RPE1
****
****
FBF1 (a.u.)
2.5
2
1.5
1
0.5
0
WT
CEP83 KO
WT
CEP83 KO
C)
WT
CEP83 KO
A549
RPE1
γ-TUB
ODF2
D)
A549
RPE1
n.s.
n.s.
ODF2 (a.u.)
5
4
3
2
1
0
WT
CEP83 KO
WT
CEP83 KO
E)
1
126
285 319
454
611
758 788
873 910
LRR
ZU5 N
ZU5 C
UPA
DD
Y2H bait: PIDD1
ANK repeats
538
1204
CCDC144C-like
DUF
1 45
207
914
1218
1523
1630 1710
Y2H prey: ANKRD26
F)
- Trp - Leu
- Trp - Leu - His
bait: PIDD1 1-758
prey: empty
bait: empty
prey: ANKRD26 538-1204
bait: PIDD1 1-758
prey: ANKRD26 538-1204

Supplementary Figure 2. Characterization of appendage-deficient cell lines and PIDD1:ANKRD26 yeast-two-hybrid interaction. (A) Representative fluorescence micrographs from the indicated cell lines co-stained with the indicated antibodies. Blow-ups without Hoechst 33342 are magnified 2.5X. Scale bar: 5 μm. (B) Dot plots showing the FBF1 average pixel intensities at individual parental centrioles. Data obtained from images as in (A). N ≥ 50 centrosomes were assessed for each condition in as many individual cells, a.u. = arbitrary units. Mann-Whitney test. (C) Representative fluorescence micrographs from the indicated cell lines co-stained with the indicated antibodies. Blow-ups without Hoechst 33342 are magnified 2.5X. Scale bar: 5 μm. (D) Dot plots showing the FBF1 average pixel intensities at individual parental centrioles. Data obtained from images as in (A). N ≥ 50 centrosomes were assessed for each condition in as many individual cells, a.u. = arbitrary units. Mann-Whitney test. (E) Schematic of the domain structures of PIDD1 and ANKRD26. The bait utilized in the screen corresponded to PIDD1$^{S446A-S588A}$ a.a. 1-758 and retrieved as prey the 538-1204 fragment of ANKRD26. ANKRD26 annotated domains: ANK repeats = Ankyrin repeats, CCDC144C-like = Coiled-coil domain similar to CCDC144C, DUF: Domain of Unknown Function. For PIDD1 domain descriptions see Fig. 14A. (F) One by one interaction between the PIDD1 bait and the ANKRD26 prey plasmid isolated from the screen. Yeasts transformed with the indicated bait and prey plasmids were tested for growth on selective plates devoid of tryptophan and leucine (-Trp -Leu) or devoid of tryptophan, leucine and histidine (-Trp -Leu - His).

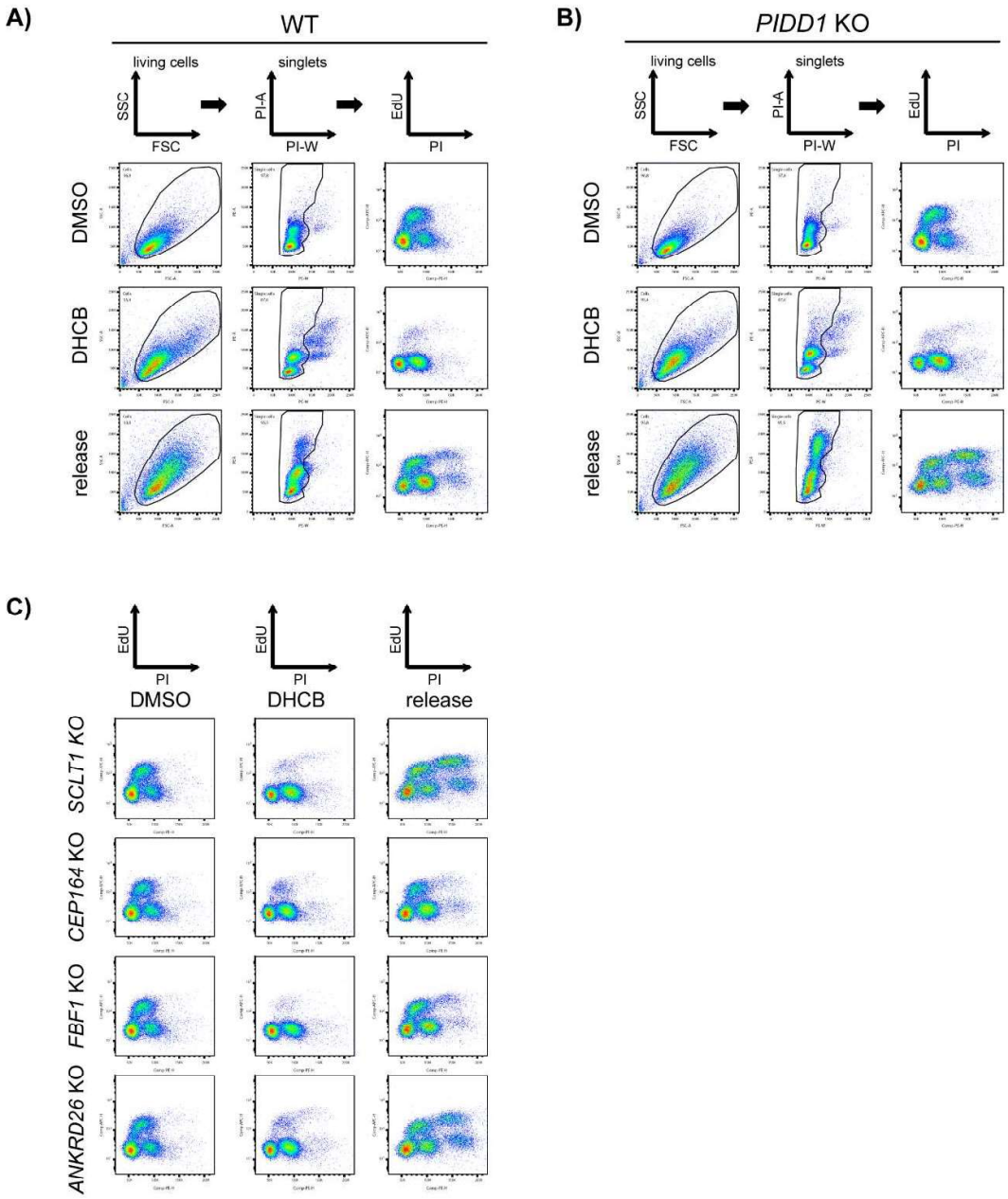

Supplementary Figure 3. Representative raw data and gating strategies relative to Fig. 12E. (A-B) Chosen gating strategy for the assessment of genome reduplication upon cytokinesis failure, displayed for RPE1 parental cells (A), showing a limited degree of genome duplication, as well as for PIDD1 KO RPE1 derivatives (B), showing a high degree of genome reduplication. RPE1 cells of the indicated genotypes were treated either with DMSO or with DHCB for 24h. A fraction of DHCB treated cells were released into fresh medium for other 24h (release), allowing to assess the degree of genome reduplication. FSC = forward scatter, SSC = side scatter, PI = propidium iodide, EdU = 5-Ethynyl-2′-deoxyuridine. (C) PI vs EdU dot plots of the indicated RPE1 genotypes treated and gated as in (A-B).

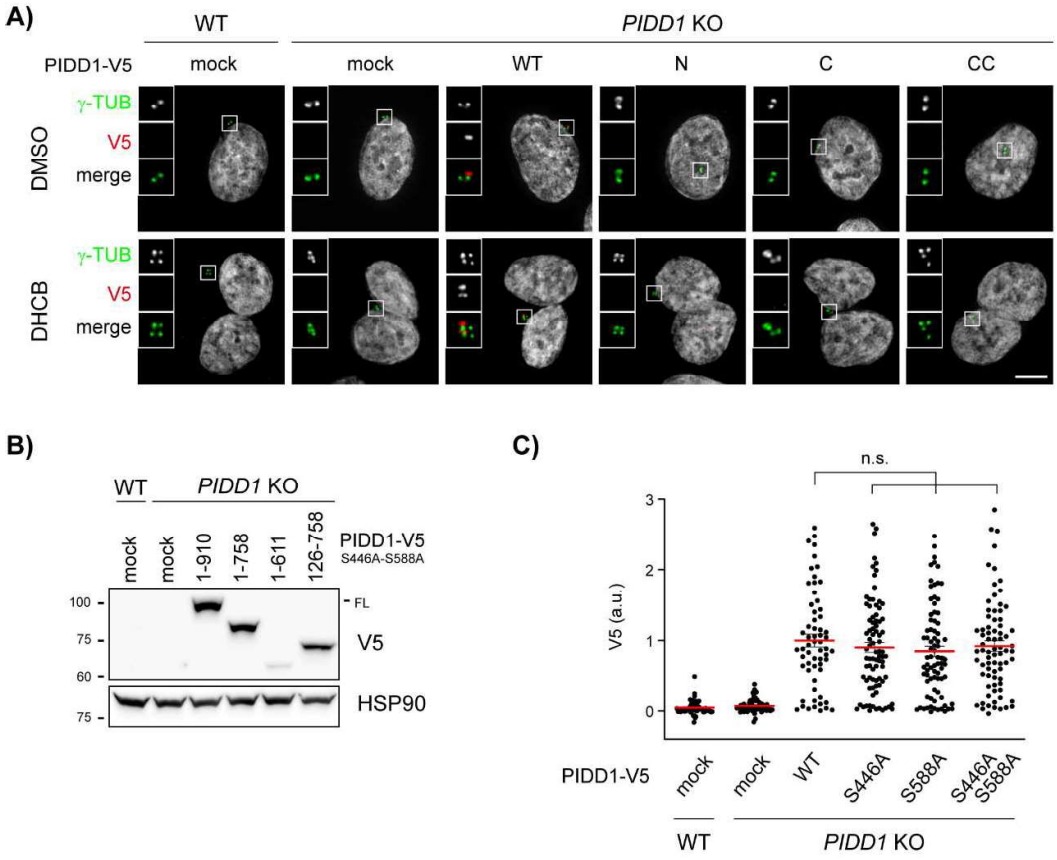

Supplementary Figure 4. Data related to Fig. 14 and 15. (A) RPE1 cells of the indicated genotypes were either left untransduced (mock) or transduced with lentiviral vectors expressing PIDD1-V5 in its wild type form or autoprocessing fragments. Cells were treated either with DMSO or with DHCB for 24h and subjected to immunostaining with the indicated antibodies. Blow-ups without Hoechst 33342 are magnified 2.5X. Representative micrographs are shown. Scale bar: 5 μm. (B) Immunoblots corresponding to fluorescence micrographs displayed in Fig. 4F. A549 cells of the indicated genotypes were either left untransduced (mock) or transduced with lentiviral vectors expressing the PIDD1-V5 non-cleavable derivative or truncations thereof. N = 2 independent experiments. (C) Dot plot showing the average V5 pixel intensities of at individual parent centrioles in A549 cells of the indicated genotypes, either left untransduced (mock) or transduced with lentiviral vectors expressing PIDD1-V5 in its wild type form or carrying the indicated point mutations. N > 50 centrosomes were assessed for each condition in as many individual cells; a.u. = arbitrary units. Kruskal-Wallis test.

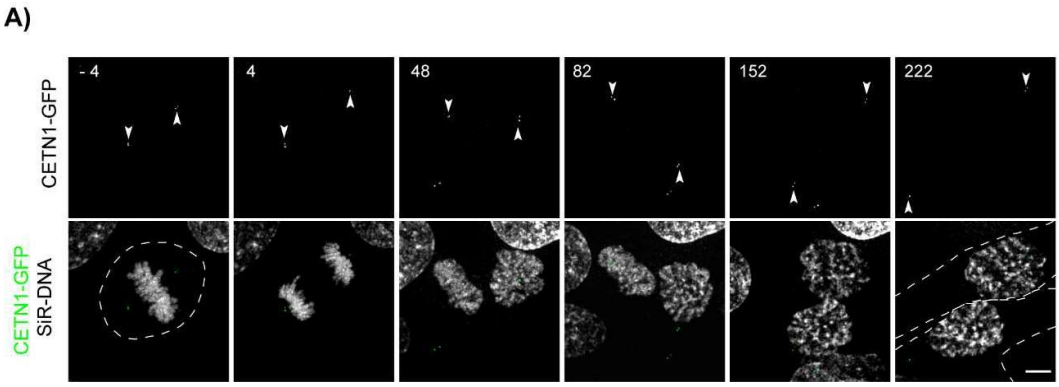

Supplementary Figure 5. Untreated control cell related to Fig. 17E. (A) Movie stills of a representative RPE1 cell stably expressing CETN1-GFP treated with DMSO, exposed to SiR-DNA and subjected to time-lapse video microscopy. The dashed line indicates the plasma membrane of the cell of interest, arrowheads indicate the centrosome position. Scale bar: 5 μm.

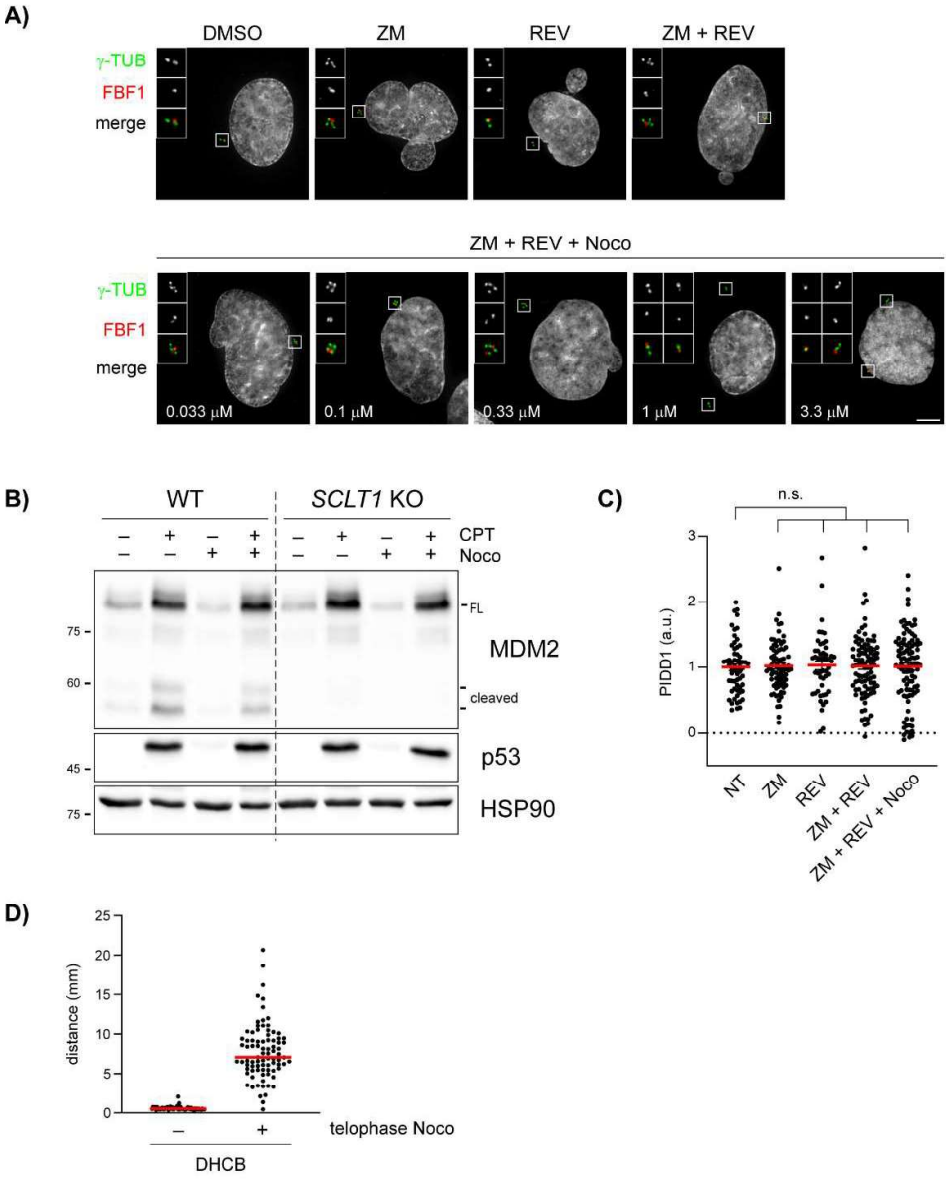

Supplementary Figure 6. Data related to Fig. 19. (A) A549 cells were either left untreated (DMSO) or treated with the indicated combination of drugs for 24h and co-stained with the indicated antibodies. Representative fluorescence micrographs are shown. Blow-ups without Hoechst 33342 are magnified 2.5X. Scale bar: 5 μm. (B) A549 cells of the indicated genotypes were either left untreated or treated with CPT and/or nocodazole (1 μM) as reported for 24h and subjected to immunoblot. N = 3 independent experiments. (C) Dot plot showing the average pixel intensities of PIDD1 at individual parent centrioles in A549 treated as in (A). 1 μM Nocodazole was used. N > 50 centrosomes were assessed for each condition in as many individual cells; a.u. = arbitrary units. Kruskal-Wallis test. (D) Distance of parent centrioles in binucleated RPE1 cells subjected to synchronization as in Fig. 19D. Cells were release in DHCB in the absence (-) or presence (+) of nocodazole during telophase. Distances were calculated in ≥ 50 individual cells per condition.

SUPPLEMENTARY TABLES

Table 1	sgRNAs for CRISPR/Cas9		
Target gene	sg#	Sequence 5'-3'	Target exon
ANKRD26	2	GCTCCTCTGCCGCCGCGCGA	1
ANKRD26	4	ATGTCTGTGACAACGAAAAC	2
CEP164	2	CTGATGTGGCTGGCGCGAGA	4
CEP83	3	AAGAATACAGGTGCGGCAGT	7
CEP83	4	GGCTGAAGTAGCGGAATTAA	7
FBF1	1	TATCAGCATCCATGCCGTCC	8
PIDD1	2	GCCGATAGCGGATGGTGATG	6
PIDD1	4	GGCCCGGCGCTGCCGTGAAG	7
SCLT1	2	GGGCCTCAGTCATATGTTCC	7
TP53	4	TCCATTGCTTGGGACGGCAA	4

Table 2	Primers for ICE analyses			
Target gene	sg#	Primer	Sequence 5'-3'	Notes
ANKRD26	2	FW	GCTTGCGACGCCTATTACCT	
		RV	GAACACTCAGCCAGACTCCC	
ANKRD26	4	FW	TTGCCATGGACATCCGCAAG	
		RV	GTTTTGAGACAGTGCACTACAGTT	
CEP164	2	FW	AATACGATTTTCTCATTGATGGAGAG	
		RV	GAGATAGCATGCTTGGATTCAAGTG	
CEP83	3	FW	TTAAGACATTTCAGATAGGTGACTTGACTCCC	
		RV	GGAAAAGCTTTGGAGTAGTCAGAGTTTTGG	
CEP83	4	FW	TTAAGACATTTCAGATAGGTGACTTGACTCCC	
		RV	GGAAAAGCTTTGGAGTAGTCAGAGTTTTGG	
FBF1	1	FW	GTGCTGACTTTGAGTCTCTCATCCC	
		RV	GCTTCTGGCAGGGAAACGAGG	
PIDD1	2/4	FW	TGGGGTGGGTTGAGGGGGC	
		RV	GGAAGTTGCCAGGGACACAGGG	
SCLT1	2	FW	CCACAATTTCAAAATAAGGAACTTTATGTCTTC	
		RV	TTGAGCAGGTTTCTTCACTGGCC	
TP53	4	FW	TACGGCCAGGCATTGAAGTC	A549
		RV	GACCCAGGGTTGGAAGTGTC	
TP53	4	FW	TTGGCGTCTACACCTCAGGA	RPE1
		RV	GCAGTCAGATCCTAGCGTCG	

Table 3		Primers for cloning	
Construct	Primer	Sequence	Notes
PIDD1-N	FW	GGCGGATCCACCATGGCTGCAACGGTGGAGGGGC	
	RV	GCCGCCGGCCGCCTAGGTGCTGTCCAGGCCCAGCAGGGGGTTGGGGATGGGCTTGCCGCTGCCGAAGTGGGGCACCTG	
PIDD1-C	FW	GGCGGATCCACCATGTCCTGGTTCCTTGTGGTTTCC	
	RV	CCGGCCGGCCGCCTAGGTGCTGTCCAGGCCCAGCAGGGGGTTGGGGATGGGCTTGCCGCTGCCGGCCTGGGCAGGCTCTGG	
PIDD1-CC	FW	GGCGGATCCACCATGTCCTGGTACTGGCTCTGG	
	RV	CCGGCCGGCCGCCTAGGTGCTGTCCAGGCCCAGCAGGGGGTTGGGGATGGGCTTGCCGCTGCCGGCCTGGGCAGGCTCTGG	
PIDD1 1-758	FW	GGCGGATCCACCATGGCTGCAACGGTGGAGGGGC	
	RV	ATGATGGCGGCCGCCTAGGTGCTGTCCAGGCCCAGCAGGGGGTTGGGGATGGGCTTGCCGCTGCCCGGCAGCTTGATGGGCAGAG	
PIDD1 126-758	FW	CATCATGGATCCACCATGCATCTGGCCCACCTGGACCTG	
	RV	ATGATGGCGGCCGCCTAGGTGCTGTCCAGGCCCAGCAGGGGGTTGGGGATGGGCTTGCCGCTGCCCGGCAGCTTGATGGGCAGAG	
PIDD1 1-611	FW	CATCATGGATCCACCATGGCTGCAACGGTGGAGGGGC	
	RV	ATGATGGCGGCCGCCTAGGTGCTGTCCAGGCCCAGCAGGGGGTTGGGGATGGGCTTGCCGCTGCCCAGCCGCTCCCAGGCCTTC	
ANKRD26-PMID	FW	GCACCAGGATCCACCATGGAGCAGAAGTTGATTAGCGAGGAAGACCTCGGATCATCTCATAGTCATGAAGAAGAAAAAGAC	
	RV	ATGATGGCGGCCGCTCACTCAGCTTGAAGTTTTTGCAC	
ANKRD26-ΔPMID A	FW	TCGTTAACGGATCCACCATG	overlapping PCR
	RV	CTAGCAGAAGACTTTGCTTTTCACTGTTCTCAGAGTTCATTTTCTTTTGAG	
ANKRD26-ΔPMID B	FW	AAAGAAAATGAACTCTGAGAACAGTGAAAAGCAAAGTCTTCTGCTAG	
	RV	GATCAGCGGGTTTAAACGGG	

Table 4		Primers for site-directed mutagenesis	
Construct	Primer	Sequence	Notes
SCLT1 PAMmut sg#2	FW	GACTACACAAGCTTTATCAAGAACATATGACTGAG	silent mutation to prevent recognition by sgRNA #2
	RV	CTCAGTCATATGTTCTTGATAAAGCTTGTGTAGTC	
PIDD1 PAMmut sg#2	FW	GGGAGCCACCGCCACTCCAATCACCATCCGCTATC	silent mutation to prevent recognition by sgRNA #2
	RV	GATAGCGGATGGTGATTGGAGTGGCGGTGGCTCCC	
PIDD1 L828E	FW	GAGTTCCGGGATGATGAGGATGAGCAGATCCG	
	RV	CGGATCTGCTCATCCTCATCATCCCGGAACTC	
PIDD1 S446A	FW	CAGGTGCCCCACTTCGCCTGGTTCCTTGTGGTTTC	
	RV	GAAACCACAAGGAACCAGGCGAAGTGGGGCACCTG	
PIDD1 S588A	FW	CAGGTCACACACTTCGCCTGGTACTGGCTCTGG	
	RV	CCAGAGCCAGTACCAGGCGAAGTGTGTGACCTG	

ACKNOWLEDGMENTS

I would like to express my deep gratitude to my advisor Prof. Luca Fava for selecting me as first PhD student of his laboratory, for mentoring me during these years, for his constant guidance and support.

Thank you also to the current and former members of the Fava lab as well as to all the CIBIO colleagues: we had interesting discussions and shared many good times together!

I would like to acknowledge the Advanced Imaging Core Facility staff for training me and for the help in getting the best out of my experiments.

A special thanks to all my new friends for the unforgettable moments spent together.

ANNEXES

Burigotto M., Mattivi A., Migliorati D., Magnani G., Valentini C., Roccuzzo M., Offterdinger M., Pizzato M., Schmidt A., Villunger A., Maffini S., Fava LL. *Centriolar distal appendages activate the centrosome-PIDDosome-p53 signalling axis via ANKRD26.* EMBO J 2021 2021;40(4):e104844. doi:10.15252/embj.2020104844

Burigotto M., Fava LL. *The PIDDosome: centrosome guardian and backup on the DNA damage response.* Molecular & Cellular Oncology 2021; doi: 10.1080/23723556.2021.1893625.